



NANOTECH TUNISIA 2015

International Nanotechnology Conference
22 – 24 April 2015

El Mouradi Hotel, Yasmine Hammamet
Hammamet – Tunisia

Organizer



www.setcor.org

Nanotech Tunisia 2015 Conference Program

Wednesday 22nd April 2015

Session I: Nanomaterials Fabrication, Characterization and Tools/ Properties

Session chairs:

Prof Adnane Abdelghani- Tunisia/ Prof Eduard Llobet - Spain

9.00-9.45	Anodic Growth and Use of Highly Aligned Refractory Metal Oxide Nanostructures A. Mozalev	Dr Alexander Mozalev , Brno University of Technology- Czech Republic
9.45-10.00	Functional ferrofluids based on levan coated magnetite nanoparticles V. Gaziyer, C. B. Cebeci, T. Morova, O. Ates, E. Toksoy Oner and S. Genc	Dr Seval Genc , Marmara University, Turkey
10.00-10.15	Manufacturing Polylactic Acid (PLA)/Nano Crystal Cellulose (NCC) by Solution Blending and Investigation of Improved Mechanical Properties. T-H. Lee , S-J Lee, J-W. Park and H-J. Kim	Mr Tae-Hyung Lee , Seoul National University- Republic of Korea
10.15-11.00	Coffee break + Poster Session I	
11.00-11.30	Multidimensional in-situ analysis of Boron/Ni composite nanowires in the new FEI Talos 200X TEM D. Delille	Dr Dominique Delille , FEI Company- Eindhoven- Netherlands
11.30-11.45	Analysis of the re-stacking structure of clay dispersed intumescent flame retardant composites J.-H. Lee , H. Kim, J.-W. Park, H.-J.Kim and J.-Y.Choi	Mr Jung-Hun Lee , Seoul National University- Republic of Korea
11.45-12.00	Synthesis and characterization of thermoelectric nanowires based on bismuth telluride M. Ben Khedim , D.Bourgault, L.Cagnon, V.Serradeil and T.Fournier,	Mrs Meriam Ben Khedim , STMicroelectronics Rousset- France
12.00-12.15	Microstructure and mechanical properties of Al ₂ O ₃ / SiO ₂ nanocomposite H. Bouhamed	Dr Hazem Bouhamed , Engineering School of Sfax (ENIS)- Tunisia
12.15-12.30	Dual mode Up/Down conversion emissions in ZnO:Er,Yb thin films R. Elleuch , R. Salhi, J.-L. Deschanvres and R. Maalej	Dr Ridha Elleuch , University of Sfax- Tunisia
12.30-14.00	Lunch break + Poster Session I	
Session Chairs:		
Dr Malika Ardhaoui- France/ Dr Imen Hafaid- Tunisia		
14.00-15.00	Carbon in Nano and Outer Space H.W. Kroto	Prof. Sir Harold W. Kroto (1996 Nobel Prize in Chemistry), Florida State University- USA
15.00-15.15	Submicron random pyramids on crystalline Si thin films fabricated by epi-PECVD R. Boukhicha , W. Chen, M. Foldyna and P. Roca Cabarrocas ¹	Dr Rym Boukhicha , LPICM, CNRS- Polytechnic School- France
15.15-15.30	Synthesis of Aluminum Nitride and Boron Nitride Thin Films by Classical Magnetron Sputtering and by High Power Impulse Magnetron Sputtering for the Thermal Management of High Temperature Devices M-A Soussou and M-A Djouadi	Dr Mohamed-Akram Soussou Gabes Faculty of Sciences, Tunisia
15.30-15.45	Tantalum nanotube arrays via porous-alumina-assisted electrodeposition from ionic liquid: electrical characterization H. Simunkova , L. Kalina, J. Bousek and A. Mozalev	Dr Helena Simunkova , Brno University of Technology- Czech Republic
15.45-16.00	Electrical, structural and optical properties of Mg-doped InP grown by MOVPE M. Ezzedini, I.Zeydi , S. Jiang, W. Guo, L. Sfaxi, S. El Kazzi and C. Merckling.	Ms Imen Zeydi , Faculty of Science Monastir- Tunisia
16.00-16.30	Coffee break + Poster Session I	

16.30-16.45	Optical properties of an exciton bound to an ionized impurity in ZnO/SiO ₂ quantum dots L. Dallali and S. Jaziri.	Dr Lobna Dallali , Bizerte Science Faculty- Tunisia .
16.45-17.00	Correlation between coating hardness and abrasion resistance of coated nanoscale structure surfaces S. Lakel , M. Ibrir and K. Almi	Prof Said Lakel , Biskra University- Algeria
17.00-17.15	Effect of the drying conditions on properties of nanocrystal-lite catalysts for n-hexane S. Raissi , M.K.. Younes and A. Ghorbel	Dr Sahar Raissi , Faculty of Sciences of Tunis- Tunisia
17.15-17.30	Sprayed volume effects on the growth of Cu ₂ ZnSnS ₄ thin films Z. Seboui , A. Gassoumi, Y. Cuminal and N. Kamoun Turki	Dr Zeineb Seboui , Tunis Science Faculty, Tunisia .
17.30-17.45	Correlation between structural and optical properties of nanostructured CuIn ₅ S ₈ thin films grown by glancing angle deposition A. Sinaoui , F. Chaffar-Akkari, B. Gallas, D. Demaille and M. Kanzari 1	Ms Azza Sinaoui , Tunis National Engineering School- Tunisia
17.45-18.00	Temperature and cross-linking degree effects on the swelling of poly(Acrylamide/1,6-Hexanedioldiacrylate) : Optimization by composite experimental designs S. Hamri , B. Dali-Youcef, K. Boudraâ, T. Bouchaour, K. Bachari and D. Lerari	Dr Salah Hamri , Center for Scientific and Technical Research in Physical and Chemical Analyses (CRAPC)- Algeria

Thursday 23rd April 2015
Session II: Nanotech in Life Sciences and Medicine

Session chairs:
Prof Larbi Sfaxi- Tunisia/ Dr Alexander Mozalev- Czech Republic

9.00-9.45	Multi-Walled Carbon Nanotubes-incorporated Biopolymers as Extraction Tools for Selected Drugs in Aqueous Matrices M. Marsin Sanagi , W. Nazihah, W.Ibrahim, N.S.M. Hanapi and W; A.W.Ibrahim	Prof Mohd Marsin Sanagi , Universiti Teknologi Malaysia- Malaysia
9.45-10.00	Tailoring the Magnetization Distribution in Ferromagnetic Nanowires and Nanotubes for (Bio) Applications K. Zuzek Rozman , S. Trafela, D. Pecko, M.S. Arshad, N. Kostevsek, S. Sturm and S. Kobe	Dr Kristina Zuzek Rozman , Jozef Stefan Institute- Slovenia
10.00-10.15	Study and research in Germany and DAAD funding programmes B. Schindler-Kovats	Mrs Beate Schindler-Kovats , DAAD Office Tunis - Tunisia
10.15-11.00	Coffee break + Poster Session II	
11.00-11.15	Multimodal FePt/SiO ₂ /Au nanoparticles with a combined magneto-photothermal effect for nanomedical applications S. Šturm , N. Kostevšek, K.Ž.Rožman and S. Kobe	Dr Sašo Šturm , Jozef Stefan Institute- Slovenia
11.15-11.30	Synthesis and characterization of iron oxide nanoparticles for potential biomedical applications M. Dardouri and A. Dakhlaoui Omrani	Ms Maïssa Dardouri , CNRSM, Technologic Park of Borj Cedria- Tunisia
11.30-11.45	Proteins as an alternative to synthetic surfactants for stabilizing nanoemulsions in the pharmaceutical field. G. Mekhloufi , A. Ali, E. Bouyer, M. Chéron and F. Agnely	Dr Ghozlene Mekhloufi , Pharmacy School, Paris Sud University- France
11.45-12.00	Fabrication of Silver Nanoparticles using different Egyptian Lactobacillus sp. and their antibacterial and antifungal activities S.A. Abdellatif and E-S. Shabaan	Prof Sawsan A. Abdellatif , Genetic Engineering and Biotechnology Research Institute- Alexandria- Egypt .
12.30-14.00	Lunch break + Poster Session II	

Session III: Nano-Electronics

Session chairs:
Prof Adnane Abdelghani- Tunisia / Prof Taleb H. Ibrahim- United Arab Emirates

14.00-14.45	CVD growth of single crystalline metal oxide nanomaterials and their application to gas sensing S. Roso , F. E. Annanouch and E. Llobet	Dr Eduard Llobet , Minos-EMaS, Universitat Rovira i Virgili- Spain
-------------	--	--

14.45-15.00	Porous anodic alumina covered by sputter-deposited WO ₃ for Laser Desorption Ionization (LDI) applications R. Calavia , D. Vilalta, P. Rafols, N. Ramirez, X. Correig, O. Yanes and E. Llobet	Mr Raul Calavia , Minos-EMaS, Universitat Rovira i Virgili- Spain
15.00-15.15	A Disposable Electrochemical Sensor based on Protein G for High-Density Lipoprotein (HDL) Detection H. Chammem , L. Mora, I. Hafaid, A. Garcia, O. Meilhac and A. Abdelghani	Ms Hanen Chammem , National Institute of Applied Science and Technology- Tunisia .
15.15-15.30	Development of an impedimetric immunosensor for human serum albumin detection N. Bohli , H.Chammam, L.Morra, Olivier Meilhac and A.Abdelghani	Dr Nadra Bohli , National Institute of Applied Science and Technology- Tunisia
15.30-15.45	Gas sensors based on WO ₃ nanoneedles decorated with Pt and Au nanoparticles A. Thamri, H. Baccar , E. Llobet and A. Abdelghani	Dr Hamdi Baccar , National Institute of Applied Science and Technology- Tunisia .
15.45-16.00	Ecotoxic evaluation of cobalt and titanium silicon oxide nanomaterials in terrestrial ecosystem S. Bouguerra , A.Gavina, M. Ksibi, M.G. Rasteiro, T. Rocha-Santos and R. Pereira.	Dr Sirine Bouguerra , Engineering School of Sfax- Tunisia
16.00-16.30	Coffee break + Poster Session II	
16.30-16.45	Analytical Efficient Model of the Tunneling Current in Ambipolar Schottky Barrier Carbon nanotube Field Effect Transistor W. Ben Ayed, M. Najari and H. Samet	Dr Montasar Najari , Gabes Faculty of Sciences- Tunisia
16.45-17.00	Flame retardant nanocomposite materials utilizing intumescent system and nano clay J.-W. Park , H. Kim, J.-H. Lee, H.-J.Kim, M.-J. Kwon and J.-Y.Choi	Mr Ji-Won Park , Seoul National University- Republic of Korea
17:00-17:15	Nanosized Iron Oxide for Fabrication of Carbon Structures via Pulsed Laser Ablation Deposition Method R. Irmawati , S.L. Liew, Y. Noorhana, A.H. Shaari	Dr Irmawati Ramli , Universiti Putra Malaysia, Malaysia

Friday 24th April 2015
Session IV: Nanotech for Energy and Environment

Session chairs:
Prof Larbi Sfaxi- Tunisia/ Dr Hamdi Baccar -Tunisia.

9.00-9.45	Magnetically Responsive Biological Waste Materials for Environmental Technology I. Safarik , E. Baldikova, Z. Maderova, K. Pospiskova and M. Safarikova	Prof Ivo Safarik , Institute of Nanobiology and Structural Biology- Czech Republic
9.45-10.00	Photoelectrochemical Water Splitting on Tungsten Oxide Nanorod Arrays via Anodizing Al/W Metal Layers M. Bendova , A. W. Hassel and A. Mozalev	Dr Maria Bendova , Brno University of Technology- Czech Republic
10:00-10:15	Increment of Solar Cell Efficiency by Selected Anti-Reflection Coating K. Omar , K.A. Salaman and Z. Hassan	Dr Khalid Omar , University of Nizwa- Sultanate of Oman
10.15-11.00	Coffee break	
11:00-11:30	Magnetic Nano-Structured Coatings for Corrosion Resistance T.H. Ibrahim and K.M. Abed	Prof Taleb H. Ibrahim American University of Sharjah- United Arab Emirates
11:30-11:45	Thermodynamic modeling and design of a solar lithium bromide-water absorption chiller C. Hamdi and A Farhat	Mr Chaker Hamdi , National Engineering School of Tunis- Tunisia
11:45-12:00	Drinking water micro-pollutants evaluation in Tunisia, case of: Pb, Hg, Cd, F W. Guissouma and J. Tarhouni,	Mrs Wiem Guissouma , National Institute of Agronomy of Tunis, Department- Tunisia
12:00-14.00	Lunch break	

Posters Session I
Nanomaterials Fabrication, Characterization and Tools
Nanotech in Life Sciences and Medicine
Wednesday 22nd April 2015

N.	Title	Author/Affiliation/Country
1	Structural, microstructural and thermal stability of FeSiB na-nopowders alloys prepared by mechanical alloying M. Ibrir , S. Alleg, S.LAKEL, Saadi BERRI, N.E. Fenineche and J.J. Suñol	Dr Ibrir Miloud , Msila University - Algeria
2	Cupric oxide nanomaterials: Hydrothermal synthesis and electrochemical properties F. Janene , H. Dhaouadi and F. Touati	Ms Fatma Janene , Tunis Science Faculty - Tunisia
3	Nucleic Acid Induced Assembly of Gold Nanoparticles R. Gary , G. Carbone, G. Petriashvili and R. Barberi	Dr Ramla Gary , universita della calabria - Italy
4	Formation of nanocrystalline B2-structured (Fe,Ni)Al in mechanically alloyed Fe ₅₀ Al ₃₀ Ni ₂₀ (%.wt) powder C. Nakib , A. Otmani, A.Djekoun and J.M. Grenèche	Ms Chafika Nakib , Skikda University - Algeria
5	Theoretical prediction of the optical properties of Zn _{1-x} BexO Alloys based optoelectronic devices S. Lakel , F. Elhamra, M. Ibrir, K. Almi and F. Okbi	Prof Said Lakel , Biskra University - Algeria
6	Acute hepatotoxicity of zinc oxide nanoparticles in Wistar rats H.Ben Miled, Z.Ben Barka, Y.Baratli, M. Tlili, H.Abdelmelek, M. Sakly, K. Ben Rhouma and O. Tebourbi	Dr Olfa Tebourbi , Science faculty of Bizerte - Tunisia
7	Synthesis, characterization and optical properties of ZnO nanostructures via solvo-hydrothermal process A. Moulahi and F. Sediri	Mr Ali Moulahi , IPEIT, University of Tunis 2 - Tunisia .
8	Correlation between structural and optical properties of SiO ₂ /(Ni:TiO ₂) Bragg reflectors processed by dip-coating sol-gel method: The effect of annealing duration and Ni content H. Sedrati and R. Bensaha	Dr Hichem Sedrati , University of Skikda - Algeria
9	Age Modulates Fe ₃ O ₄ Nanoparticles Liver Toxicity Y. Baratli , M. Tlili, H. Ben Miled, Z. Ben Barka, L. Ben Taher, H. Abdelmelek, O. Tebourbi and B. Geny	Mrs Yosra Baratli , Science faculty of Bizerte - Tunisia

Posters session II

Nano-Electronics/ Nanotech for Energy and Environment

Thursday 23rd April 2015

N.	Title	Author/Affiliation/Country
1	The application of electrochemical impedance spectroscopy to study of enzyme kinetics Z. Fohlerová , M. Jílek, M. Pospíšilová and J. Hubálek	Dr Zdenka Fohlerová , Brno University of Technology- Czech Republic
2	Optimization of the electromagnetic wave propagation in a tri-layer electrode ZnO/Ag/ZnO for solar cells application D. Hatem , MS. Belkaid and M. Mesrouk	Mrs Djedjiga Hatem , Mouloud Mammeri University- Algeria
3	Use Hydrogen in the Steel Industry M. Kahalerras , M. T. Abedghars,	Mr Mounir Kahalerras , URASM /CSC-Annaba- Algeria
4	Single and binary adsorption system of lead and zinc ions from aqueous solution, by use of ammonium activated clays: kinetics and thermodynamics study. A. Gharsalli , M. Bagane and S. Ammar	Mr Amor Gharsalli , National Engineering School of Gabes- Tunisia .
5	3-D Design, Electro-Thermal Simulations of Metal Oxide Gas Sensor Based on a High Temperature and Low Power Consumption Micro- Heater Structure and Geometrical Optimization of Spiral Platinum Micro-heaters using COMSOL A. A. Abdeslam , F. Kerrou and K. Aguir	Mr Aimer Amer Abdesslam , Constantine 1 University- Algeria
6	Effect of cavity length of quantum well laser K. Aouni and F. Kerrou	Ms Khadoudja Aouni / Mr Aimer Amer Abdesslam , Constantine 1 University- Algeria
7	White organic light-emitting diode using Rubrene A. Sidi Said , M. Belkaid, R. Antony, S. Oussalah and D. Hatem	Mrs Djedjiga Hatem , Mouloud Mammeri University- Algeria
8	Laser-assisted photocatalysed degradation of pollutants using semi-conductors in electronic contact with gold nanoparticles Z. Chehadi , J. Toufaily, J-S. Girardon, M. Capron, F. Dumeignil, T. Hamieh, R. Bachelot and S. Jradi	Ms. Zeinab Chehadi , University of technology of Troyes- France
9	The study of functionalization rule in the biosensing approaches H. Ben Fredj , M.B. Mejri, A. Abdelghani	Dr Haykel Ben Fredj , INSAT - Tunisia
10	Surface Potential Decay and Potential Return of Corona Charged Biomedical Polymer: Simulation and Experimental Hitoum Nabil , S. Sahli, Z. Ziari, A. Bellel	Mr HITOUM Nabil Constantine 1 University, Algeria

Oral Presentations

Anodic Growth and Use of Highly Aligned Refractory Metal Oxide Nanostructures

A. Mozalev

Central European Institute of Technology (CEITEC), Brno University of Technology, Brno, Czech Republic

Abstract: Refractory metal (including valve metal) oxides possess various useful properties, such as superconductivity, magneto-resistance, catalytic activity, electrochromism, gas sensitivity and many more. Nanostructuring of metal oxides is an active and competitive area of research as it offers unprecedented opportunities for the development of advanced materials and microsystem components at the nanoscale with improved performances or substantially enhanced properties. Alignment of nanostructures over a large area of flat and patterned substrates is a prerequisite to use their collective properties, for example, in gas sensors, energy conversion, distribution and storage microdevices.

This presentation demonstrates an approach to achieve electrochemical fabrication of self-organized high aspect ratio metal oxide layers with meso-scale feature sizes *via* electrochemical anodizing of valve metal bilayers comprising a thin layer of Al superimposed on a layer of different metal (Mozalev *et al.*; 2014). The Al layer is first converted into its nanoporous oxide, this being sequentially followed by anodizing the underlying metal through the alumina nanopores. In this approach, the alumina layer is used not just as a porous mask but as part of the complex electrochemical system, included in a series of electrochemical and solid-state reactions.

Several highly promising geometries - *nanodots*, *nanocolumns*, *nanocapsules* and *nanotubes* - can be produced under controlled electrochemical conditions (Mozalev *et al.*; 2014). The detailed morphological features, such as the shape, size and mutual arrangement of nanostructures can be precisely controlled by a variation of the anodization parameters. Moreover, a high temperature annealing can be used to crystallize the as-anodized amorphous nanostructures to achieve a variety of crystalline modifications. Different doping and band-gap engineering approaches are feasible and will be discussed.

Up to date, nanostructured metal oxide films have been successfully derived from the *Al/Ta*, *Al/Nb*, *Al/Ti*, *Al/Zr* and *Al/Zr-W* bilayers. The experimental findings have helped better understand the ion and proton transport processes determining the growth and post-formed behavior of these metal oxide nanostructures.

The films' formation-structure-properties have also been studied in pursuit of new functionalities and more potential applications in microelectronics, op-

tics, optoelectronics, functional coating including self-cleaning surfaces, proton conducting membranes, chemiresistive gas sensors, including the most recently developed 3-D metal-oxide-metal nanostructures that merge the benefits of advanced nanocomposite inorganic materials with the flexibility of non-lithographic electrochemical technologies based on anodization of aluminium and on the porous-anodic-alumina-assisted anodizing of a variety of refractory metals (example in Fig. 1).

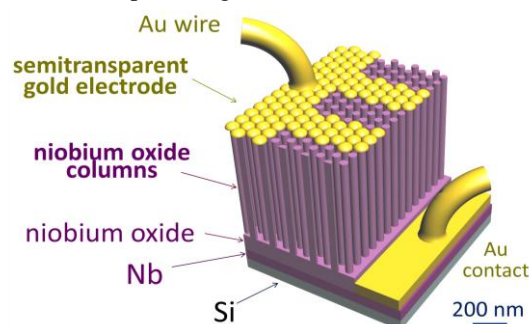


Figure 1. Computer modelled view of a 3-D nanofilm based on anodized Al/Nb layers on a Si substrate

Additionally to the above applications, the films have a high potential for utilization in dye-sensitized solar cells, photocatalytic and photoelectrochemical water splitting. The talk will address most promising and impressive applications, the well established and potential.

Research leading to these results was supported in part by GAČR grant no. 14-29531S. More contributions to this work of research institutions, relevant individuals and funding organizations will be acknowledged through the talk.

Keywords: anodizing, porous anodic alumina, refractory metal, metal oxide, nanostructure, gas sensors

References:

Mozalev, A. et al (2014), Formation-structure-properties of niobium-oxide nanocolumn arrays via self-organized anodization of sputter-deposited aluminum-on-niobium layers, *J. Mat. Chem. C* (2014) 2, 4847–4860.

Mozalev, A. et al., Smart Anodizing of Tungsten through the Alumina Nanopores: from Nanocolumns to Nanocapsules and Nanotubes. 65th Annual Meeting of the International Society of Electrochemistry, 2014. 460.

Functional ferrofluids based on levan coated magnetite nanoparticles

V. Gaziyer^{1, a}, C. B. Cebeci^{1, b}, T. Morova^{1, b}, O. Ates², E. Toksoy Oner^{1, b}, S. Genc^{1, a, *}

¹Marmara University, Engineering Faculty

^a Metallurgical and Materials Engineering Department

^b Bioengineering Department

²Nisantasi University, Medical Techniques and Services Department

Abstract: Ferrofluids (FF) are stable colloidal dispersions of very fine superparamagnetic particles. The design and synthesis of ferrofluids has been under intensive investigation due to their broad application areas. Different kinds of FFs such as water-based or organic liquid based FFs have been obtained and widely used in dynamic loudspeakers, computer hardware, dynamic sealing [Scherer *et. al.*; 2005], and environmental engineering [Peng *et. al.*; 2010]. The application of aqueous FFs is attracting great attention in biological and medical diagnosis and therapy, in pharmacy, and in biosensors [Brusentsov *et. al.*; 2002, Liao *et. al.*; 2011]. The particle content, saturation magnetization, suspension viscosity and surfactants for stabilizing the FF are vital and dominate the process performances. Prevention of particle agglomeration is one of the critical issues to be overcome in producing stable ferrofluids. Thus, nanoparticle stabilizers such as organic surfactants or polymeric compounds have been used in order to modify nanoparticle surface and/or increase their dispersion stability [Shen *et. al.*; 1999]. In this research, nano-sized magnetite (Fe_3O_4) that are particles produced by co-precipitation technique are coated with Levan polysaccharide. Levan is a fructose homopolysaccharide that is produced by a variety of microorganisms in sucrose-based media and it is mainly associated with high-value applications. Levan used in this study is obtained from the halophilic *Halomonas smyrnensis* AAD6^T bacteria isolated from Turkey [Kazak, *et. al.*; 2014]. In this study, we'll discuss the dispersibility and stability of the aqueous dispersions of levan coated Fe_3O_4 based ferrofluids as well as the magnetic, rheological properties depending on the concentrations of the particles and concentrations of the levan polysaccharide.

Keywords: Ferrofluids, Magnetic nanoparticles, Levan, rheological properties, stability

*Corresponding Author

References:

Brusentsov, N., Nikitin, L., Brusentsova T., Kuznetsov, A., Bayburtskiy, F., Shumakov, L., Jurchenko N., (2002), Magnetic fluid hyperthermia of the mouse experimental tumor, *Journal of Magnetism and Magnetic Material*, 252, 378–380.

Kazak, H., Ates, O., Ozdemir, G., Arga, K.Y. and Toksoy Oner, E. "Effective stimulating factors for microbial levan production by *Halomonas smyrnensis* AAD6^T", *Journal of Bioscience and Bioengineering*, 2014, doi: 10.1016/j.jbiosc.2014.09.019.

Liao, Z., Wang, H., Lv, R., Zhao, P., Sun, X., Wang, S., Su, W., Niu, R., Chang, J., (2011), Polymeric liposomes-coated superparamagnetic iron oxide nanoparticles as contrast agent for targeted magnetic resonance imaging of cancer cells, *Langmuir*, 27, 3100–3105.

Peng, Q., Liu, Y., Zeng, G., Xu, W., Yang, C., & Zhang, J. (2010). Biosorption of copper (II) by immobilizing *Saccharomyces cerevisiae* on the surface of chitosan-coated magnetic nanoparticles from aqueous solution, *Journal of hazardous materials*, 177(1), 676-682.

Scherer, C., Figueiredo Neto, A., (2005), Ferrofluids: properties and applications, *Brazilian Journal of Physics* 35, 718–727.

Shen L, Laibinis PE, Hatton TA (1999) Bilayer surfactant stabilized magnetic fluids: synthesis and interactions at interfaces. *Langmuir*, 15:447–453

Manufacturing Poly(lactic acid) (PLA)/Nano Crystal Cellulose (NCC) by Solution Blending and Investigation of Improved Mechanical Properties.

T-H. Lee¹, S-J Lee¹, J-W. Park¹, H-J. Kim^{1*}

¹Laboratory of Adhesion & Bio-Composites, Program in Environmental Materials Science, Research Institute for Agriculture & Life Sciences, Seoul National University, Seoul 151-921, Republic of Korea.

Abstract: PLA was reinforced by nano crystal cellulose (NCC). The main method to make NCC is acid hydrolysis. The crystalline regions of cellulose have good resistance to acid, but the other regions, disordered or paracrystalline regions, are hydrolyzed by acid attack. In resultingly, the remains are NCC (Habibi *et al.*; 2010). PLA/NCC composites were prepared by solution blending method. In common with other nano materials, it is important to make well dispersed nano composite without aggregation of nano materials. But, in generally, nano or micro celluloses including NCC have poor surface adhesive with general polymer to fabricate composites. So, there are some methods to make cellulose/polymer composite with no dispersion problem. In this research, treated and non-treated NCC were dispersed in polar solvent by ultra-sonication process. Some researchers studied the methods to disperse NCC to the polar and non-polar organic solvents with sonication, surfactant, and so on (Viet *et al.*; 2007). The dispersed NCC was blended with PLA solution. And then, PLA/NCC solution was dried in oven. Imaging analysis was conducted to confirm dispersion of NCC in matrix. And mechanical and viscoelastic properties of composites were measured by tensile strength test and dynamic mechanical analysis. By the cellulose crystal, the tensile strength of PLA was improved, and its elongation property was also enhanced. By the results of mechanical measurements and imaging analysis, the dispersion of NCC in the PLA was checked. In this research, NCC was well dispersed to PLA without any surfactant or dispersion agent.

Keywords: nanocomposites, nano crystal cellulose, polylactic acid, solution blending, ultra-sonication

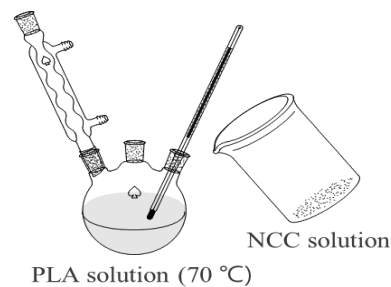
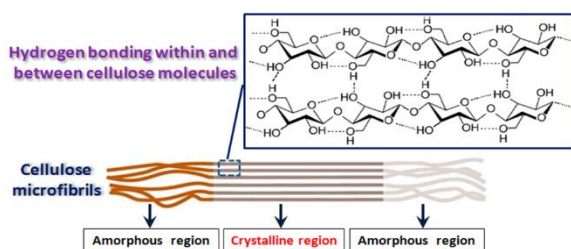


Figure 1: Schematic illustration of cellulose structure before acid hydrolysis, and solution blending to make PLA/NCC composite (Zhou *et al.*; 2012).

References:

- Youssef Habibi, Lucian A. Lucia, and Orlando J. Rojas (2010) Cellulose Nanocrystals: Chemistry, Self-Assembly, and Applications, *Chem. Rev.* *110*. 3479-3500.
- David Viet, Stephanie Beck-Candanedo and Derek G. Gray (2007) Dispersion of Cellulose Nanocrystals in Polar Organic Solvents, *Cellulose*. *14*. 109-113.
- K. Oksman, A.P. Mathew, D. Bondeson, I. Kvien (2006) Manufacturing process of cellulose whiskers/polylactic acid nanocomposites, *Composites Science and Technology*. *66*. 2776-2784.
- István Siro', David Plackett (2010) Microfibrillated cellulose and new nanocomposite materials: a review, *Cellulose*. *17*. 459-494.

Chengjun Zhou, Qinglin Wu (2012) Recent development in applications of cellulose nanocrystals for advanced polymer-based nanocomposites by novel fabrication strategies, *Nanocrystals-Synthesis, Characterization and Applications*.

Multidimensional in-situ analysis of Boron/Ni composite nanowires in the new FEI Talos 200X TEM

D. Delille*

FEI Company, Achtseweg noord 5, P.O. Box 80066, 5600 KA, Eindhoven

*Corresponding author: Email dominique.delille@fei.com

Abstract: Recent advances in EDX technology in the S/TEM and the growing use of high sensitivity windowless SDD detectors showing large collection angle have led to a strong renewal of interest for in-situ experiments on nanostructures. In the present study, the FEI Chemi-STEM Technology [1] was used on an FEI Talos F200A S/TEM to perform the fast 2D and 3D chemical mapping of B/Ni composite nanowires at a nanometer scale and at various temperatures by EDX (energy-dispersive X-ray spectroscopy), thanks to the newly developed Velox[™] software.

Successful synthesis of crystalline nanowires composed of the refractory light materials such as Boron can enable novel applications for nano-electronics [2-5]. Indeed for such applications, the ideal 1D nanoscale interconnects are expected to be composed of electrically conductive ceramics or refractory elements possessing high crystallinities and high conductivities irrespective of chirality or crystallographic orientation. Boron/Nickel composite nanostructures were prepared using a CVD-based synthetic procedure with a Ni-based compound catalyst. The properties of this binary nanomaterial at room temperature are compared to those achieved from heating experiments up to 1000 °C. 2D-3D EDX chemical mappings show clearly the core-shell structure of the wires: B in the shell and Ni in the core. This is amplified at elevated temperatures of about 500 °C. At about 1000 °C, EDX maps reveal also that Ni vanishes from the core, leaving behind hollow B nanowire (nanotube) structures.

EDS compositional analysis in TEM has revealed a presence of Boron crystalline nanowires having Ni core structure. Such composite nanostructures are created as a result of the CVD based synthetic procedure using Ni based compound as catalytic element. The 3D EDS compositional analysis and properties of such binary nanomaterial are discussed.

Details of the experimental setup will be discussed together with the proposal of a growth model. Potential electro-mechanical properties of these composite nanostructures will be evaluated and discussed as well in the oral presentation.

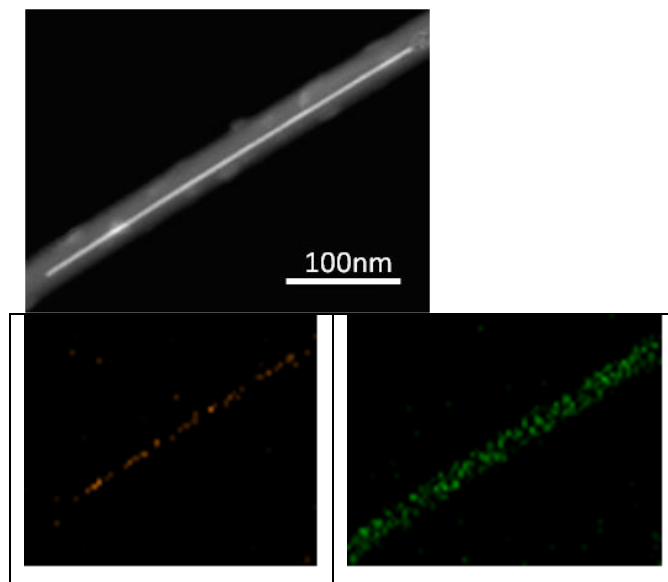


Fig. 1. (top) STEM DF image of Boron/Ni composite nanowire ; (left) Ni EDS map; (right) Boron EDS map;

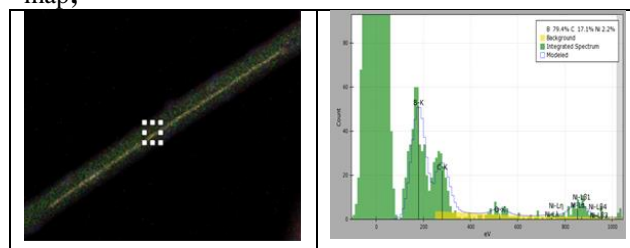


Fig. 2. (left) combined EDS Boron/Ni map with indicated area where the EDS spectrum is acquired (right)

References:

- [1] P. Schlossmacher et al., *Microscopy Today* 18(4) (2010)
- [2] CJ Otten, et al., "Crystalline Boron nanowires", *J Am Chem Soc.* 2002 May 1;124(17):4564-5
- [3] D. Wang et al., "Electrical transport in boron nanowires", *APL* 2003, 183(25):5280-82
- [4] W. Ding et al., "Mechanics of crystalline boron nanowires", *Comp. Sci. and Techn.* 2006, 66:1109-21
- [5] J. Tian, et al., "Boron nanowires for flexible electronics", *APL* 2008 93:122105-7-5

Analysis of the re-stacking structure of clay dispersed in intumescent flame retardant composites

J.-H. Lee¹, H. Kim¹, J.-W. Park¹, H.-J. Kim¹, J.-Y. Choi²

¹ Seoul National University, Laboratory of Adhesion & Bio-Composites, Program in Environmental Materials Science, Seoul, Republic of Korea

² Korea Environment Merchandise Testing Institute, Republic of Korea

Abstract: Clay composite material is a nano-composite that reinforces the strength and variety of physical properties through superior aspect ratio of clay. Dispersion of clay is classified by degree of dispersion in terms of micro dispersion, intercalated and exfoliated. According to the degree of these dispersion, clay composite would be to express the various physical properties. The complex composite flame retardant systems that utilize clay and intumescent systems are known to have a structure that is re-stacking the surface at the combustion process. These re-stacking systems will be realized combustion delay effect by forming a heat insulating layer from the surface. Accurate analysis of dispersion and re-stacking clay is essential for analysis of heat insulating effect. And can be utilized as an element for investigating the properties of the surface such as carbide layer generated after combustion. In the state of the composite material, clay has been exfoliated. It was predicted to intercalated state is after combustion. Verifying the clay dispersibility in the state of the composite material was made through the imaging analysis and XRD. After combustion has a structure that is present only in the carbide layer, validation samples is prepared by using molding techniques. In particular, the interlayer distance of re-stacking structures are calculated through the diffraction analysis of TEM. Thus, the structure of the interlayer material is confirmed, it was possible to confirm that the interlayer distance is maintained by carbides that generated during combustion.

Keywords: flame retardant, intercalated, exfoliated intumescent system, nano clay, re-stacking

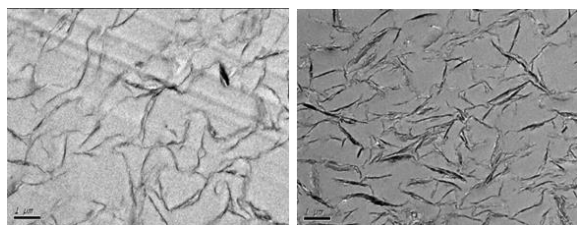


Figure 1 : Imaging analysis of clay dispersed in composites. At composite state, clay is well dispersed in composites that called “exfoliated”

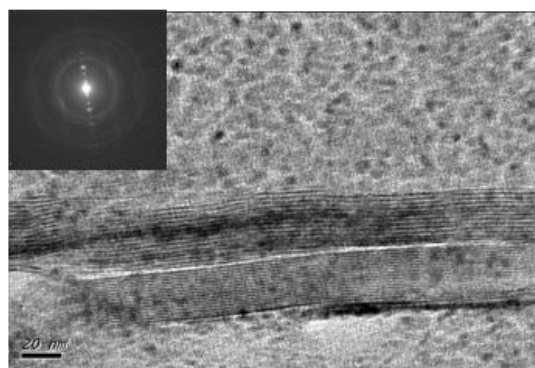


Figure 2: Re-stacking clay after combustion test. Re-stacking clay shows specific pattern. The pattern can be analyzed by diffraction analysis. Major peak means 9.76 \AA , this size is single cyclic carbon. The carbon layer is formed by combustion process.

References:

- Beyer G. (2002) Nanocomposites: a new class of flame retardants for polymers. *Plast Addit Compd*
- Landrock AH. (1983) Handbook of plastics flammability and combustion toxicology. Park Ridge, NJ: Noyes Publications
- Lu SY, (2002) Hamerton I. Recent developments in the chemistry of halogen-free flame retardant polymers. *Progr Polym Sci*
- Crummett WB. (2002) Decades of dioxin. Princeton, NJ: Xlibris Corp
- Bourbigot S, Le Bras M. (2004) Fundamentals: flame retardant plastics. In: Troitzsch J, editor. *Plastics flammability handbook: principles, regulation, testing and approval*. Munich, Germany/Cincinnati, OH: Hanser Publishers/Hanser Gardner Publications Inc.;
- Lomakin SM, Haslam E. (1999) Ecological aspects of polymer flame retardancy (new concepts in polymer science). Leiden, The Netherlands: Brill Academic Publishers

Synthesis and characterization of thermoelectric nanowires based on bismuth telluride

M.Ben Khedim^{a,b,c*}, D.Bourgault^{a,b}, L.Cagnon^{a,b}, V.Serradeil^c, T.Fournier^{a,b}

^aUniv. Grenoble Alpes, Institut NEEL, F-38042 Grenoble, France

^bCNRS, Institut NEEL, F-38042 Grenoble, France

^cTechnology R&D, STMicroelectronics, 13106 Rousset, France

Abstract:

Bismuth antimony telluride ($\text{Bi}_x\text{Sb}_{2-x}\text{Te}_3$) and bismuth tellurium selenide ($\text{Bi}_2\text{Te}_{3-x}\text{Se}_x$) nanowires, with diameter of 60nm, have been potentiostatically electrodeposited from perchloric baths using anodic alumina membrane.

Bi_2Te_3 , as the most efficient thermoelectric materials at room temperature, has been doped in order to enhance its efficiency. Nanowires electrochemical synthesis is considered as the best alternative to vacuum based methods due to its simplicity, rapidity, and low cost. In addition, compounds composition can be controlled by adjusting the initial electrolytes concentration and by varying between continuous and pulsed potential deposition, which improve the nanowires quality.

Several groups focused on binary alloys (Bi_2Te_3 , Sb_2Te_3 ..). Some others focused on the ternary alloys ($\text{Bi}_x\text{Sb}_{2-x}\text{Te}_3$ and $\text{Bi}_2\text{Te}_{3-x}\text{Se}_x$), but they reported essentially the structural, morphological and composition properties. Meanwhile only few groups investigated their thermoelectrical properties.

In this study, the nanowires morphology and stoichiometry were investigated by SEM and EDX, while structure and phases by XRD. This work reveals that the deposition potential strongly influences the nanowires chemical composition and morphology. For the low deposition over-potentials, the deposition rate is fairly slow and nanowires have almost a single crystalline structure; whereas for higher deposition over-potentials, fast growth rate leads to dendritic polycrystalline ones.

Transport properties (electrical conductivity, Seebeck coefficient) were investigated on nanowire arrays and single nanowires in order to study 1D structure effect on ternary compounds. First electrical conductivity measurements exhibit a high resistivity. In addition, the contact resistance's problem between nanowires and metals is revealed through the resistance measurement of single and assembled nanowires. For as-deposited nanowire arrays, Seebeck coefficient of $-45\mu\text{V/K}$ was obtained for the n-type and $+165\mu\text{V/K}$ for the p-type.

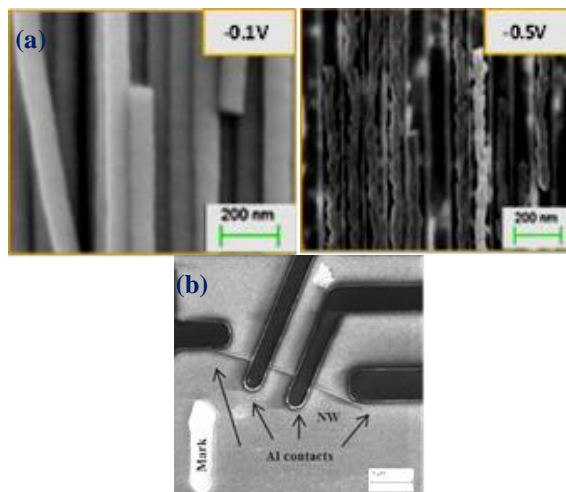


Figure 1: (a) The influence of the deposition potential on the morphology of as-deposited p-type nanowire arrays. (b) SEM image of four-probe setup on a single nanowire.

References:

- M.S.Dresselhaus, J.P.Heremans. (2006). Recent developments in low-dimensional thermoelectric materials. *In Thermoelectrics Handbook: Macro to Nano*, D. M. Rowe, CRC Press. Boca Raton, FL, p.39.
- H. Masuda, K. Fukuda. (1995). Ordered metal nanohole arrays made by a two-step replication of honeycomb structures of anodic alumina. *Science*, 268, p1466.
- DelFrari.D, Diliberto.S, Stein.N, Boulanger.C, Lecuire.JM. (2005). Comparative study of the electrochemical preparation of Bi_2Te_3 , Sb_2Te_3 , and $(\text{Bi}_x\text{Sb}_{1-x})_2\text{Te}_3$ films. *Thin Solid Films*, 483, p.44.
- S.Bäbler, T.Böhnert, J.Gooth, C.Schumacher, E.Pippel, K.Nielsch. (2013). Thermoelectric power factor of ternary single-crystalline Sb_2Te_3 and Bi_2Te_3 based nanowires, *Nanotechnology*, 24, p.495402.
- S.B. Cronin, Y-M. Lin, O. Rabin, M.R. Black, G. Dresselhaus, M.S. Dresselhaus. (2000). 4-point resistance measurements of individual Bi nanowires. *Synthesis, Characterization and Applications: MRS Symposium Proceedings, Boston*, 635, C5-7.

MICROSTRUCTURE AND MECHANICAL PROPERTIES OF Al₂O₃ / SiO₂ NANOCOMPOSITE

H. BOUHAMED*

Laboratoire de Chimie Industrielle (LCI), Ecole Nationale d'Ingénieurs de Sfax (ENIS), BP 1173 - 3038 Sfax,
Tunisia

*To whom correspondence should be addressed. E-mail : hazem.bouhamed@gmail.com

Abstract: Synthesis and characterization of alumina based ceramic matrix nanocomposite reinforced by x wt.% of nanometric silica have been investigated. Pressureless sintering has been found to be a good technique to maintain the quality of the dispersion homogeneity during the aqueous processing of (Al₂O₃-SiO₂) nanocomposite. XRD study has shown the presence of the characteristic peaks of both alumina and mullite phases, proof of the stability of a crystalline alumina-mullite nanocomposite. SEM analysis has revealed that the mullite phase has been located either within the alumina grains or at the grain boundaries. Consequently, the mullites have shown positive results in the prevention of the alumina grains growth and the densification of the material by occupying an important volume of pores. Mechanical measurements have confirmed that the inclusion of silica nanoparticles (10 nm) to the nanometric alumina (50 nm) matrix can effectively improve the microhardness and the Young's modulus of the elaborated alumina-mullite nanocomposite, leading the samples to achieve about 920 HV and 109 GPa, by incorporating 50 wt% of silica and sintering at 1550°C for 2 h.

Keywords: Nanocomposite, Alumina, Silica, Mullite, Pressureless sintering, Characterization, Mechanical properties.

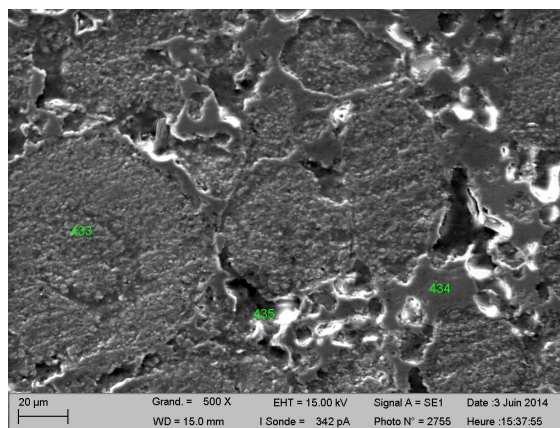


Figure 1: SEM micrograph of (80%Al₂O₃-20%SiO₂) sintered at 1550°C during 2 h

Dual mode Up/Downconversion emissions in ZnO:Er,Yb thin films

R. Elleuch^{1,3*}, R. Salhi², J.-L. Deschanvres³, R. Maalej¹

¹ Laboratoire Géossouces, Matériaux, Environnement et Changements Globaux, Faculté des Sciences de Sfax, Université de Sfax, 3018 Sfax, Tunisia

² Laboratoire de chimie industrielle, Ecole Nationale d'ingénieurs de Sfax Université de Sfax, 3018 Sfax, Tunisia

³ Laboratoire des Matériaux et du Génie Physique, 3 Parvis Louis Néel BP 257, 38016 Grenoble, France

Abstract: At present, more than 80% of the global commercial solar cells are based on crystalline silicon (c-Si). The typical power conversion efficiency of c-Si solar cells is about 18%. A major problem limiting the conversion efficiency of the cells is their insensitivity to a full solar spectrum. The spectral distribution of sunlight at Air Mass 1.5 global (AM 1.5G) consists of photons with wide wavelengths ranging from ultraviolet to infrared (280–2500 nm), but current PV cells only utilize a relatively small fraction of the solar photons. This is attributed to the fact that each cell responds to a narrow range of solar photons with energy matching the characteristic bandgap of the material. Different technologies are being sought to further enhance the c-Si cell conversion efficiency. Placing on the front and rear side of a traditional bi-facial photovoltaic solar cell a thin photon conversion layer, is the most suitable used approach (Shalav *et al.*, 2007). Trivalent lanthanide ions are the prime candidates to achieve efficient spectral conversion because of their rich energy-level structure (known as the Dieke diagram) that allows for facile photon management. Upconversion of sub-bandgap light is exploited to reduce non-absorption energy losses. The upconverter transforms two (or more) transmitted sub-bandgap (Infra-red) photons into one usable above bandgap photon, which is subsequently absorbed by the solar cell to generate electron-hole pairs. The maximum efficiency was calculated to be 47.6% for non-concentrated light (Trupke *et al.*, 2007a). Quantum-cutting through downconversion is able to split one incident high-energy photon into two (or more) lower energy photons with a conversion efficiency higher than 100%. This process could minimize the energy loss caused by thermalization of hot charge carriers after the absorption of high-energy photons, if the downconverted photons can be absorbed by solar cells. A recent quantum-cutting model can achieve a conversion efficiency of up to 38.6% (Trupke *et al.*, 2007b).

The biggest hindrance of using thin film converter is their low luminescent efficiency compared to those in powder and bulk counterparts. Thus, there have been enormous efforts to improve luminescent efficiency in semiconductor thin-film-integrated c-Si solar cells. In this framework, we

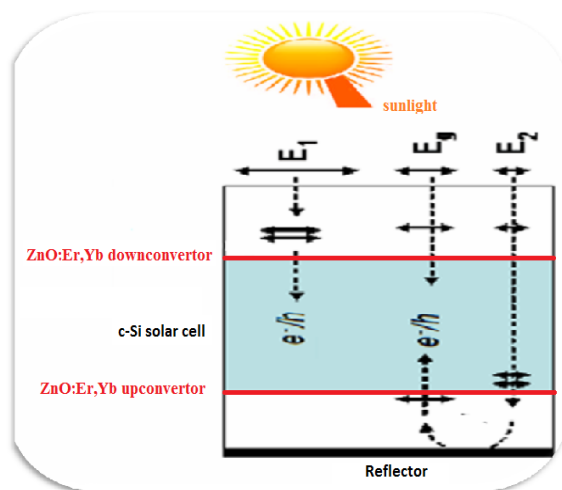


Figure 1: Figure illustrating the placement of the ZnO:Er,Yb DC/Upconvertors on the front/side of the c-Si solar cell for boosting his efficiency.

present a bifunctional ZnO:Er,Yb luminescent thin film used as dual mode Up/Downconversion photons, which can be used as converter layers for boosting c-Si solar cell. Films (with surfaces of 3 inches x 3 inches) with hexagonal phase structure are deposited at 430°C by an aerosol assisted chemical vapor deposition process liquid source in atmospheric pressure. Annealing treatments at 1000°C leads to enhance the crystallinity and the Up/Downconversion emissions in the visible-infrared ranges, which are absorbed by the c-Si cells.

Keywords: AACVD process, ZnO:Er,Yb luminescent thin film, Up/Downconversion, Boosting c-Si solar cell efficiency.

References:

Shalav, A., Richards, B.S., Green, M.A., (2007) Solar Energy Materials & Solar Cells, 91, 829–842.

Trupke, T., Green, M. A., Würfel, P., (2002) J. Appl. Phys., 92, 4117–4122.

Trupke, T., Green, M. A., Würfel, P., (2002) J. Appl. Phys., 92, 1668–1674.

Chemistry in Nano and Outer Space

Harold Kroto

Chemistry and Biochemistry Department,
The Florida State University, Florida, USA

Abstract: As the 21st Century unfolds, the top-down techniques for creating the materials, which have served us so well up till now, are approaching fundamental limits. Fortunately ingenious synthetic chemistry-based approaches are now being developed which are focused on the creation of new materials with extended, exactly-specified atomic and molecular infrastructures. These bottom-up chemical assembly methods are the crucial key to the nanoscale structure control necessary in order to achieve the paradigm shifting technical advances that are promised. As the synthetic problems are overcome, so nanoscale structures are being created with novel advanced function, vastly improved effective tensile strengths, infinitely more efficient electronic and magnetic behavior and the “intelligence” needed for medical applications etc. This intrinsically modern, synthetic perspective has evolved almost overnight and the associated new materials field has acquired a new name, Nanoscience & Nanotechnology (N&N). It is of course not new at all as biology has done things this way since the first organisms appeared. All living systems are created by bottom-up synthesis ie atom-by-atom, protein molecule by protein molecule assembly on the basis of a chemically coded blue-print stored in DNA. If life can do it - so can Chemists. In fact, the cross-disciplinary field of N&N which conflates condensed matter physics, molecular biology and materials engineering and may be considered the “Frontier Chemistry of the 21st Century”. Over the last decade or so, we have examined a wide range of methods for nanostructure formation and from these studies important new insights have been gained. We have focused particular attention on the factors governing the creation of materials with intrinsically 1- and 2-D nanoscale infrastructures. Although some advances in materials behaviour have already been achieved the technological paradigm shift that N&N promises will require further improvement of fine control over bottom-up (chemical) self-assembly.

As these new approaches were starting to develop, a totally unexpected new form of pure carbon with fascinating properties was discovered. This was the family of carbon cage molecules, the Fullerenes (Buckyballs) together with their elongated cousins the Nanotubes (or Buckytubes). This breakthrough came about partly as a consequence of the discovery, by radioastronomy, that colossal quantities of molecules existed in space and partly as a consequence of

technical laboratory advances in studying clusters of atoms. Molecular radioastronomy surveys have shown that the very cold interstellar medium was a veritable Pandora's Box, full to the brim with fascinating and exotic molecules, dust particles and also some highly puzzling material responsible for some as yet unidentified spectroscopic features. The fact that C₆₀, Buckminsterfullerene had been hiding from us and only sighted at the end of the 20th Century suggested (at least to me) that it might have been hiding in the dark recesses of the Galaxy since time immemorial. This conjecture was confirmed last year by NASA's Spitzer satellite born telescope. This is yet another example of the remarkably synergistic relationship between terrestrial and space science. In these difficult times it lends useful support for the fundamental value of "Blue Skies" or perhaps more accurately "Black Skies" cross-disciplinary research.

Submicron random pyramids on crystalline Si thin films fabricated by epi-PECVD

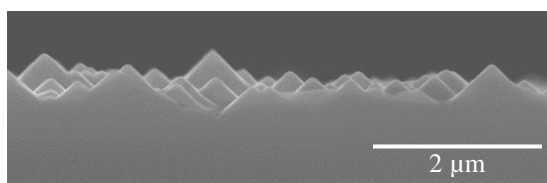
R. Boukhicha¹, W. Chen¹, M. Foldyna¹, P. Roca i Cabarrocas¹

¹LPICM, CNRS, Ecole Polytechnique, Palaiseau, France

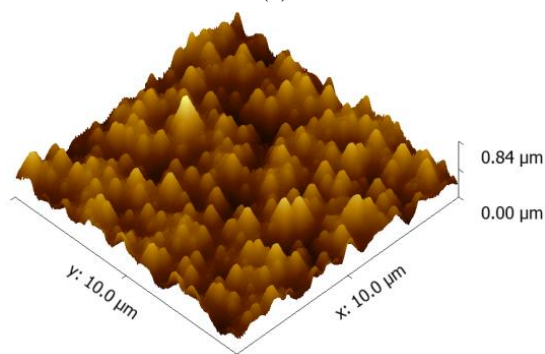
Abstract: Surface texturing is of great interest in applications for solar cells. By texturing the front surface, the reflectivity is reduced and the amount of trapped light in the solar cell increases due to the enhanced absorption. Light trapping by random pyramids is the state of the art for industrial crystalline silicon (cSi) solar cells (Campbell *et al.* 2001).

In this work, we propose to extend the knowledge of texturing on cSi solar cells (Moreno *et al.*, 2014) to thin films cSi solar cells. We produce random roughness on epitaxial crystalline silicon thin film grown by PECVD at low temperature (200°C). The texture can be done in a single process step by a wet or dry etching technique.

When performing a wet texturing, the Si(100) plane etches faster compared to the Si(111) plane leading to the formation of pyramids. Figure 1 shows random pyramids formed after 4 minutes etch of a 8 μm cSi thin layer characterized by scanning electron microscopy (a) and atomic force microscopy (b).



(a)



(b)

Figure 1: (a) SEM image of a cSi thin film etched by 3 wt% KOH during 4 minutes (b) the corresponding AFM image.

Figure 2 shows the decrease of the reflectance as a function of the wavelength for a textured cSi thin film etched for varying times from 1 to 7 minutes.

The observed reduction of the amount of reflected light from the film leads to a significant increase of the short-circuit current density in the solar cell.

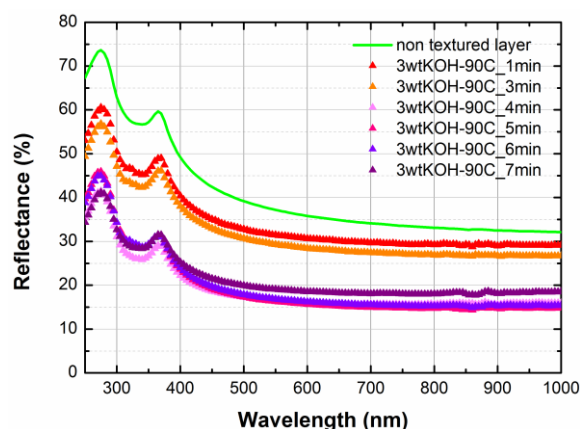


Figure 2: Spectral total reflectance measured on cSi thin film etched for varying times by a 3 wt% KOH solution at 90 °C.

We will demonstrate the performance improvements directly on HIT thin film solar cells fabricated on described epi-PECVD films (Cariou *et al.*, 2011).

Keywords: texturing, light trapping, thin films solar cells, photovoltaic application.

References:

Campbell, P., Green, M. A. (2001), High performance light trapping textures for monocrystalline silicon solar cells, *Solar Energy Materials and Solar Cells*, 65, 369–375

Moreno, M., Murias, D., Martinez, J., Reyes-Betanzo, C., Torres, A., Ambrosio, R., Rosales, P., Roca i Cabarrocas, P., Escobar, M. (2014), A comparative study of wet and dry texturing processes of c-Si wafers for the fabrication of solar cells, *Solar Energy Materials and Solar Cells*, 94, 733–737

Cariou, R., Labrune, M., Roca i Cabarrocas, P. (2011), Thin crystalline silicon solar cells based on epitaxial films grown at 165°C by RF-PECVD, *Solar Energy Materials and Solar Cells*, 95, 2260–2263

Synthesis of Aluminum Nitride and Boron Nitride Thin Films by Classical Magnetron Sputtering and by High Power Impulse Magnetron Sputtering for the Thermal Management of High Temperature Devices

M-A Soussou,^{1,2,*} M-A Djouadi,²

¹LaPhyMNE, University of Gabes, Cité Erriadh, 6072 Zrig, Gabes, Tunisia

²Institut des Matériaux Jean Rouxel (IMN), Université de Nantes, CNRS, 2 rue de la Houssinière, BP32229, 44322 Nantes Cedex3, France

Abstract: This work is dedicated to the development of a low temperature aluminium and boron nitrides (AlN and BN) thin film deposition process by reactive magnetron sputtering. This process is suitable for the requirement of microelectronics technologies. In order to elaborate high crystalline quality films, we optimized the classical magnetron sputtering process and, then, set-up the newly emerging technique of High Power Impulse Magnetron Sputtering (HiP-IMS). Thanks to their high thermal conductivities, the synthesized materials will allow a lowering of the thermal resistance of devices and an increasing of their performances.

First, a complete analysis of the DC discharge was conducted in order to optimize the numerous plasma parameters in correlation with the material properties. Our study showed that it is possible to obtain a good crystalline quality of aluminium nitride thin films.

Second, we have demonstrated for the first time that HiPIMS process can be used for the deposition of insulating material as AlN and BN. Thanks to an adaptation of the whole process including the pulsed power supply we overcome all technical problems and deposit such dielectric materials. Thanks to time-resolved diagnostic of the discharge, this process was optimised and allowed an improvement of AlN films' crystalline quality both at the interface with the substrate and at the "bulk" of the film.

Third, thermal properties of AlN films were measured and linked to their microstructures. A thermal conductivity as high as $200 \text{ W}\cdot\text{m}^{-1}\cdot\text{K}^{-1}$ was obtained.

Keywords: low temperature plasma process, DC magnetron sputtering, HiPIMS, thin films, thermal management, high power devices, aluminium nitride, boron nitride

Tantalum nanotube arrays *via* porous-alumina-assisted electrodeposition from ionic liquid: electrical characterization

H. Simunkova¹, L. Kalina², J. Bousek^{1,3}, A. Mozalev³

simunkova@feec.vutbr.cz

¹Department of Microelectronics, Brno University of Technology (BUT), Czech Republic

²Materials Research Centre, Faculty of Chemistry, BUT, Czech Republic

³Central European Institute of Technology (CEITEC), BUT, Czech Republic

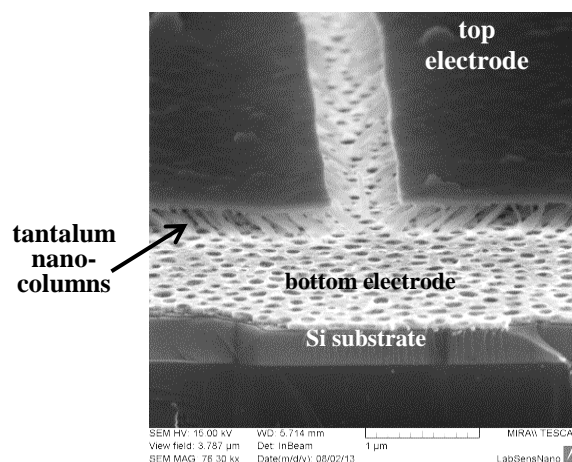
Abstract: Electrochemical formation and electrical characterization of tantalum and tantalum oxide nanostructures is an active and competitive area of research for the development of 3-D structures with an enlarged surface-to-volume ratio and different interfaces, such as metal/insulator or metal/semiconductor, used in microelectronics, e.g., metal-insulator-metal (MIM) capacitors, resistive switchers or emerging random access memories (RAMs) including resistive RAMs (RRAMs).

Electrodeposition (ED) of tantalum at a room or medium temperature (up to 200°C) using ionic liquids (ILs) has been a challenging process over the last decade. The success of first work on ED of Ta over a planar substrate (Borisenko *et al.*; 2009) inspired us to advance the technique striving to create an array of well-aligned spatially ordered tantalum and tantalum oxide nanostructures via electrodeposition from IL through nanopores in a thin-film alumina template prepared by anodizing of aluminium on a conducting substrate.

The porous anodic alumina template, having ~100-nm wide and 1- μ m long pores of $\sim 10^9$ cm⁻² population density, was prepared by anodization of a layer of Al over a W/Ti bilayer sputter-deposited onto an oxide-coated Si wafer. ED of Ta was carried out using IL 1-butyl-1-methylpyrrolidinium bis(trifluoromethylsulfonyl) imide, ([BMP]Tf₂N) (Solvionic, 99.9%), containing 0.25M TaF₅ (Alfa Aesar, 99.9 %) and 0.25M LiF (Alfa Aesar, 99.99%).

Microscopically flat continuous Ta films (400 nm thick, well adherent to the substrate) and the free-standing arrays of Ta nanotubes filling the alumina pores were achieved via potentiostatic ED. Linear sweep voltammetry revealed that the reduction of tantalum in the IL proceeds in a series of steps from Ta(V) to a final insoluble Ta-containing product. An optimal combination of process variables, such as the potential, IL temperature and polarization time, were determined and optimized. XPS analysis revealed the presence of C, Ta, O, Li and F in the outer region of the electrodeposited coatings. The coatings annealed at 600°C at 10⁻⁵ Pa were fluoride- and lithium-free, and their surface region comprised Ta₂O₅ (~70at.%), Ta₂O, Ta and tantalum carbide (~30at.%). SEM study of filling the pores with tantalum metal re-

vealed that a prolonged deposition time caused the deposit to come out from the pores and make either a dot-like or a netlike coverage on the template surface,



which may develop to a complete uniform Ta over-layer across the template (Fig. 1).

Figure 1: SEM image of a 3-D nanofilm prepared *via* electrodeposition of Ta metal in pores of an anodic alumina template (dissolved afterwards)

The current-voltage characteristics recorded along the alumina-templated Ta nanotubes revealed a bipolar resistive switching event in the films, when the behavior changes abruptly and reversely from a high resistance state to a low resistance state in a smaller voltage range. Electrochemical impedance spectroscopy measurements of the as deposited and partly anodized nanocoatings revealed the development of various semiconductor/metal interfaces and combinations, the results to be discussed in due course.

Research leading to these results was supported in part by project CZ.1.07/2.3.00/30.0039 of BUT, by GAČR grant no.14-29531S and by project CZ.1.05/2.1.00/01.0012.

Keywords: electrodeposition, porous anodic alumina, tantalum, ionic liquid, 3-D nanostructure

References:

Borisenko N., et al. (2009) *Electrochimica Acta* 54, 1519-1528

Electrical, structural and optical properties of Mg-doped InP grown by MOVPE

M. Ezzedini,^{1,2,4} I. Zeydi,⁴ S. Jiang,² W. Guo,² L. Sfaxi,³ S. El Kazzi,² C. Merckling²

¹KACST-Intel Consortium Center of Excellence in Nano-manufacturing Applications (CENA), Riyadh, Saudi Arabia

²imec, Kapeldreef 75, Leuven, Belgium

³Laboratoire de Micro-Optoelectroniques et Nanostructures, Université de Sousse, Tunisia

⁴Laboratoire de Micro-Optoelectroniques et Nanostructures, Université de Monastir, Tunisia

Abstract: We report on the electrical, optical and structural properties of epitaxial Mg-doped InP layers by Metal Organic Vapor Phase Epitaxy (MOVPE). The hole carriers concentration and (Mg) incorporation efficiency are studied using Hall effects measurements, high-resolution X-ray diffraction photoluminescence (PL) spectroscopies and SIMS. P-type InP layers with hole concentration up to $2.3 \cdot 10^{18} \text{ cm}^{-3}$ are demonstrated. From the PL measurements, the InP(Mg) samples has a near emission band to band (B-B), a Mg-related emission band-acceptor (B-A) and donor-acceptor (D-A) transition.

I. INTRODUCTION

The growth of high quality III-V layers is of great interest for the realization of optoelectronic and microelectronic devices. InP example, which can be both n- or p-type doped, shows to be a very promising material for the microwave range in photodetectors applications [1] due to their intrinsic properties. On the other hand, there has been a rising interest in integrating this material and other high electron mobility materials such as InGaAs on Si substrates for the next generation of high performance complementary metal oxide semiconductor (CMOS) devices [2, 3]. Because for a n-type channel device, ideally the buffer underneath need to be p-type doped in order to isolate the device from leakages. In the past, structures grown by Metal Organic Molecular Beam Epitaxy (MO-MBE) have first relied essentially on Be effusion cells for p-type doping. While the material grown by this method was suitable for device fabrication, the MO-MBE technique by combining metal organic and solid source led to other consequences related to reliability and reproducibility. As gaseous Be sources for instance showed to be quite toxic and thus were generally not used and other dopant elements were hence required. In the same vein, Diethylzinc (Zn) has been reported to yield efficient p-type doping of III-V semiconductors for Metal Organic Vapor Phase Epitaxy (MOVPE) but is presenting a high diffusivity in Si which is not compatible with FEOL integration. Last option could be Mg that showed to be more thermally stable than Zn as a p-type dopant for MOVPE.

In this paper, properties of the in-situ Mg-doped InP grown by MOVPE are reported. In particular, we study the influence of the Mg incorporation on the electrical and structural properties on InP. A systematic investigation of electrical, structural and optical characterizations was carried out on a series of samples using Hall effect high resolution X-ray diffraction (HR-XRD),

photoluminescence (PL) and Secondary ion mass spectrometry (SIMS).

II. EXPERIMENTS

The first three samples used in this work were (S1, S2 and S3) with a 0.5 μm -thick Mg-doped InP layers. All the sample were grown on Semi-Insulating (SI) Fe-doped InP (001)-oriented-substrates in an Aixtron Crius MOVPE reactor. Trimethylgallium (TMGa), trimethylindium (TMIn), Trimethylaluminium (TMAI), tertiarybutylphosphine (TBP), tertiarybutylarsine (TBAs) and bis (cyclopentadienyl) magnesium (Cp_2Mg) were used as precursors. These precursors were introduced into the reactor with H_2 as the carrier gas. The typical growth conditions used was temperature of 560°C with a V to III ratio equal to 50. To study the Mg doping influence on InP, the Cp_2Mg flow during growth of the doped InP layer was varied from 150 sccm (0.5 $\mu\text{mol}/\text{min}$) for sample S1 going to 200 sccm (0.673 $\mu\text{mol}/\text{min}$) for S2 and up to 250 sccm (0.841 $\mu\text{mol}/\text{min}$) for sample S3.

Samples	Conductivity	Resistivity [ohm/sq]	Hole concentration (cm^{-3})	Mobility (cm^2/Vs)
S1	N-type	4433	$1.861 \cdot 10^{18}$	15
S2	P-type	1015	$1.75 \cdot 10^{18}$	70
S3	P-type	788	$2.31 \cdot 10^{18}$	68

Table I: Electrical properties of Mg-doped InP samples.

The Photoluminescence (PL) measurement was used to examine the optical transition of the Mg-doped InP structures. The electrical properties of Mg-doped InP samples were studied using Hall measurement at 300K temperature. Furthermore, the quality of the layers structure was assessed by High-resolution X-ray diffraction (HR-XRD) measurement in the vicinity of the (004) reflection in a coupled omega scan, Omega-2Theta and the reciprocal space mapping (RSM) scan. Secondary ion mass (SIMS) was used to characterize doping profiles across the interface.

III. RESULTS AND DISCUSSION

Hall measurement results for samples S1, S2, and S3 are summarized in Table 1. For the sample S1, S2 and S3, when the

Mg-doped InP is grown with the lower Cp_2Mg flow (S1: 150 sccm), the carriers were n-type with an extremely low electron mobility ($15 \text{ cm}^2/\text{V.s}$). However p-type conductivity is obtained using a higher Cp_2Mg flow (samples S2 and S3, respectively). To study the incorporation for p-doped InP, PL measurements at 77 K were performed on all the samples. For the Mg-doped InP, different peaks are clearly visible corresponding to band-to-band transition (B-B) the band-acceptor transition (B-A) and donor acceptor transition (D-A) [4, 5] in Figure. 1.

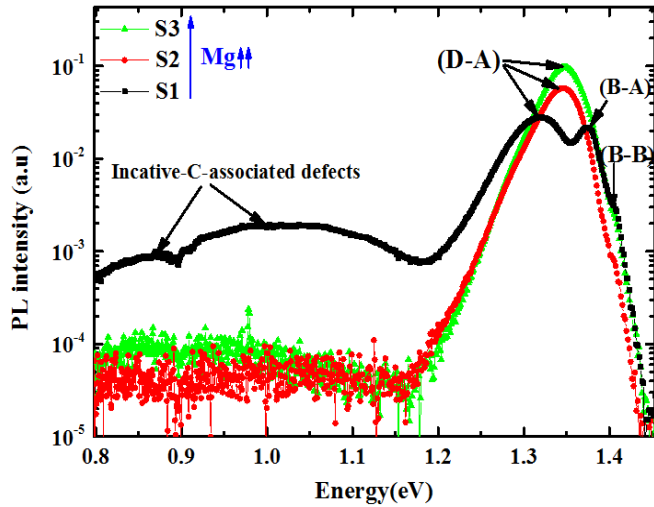


Figure 1. 77 K PL spectra obtained from samples (a) S1, S2 and S3.

To investigate the material quality, all the epilayer were characterized by HR-XRD. Typical (004) Bragg reflection RSM of the sample S1, S2 and S3 Mg-doped InP was studied. These measurements show that as expected InP (Mg) layer overlap on the InP substrate during the homoepitaxy. On the reciprocal map for the sample S3, the InP(Mg) Bragg reflection consists in a diffuse reflection spot related to the mosaicity of the Mg-doped InP layer [6,7] (Figure. 2).

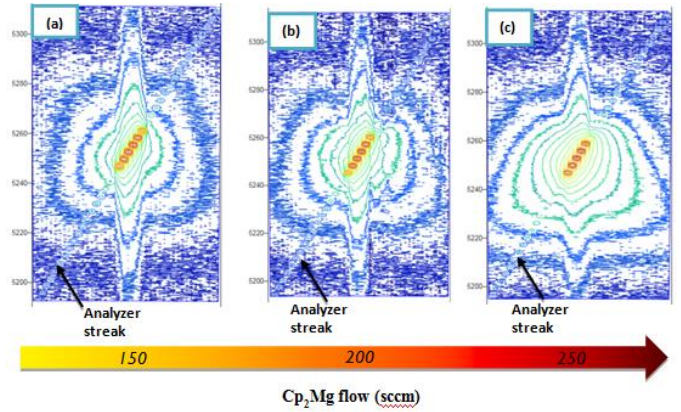


Figure 2. Measured symmetric (004) triple axis RSM of (a) Mg-doped InP, (a) sample S1 and (b) Sample S2 and (c) sample S3.

IV. CONCLUSION

A series of Mg-doped InP and Mg were grown by Metal Organic Vapor Epitaxy. We have demonstrated that Mg is an acceptor for InP semiconductor leading to an efficient p-type doping using bis(cyclopentadienyl) magnesium as precursors in MOVPE. On the other hand, the InP(Mg) crystalline quality is affected by a strong mosaicity in the layer attributed by the presence of defects generated during InP(Mg) homoepitaxy. Moreover, we demonstrated that Mg is an acceptor for the InP.

REFERENCE

- [1] H. Burkhard, H. W. Dinges, and E. Kuphal, "Optical properties of $\text{In}_{1-x}\text{Ga}_x\text{P}_{1-y}\text{As}_y$, InP, GaAs, and GaP determined by ellipsometry," *J. Appl. Phys.* Vol. 53 pp. 655-662, January 1982.
- [2] C. Merckling, N. Waldron, S. Jiang, W. Guo, O. Richard, B. Douhard, A. Moussa, D. Vanhaeren, H. Bender, N. Collaert, M. Heyns, A. Thean, M. Caymax, and W. "Applied Physics. Vol. 114, pp. 033708-033717, July 2013.
- [3] M. Paladugu, C. Merckling, R. Loo, O. Richard, H. Bender, J. Dekoster, W. Vandervorst, M. Caymax, and M. Heyns, "Site Selective Integration of III-V Materials on Si for Nanoscale Logic and Photonic Devices," *J. Cryst. Growth Des.*, vol.12, pp. 4696-4702, August 2012.
- [4] Y. Moon, S. Si, E. Yoon, and S. J. Kim, "Low temperature photoluminescence characteristics of Zn-doped InP grown by metalorganic chemical vapor deposition," *J. Appl. Phys.*, vol. 83, pp. 2261-2265, November 1998.
- [5] P. A. Postigo, M. L. Dotor, P. Huertas, F. Garcí, D. Golmayo, and F. Briones, "Electrical and optical properties of Be-doped InP grown at low temperature by solid source atomic layer molecular beam epitaxy," *J. Appl. Phys.*, vol. 85, pp. 6567-6570 February 1999.
- [6] H.W. Dong, Y.W. Zhao, Y.P. Zeng, J.H. Jiao, J.M. Li, L.Y. Lin, "Influence of semi-insulating InP substrates on InAlAs epilayers grown by molecular beam epitaxy," *Journal of Crystal Growth*, vol.250, pp. 364-369, August 2002.
- [7] M. Ezzedini, S. Jian², W. Guo, L. Sfaxi, S. El Kazzi, E. Vancoille, M. Caymax, C. Merckling, "Influence of Cp_2Mg flow for InP p-type doping in MOVPE," unpublished

Optical properties of an exciton bound to an ionized impurity in ZnO/SiO₂ quantum dots

L.Dallali^{a,*}, S.Jaziri^a.

^a Département de Physique, Faculté des Sciences de Bizerte, 7021 Jarzouna, Bizerte, Tunisie.

Abstract: Zinc Oxide (ZnO) has a wide range of applications in optical ultraviolet devices such as light-emitting diodes, laser diodes, gas sensors, optical wave-guide and solar cells. Nanostructures and heterostructures are made of ZnO, which is an exceptionally important semiconductor with a wide band gap energy. Due to the large binding excitons energy of 60 meV, the exciton has long life at room temperature. It has also been attracting much attention because of its high luminescent efficiency and non-ohmic properties. It has been proven that impurity states play a very important role in some optoelectronic devices. Without impurity, there would be no diode, no transistor, and neither of semiconductor science and technology. A deep understanding of the effect of impurities on the exciton states of semiconductor nanostructures is a fundamental question in semiconductor physics since their presence can dramatically alter the performance of quantum devices. The energy of the ground and the excited states for the exciton and the binding energy of the acceptor-donor exciton complexes (A^-, X) and (D^+, X) as a function of the radius for an impurity position located in the center in the spherical ZnO quantum dots (QDs) embedded in a SiO₂ matrix are calculated using the effective mass approximation under the diagonalization matrix technique including a three-dimensional confinement of carrier in the QD and assuming a finite depth (Dallali et al., 2009, 2011). Numerical results show that the binding energy of the acceptor-donor exciton complexes is very sensitive to the quantum dot size (Dallali et al., 2011). (Figure 1). These results could be particularly helpful since they are closely related to experiments performed on such nanoparticles. This may allow us to improve the stability and efficiency of the semiconductor quantum dot luminescence which is, in fact, considered critical.

Keywords: ZnO QD, Acceptor – Donor complex exciton, Binding energy.

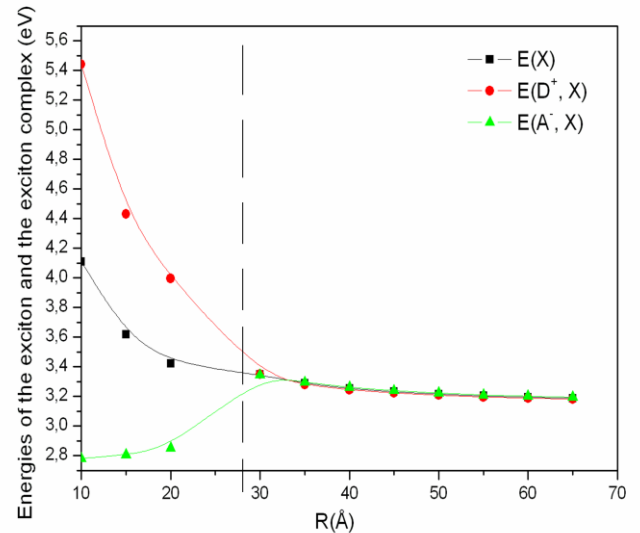


Figure 1: Energies of the exciton and the exciton complex, XC , in ZnO/SiO₂ QDs as a function of the dot radius. Impurity being located in the center.

References:

- Dallali, L., Jaziri, S., Martínez-Pastor, J. (2011), Optical properties of acceptor–exciton complexes in ZnO/SiO₂ quantum dots, *Solid State Commun.* 151 1355–1358
- Dallali, L., Jaziri, S., J, el.Haskouri., P, Amorós., Martínez-Pastor, J. (2011), Energy of excitons and acceptor–exciton complexes to explain the origin of ultraviolet photoluminescence in ZnO quantum dots embedded in a SiO₂ matrix, *Solid State Communications* 151 822–825
- Dallali, L., Jaziri, S., J, el.Haskouri., P, Amorós.(2009), Optical properties of exciton confinement in spherical ZnO quantum dots embedded in SiO₂ matrix), *Superlattices and Microstructures* 46 907- 916.

Correlation between coating hardness and abrasion resistance of coated nanoscale structure surfaces

Said LAKEL^{1,2}, M. IBRIR³, K. ALMI¹

¹ Laboratoire de physique des Matériaux - Université de LAGHOUAT – BP 37G, Laghouat, Algeria

² Laboratoire de Matériaux Semi Conducteurs et Métalliques, Université de Biskra, Algeria

³ Laboratory of Physics of Materials and its Applications, University of M'sila, Algeria

Abstract: One of the most commonly used tribological thin-film coatings is Chromium Nitride (CrN), typically deposited by PVD process [1]. Examples of current applications of this coating include cutting and forming tools: ICE piston ring, hydrodynamic pumps, etc. [2,3,4]. In selecting coating for tribological applications, one of the critical parameter is the specific wear rate κ_c of the coating. Micro-scale abrasion testing has been used to evaluate the specific wear rate κ_c of chromium-nitride (CrNx) with nanoscale structure coatings on identical a DIN 1.4301 steel substrates. Two different abrasives, SiC and diamond were used. The hardness of the films was found to be in the range of 8-38 GPa. The aim of this paper is to evaluate the abrasion resistance of hard coatings, and high abrasive wear resistance $\Omega_c=(1/\kappa_c)$ of these coatings are compared. The results were compared to those of a chromium nitride reference coating. The results obtained show an excellent correlation between coating hardness and abrasion resistance. The micro-abrasion testing employed offers a simple and inexpensive method for pre-selecting and ranking of coating materials for tribological applications.

Keywords: wear resistance, wear, Calowear, Tribology.

References:

[1] P. Wieceńska, J. Smolikb, H. Garbacza, K.J. Kurzydłowska *Surface and Coatings Technology* Volume 240, 15 February 2014, Pages 23–31

[2] Bagcivan, N., Bagcivan, N., Bobzi, K., and Theiß S., 2013 *J. Phys. D: Appl. Phys.* **46** 084001

[3]. Mo J L, Zhu M H, Leyland A and Matthews A 2013 *Surf. Coat. Technol.* 215 170

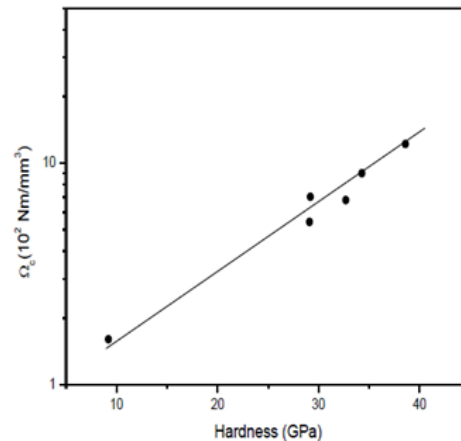


Figure 1: Abrasive wear resistance as a function of hardness (H) of Cr-N coatings.

Effect of the drying conditions on properties of nanocrystallite catalysts for n-hexane

S. Raissi, * M.K. Younes, A. Ghorbel

University of Tunis El Manar, Faculty of Sciences of Tunis, Laboratory of Material Sciences and Catalysis, Tunis, Tunisia

Abstract: Heavy naphtha constitutes a considerable portion of the petroleum products. However, it is essential to treat this portion in order to improve its characteristics and transform it into valuable products. Plastic chemicals and petroleum gases LPG can be obtained principally by cracking of light naphtha into propylene and ethylene and by liquefying high octane gasoline issued from the isomerization of light alkanes.

Different catalysts were used to study the conversion of n-hexane into its isomers or into its derived compounds. Sulphated zirconia doped transition metals seems to be a good catalysts for the type of these reactions. The aim of this work is focused on the study of the drying mode and the calcination temperature effects on the properties of sulfated zirconia doped chromium.

The sol-gel method was used for the preparation of solids because it offers homogenous materials with nanometric size. The obtained gels were dried either under an atmospheric pressure to obtain xerogels or in the hypercritical conditions of the solvent to obtain aerogels. The two kinds of solids were then calcined under a flow of oxygen at 673 K or at 973 K.

The aerogel catalysts have a good catalytic activity in isomerisation which is enhanced by calcination temperature, However the xerogel ones are completely inactive and do not ensure the hexane transformation by isomerisation, cyclisation nor cracking.

The n-hexane conversion by isomerisation into only to monobranched isomers methyl-2-pentane (M2P) and methyl-3-pentane (M3P) seems take place with a mechanism which starts by the apparition of hexene by deshydrogenation on oxo chromium sites. Then acid sites transform it into protonated cyclopropane intermediate. This later will either be rearranged to give isomerization products: M2P and M3P or to be decomposed into smaller alkane principally ethane, isobutene and propane. The XPS spectroscopy revealed specific sulphate groups on aerogels surface that could be the site responsible of the catalytic activity of those solids in isomerisation reaction.

Keywords: nanoporous sol-gel, sulfated zirconia, effect of drying, XPS spectroscopy, catalysis, n-hexane conversion.

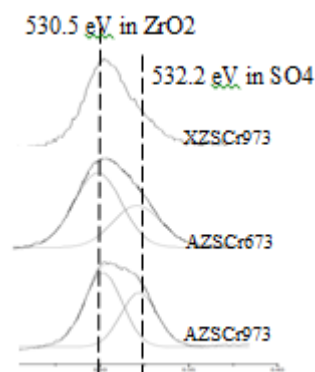


Figure 1: Catalytic activity is closely related to the preparation conditions. Drying under hypercritical conditions, as shown in the figure, the XPS study, active sites formed by sulphate groups are present on the surface of aerogels.

References:

Kammoun N, Younes MK, Ghorbel A, Mamede A, Rives A (2012) Comparative study of the texture and structure of aerogel and xerogel sulphated zirconia doped with nickel, *Por. Mat.* 19, 375-382

Raissi S, Younes MK, Ghorbel A, (2014) Mesoporous aerogels based on sulphated zirconia doped with cobalt as hexane isomerization catalysts, *Mater. Sci. Eng.*, 4, 105-111

Sprayed volume effects on the growth of $\text{Cu}_2\text{ZnSnS}_4$ thin films

Zeineb Seboui¹, Abdelaziz Gassoumi¹, Yvan Cuminal² and Najoua Kamoun Turki¹

¹Laboratoire de Physique de la Matière Condensée, Faculté des Sciences de Tunis (2092)

El Manar, Tunisia.

²IES, Université de Montpellier 2, France

Abstract

The influence of sprayed volume V_{sp} on the properties of $\text{Cu}_2\text{ZnSnS}_4$ (CZTS) thin films prepared by spray pyrolysis using a methanolic solution is investigated. Energy dispersive X-ray spectroscopy (EDX) indicates that CZTS thin films are Zn-poor and S-poor. From the results of X-ray diffraction analysis, CZTS films are amorphous at lower V_{sp} , however they become polycrystalline at higher V_{sp} . The (112) preferential orientation of the CZTS kesterite structure becomes sharper and higher with increasing V_{sp} . Raman spectroscopy reveal a good quality of CZTS film and a reduction of secondary phase at higher V_{sp} . The opto-electrical behavior shows also a drastic effect with increasing sprayed volume. The CZTS film grown at higher V_{sp} can meet the

requirement for application as an absorber in solar cell devices. The crystalline parameters of the latter are injected in WIEN2k code (Blaha et al., 2001), in order to calculate the band structure and the density of states (DOS). The calculation is made using the modified Becke Johnson (MBJ) approach (Tran et al., 2009), which is implemented in WIEN2k code.

Keywords: Raman, electrical, optical, structure band, density of states.

References

1. P. Blaha, K. Schwarz, G.K.H. Madsen, D. Kavanicka, J. Luitz, WIEN2K, an Augmented Plane Wave Plus Local Orbitals Program for Calculating Crystal Properties, Vienna University of Technology, Austria, 2001.
2. F. Tran, P. Blaha, Physical Review Letters, 102 (226401) (2009), pp.1-4.

Correlation between structural and optical properties of nanostructured CuIn_5S_8 thin films grown by glancing angle deposition

A. Sinaoui ^{1,*}, F. Chaffar-Akkari ¹, B. Gallas ², D. Demaille ², M. Kanzari ¹

¹Laboratoire de Photovoltaïque et Matériaux Semiconducteurs - ENIT - Université Tunis ElManar, BP 37, Le belvédère 1002 Tunis, Tunisie

²Institut des NanoSciences de Paris-CNRS-Université Pierre et Marie Curie, 140 rue de Lourmel, 75015 Paris, France

Abstract

CuIn_5S_8 thin films were grown by thermal evaporation method using Glancing Angle Deposition (GLAD) technique. During the deposition, the incident angle α between the particle flux and the normal to the substrate was fixed at $\alpha = 0^\circ$, 60° and 85° and the substrate rotation speed was set at $\omega = 2$ rpm.

X-Ray Diffraction (XRD), scanning electron microscopy (SEM) and UV- Vis- NIR spectra were used to characterize the structural, morphological and optical properties of the nanostructured CuIn_5S_8 thin films.

Under the GLAD conditions, we demonstrate that without substrate rotation, the oblique angle deposition films showed an inclined columnar structure, with columns tilting in the direction of the incident flux due to the shadowing effect, while with substrate rotation, the columns were grown vertically due to shadowing symmetry (Chen *et al.*, 2013) (figure 1).

Physical properties of the produced architectures are affected by the columnar structure, such as refractive index and packing density which decrease with the increase of the incident angle for both structures. This decrease is attributed to the shadowing effect which dominates the growth process at high incident angle (Sinaoui *et al.*, 2013). In particular, the optical birefringence of the columnar structure reaches its maximum at the flux angle $\alpha = 60^\circ$, while the helical structures exhibit a low value of optical birefringence due to the shadowing symmetry created by adding a continuous rotation during the deposition.

Therefore, the glancing angle deposition technique is a promising way to create a columnar structure with enhanced birefringent property.

Keywords

CuIn_5S_8 thin films, GLAD, inclined columns, helical structure, refractive index, birefringence

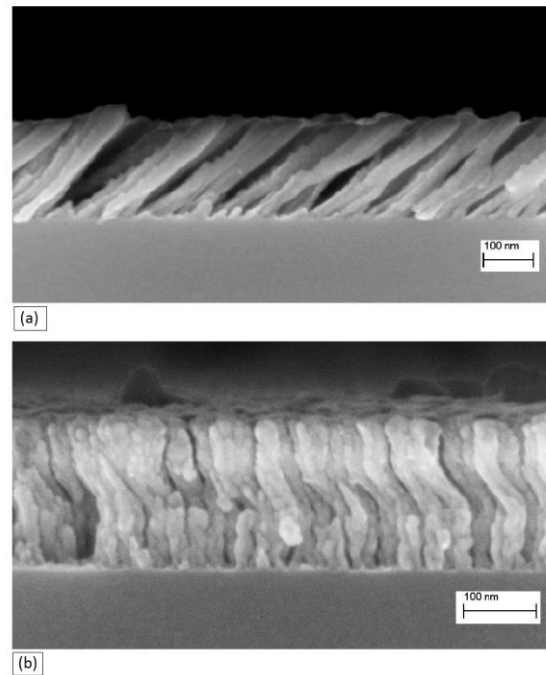


Figure 1

Illustrating the Cross sectional SEM images of CuIn_5S_8 films deposited at $\alpha = 85^\circ$, respectively, without (a) and with substrate rotation (b).

The cross-sectional view (Figure 1.a) reveals a columnar structure with columns which are inclined towards the direction of the incoming vapor flux. While, with substrate rotation, the cross-sectional view (Figure 1.b) reveals a helical columnar structure separated with voids.

References

Sinaoui, A., Khemiri, N., Chaffar-Akkari, F., Gallas, B., Kanzari M., (2013), Comparative study of structural and morphological properties of nanostructured $\text{CuIn}_{2n+1}\text{S}_{3n+2}$ ($n = 0, 1$ and 2) thin films produced by oblique angle deposition, *Eur. Phys. J. Appl. Phys.*, 64: 20301

Chen, S., Liang, J., Mo, Y., Luo, D., Jiang, S., (2013), Onset of shadowing-dominated growth of Ag films in glancing angle deposition: Kinetic Monte Carlo simulation, *Applied Surface Science*, 264, 552-556

Temperature and cross-linking degree effects on the swelling of poly(Acrylamide/1,6-Hexanedioldiacrylate) : Optimization by composite experimental designs

S. Hamri,^{1,2} B. Dali-Youcef,² K. Boudraâ,^{3,2} T. Bouchaour,² K. Bachari¹ and D. Lerari,¹

¹Center for Scientific and Technical Research in Physical and Chemical Analyses (CRAPC), Tipaza, Algeria.

²University of Tlemcen, Laboratory of Macromolecules Research (LRM), Tlemcen, Algeria

³University Dr. Tahar Moulay, Department of Biology, Faculty of Sciences and Technology, Saïda, Algeria.

Abstract: Hydrogels are cross-linked three-dimensional polymeric structures able to imbibe high amount of water or biological fluids without dissolving in aqueous surrounding environment due to the presence of critical cross-links in their structure (Rodrigues et al.; 2007). However, this class of materials are often sensitive to changes in their various external environmental conditions such as temperature, pH and ionic strength, the reason for which they are referred to as smart materials, used in many biomedical applications (Hamidi et al.; 2008, Pourjavadia et al.; 2006).

In this contribution, we study the degree of cross-linking and temperature effects on the formation of poly(acrylamide) hydrogel noted as PAM. This system was prepared by photo-chemical method using Eosin Y dye, as new photosensitizer (Figure 1), tri-ethanolamine (TEOA) as electron donor and 1,6-Hexanedioldiacrylate (HDDA) (1wt %, 4wt %) as crosslinker. The response surface was examined using modde software calculator. This method of optimization consists in determining the factors which influence the swelling of the poly (Acrylamide/HDDA). Interestingly, A minimum of experiences are sufficient to obtain a response surface that covers the entire range studied. Consequently, it will be possible to determine the response values in points where no experiments were carried out.

Keywords: Eosin Y, Photo-polymerization, Composite experimental designs, Swelling.

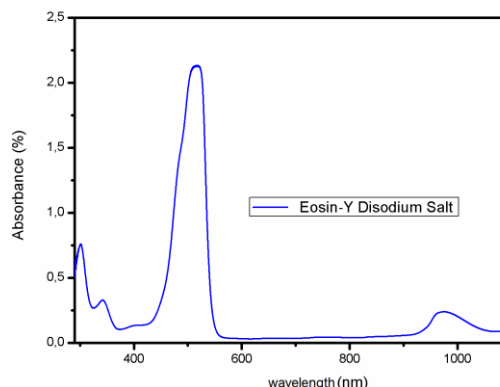


Figure 1: Visible spectrum of Eosin Y Disodium Salt in distilled water, $C_{(\text{Eosin Y})}=1,41 \cdot 10^{-5}$ g/mL, at $T=20^{\circ}\text{C}$.

References:

- Rodrigues IR, Forte MMC, Azambuja DS, Castagno KRL (2007) Synthesis and characterization of hybrid polymeric networks (HPN) based on poly (vinyl alcohol)/chitosan. *React. Funct. Polym.* 67:708–715.
- Hamidi M, Azadi A, Rafiei P (2008) Hydrogel nanoparticles in drug delivery. *Adv. Drug. Del. Rev.* 60:1638–1649.
- Pourjavadia, Mahdavnia GR (2006) Superabsorbency, pH-sensitivity and swelling kinetics of partially hydrolyzed chitosan-g-poly(acrylamide) hydrogels. *Turk J. Chem.* 30:595–608.

Multi-Walled Carbon Nanotubes-incorporated Biopolymers as Extraction Tools for Selected Drugs in Aqueous Matrices

Mohd Marsin Sanagi,^{1,2,*} Wan Nazihah Wan Ibrahim,^{1,3} Nor Suhaila Mohamad Hanapi^{1,3}
Wan Aini Wan Ibrahim¹

¹Department of Chemistry, Faculty of Science, Universiti Teknologi Malaysia, 81310 Johor Bahru, Johor, Malaysia

²Ibnu Sina Institute for Fundamental Science Studies, Universiti Teknologi Malaysia, 81310 Johor Bahru, Johor, Malaysia

³Faculty of Applied Science, Universiti Teknologi MARA, 40450 Shah Alam, Selangor, Malaysia

Abstract: Emergence of unregulated pharmaceutical residues in environmental has attracted current health issues. The chronic exposure to these substances can be a risk to human health. In the lights of these issues, analytical chemists are urged to determine and isolate these drugs from disrupting the ecosystem. Considering that these substances are present at trace concentrations and in complex matrices (ng/L - $\mu\text{g/L}$), highly sensitive and selective analytical methods are needed for sample preconcentration prior to their determination. Aligned with the 'green chemistry' concept, biopolymers has inspired worldwide attention as they offer economical and environmental friendly materials. Their natural parts guarantees biodegradability as well as biocompatibility. Apart from that, biopolymers possess high hydrophilicity and native ligands which offer potential further modifications and excellent adsorption behavior. These prompted the investigation on biopolymer adsorbents of blended agarose/chitosan incorporated with multi-walled carbon nanotubes (Agr-Ch-MWCNT) as extraction tool for the determination non-steroidal anti-inflammatory drugs (NSAIDs) in aqueous matrices. Preparation of adsorbent via homogeneous solution method showed high compatibility and good dispersion of MWCNTs in the agarose/chitosan matrix. FESEM micrograph confirms that MWCNTs were completely adhered onto the agarose/chitosan surface with absence of agglomeration (Mustafa, *et al.*, 2012). Besides, incorporation of MWCNTs increased the surface area of polysaccharides up to $40.25 \text{ m}^2/\text{g}$ compared to pristine biopolymers that offer additional active sites for adsorbent-adsorbate interaction (Crini, 2005). The synthesized biopolymer adsorbent was applied as extraction medium for determination selected NSAIDs (naproxen, diclofenac sodium salt and mefenamic acid) in the environmental water samples. The extraction setup is simple by dipping hypodermic needle pierced through 4 pieces of the Agr-Ch-MWCNT (5 mm diameter), alternately separated by silicon septum in a stirred 10 mL sample solution for analyte adsorption process (Figure 1). The entrapped analyte within the adsorbents was the adsorbed into $100 \mu\text{L}$ of iso-propanol by ultrasonication prior to high performance liquid chromatography (HPLC) analysis. Several important param-

eters, such as addition of salt, sample pH, sample volume, extraction time, desorption solvent, desorption time, conditioning solvent, stirring speed and concentration of MWCNTs in biopolymers matrix were comprehensively optimized. The Agr-Ch-MWCNT demonstrated high affinity for NSAIDs spiked in tap water, well water and river water with excellent relative recoveries (94.3 to 109.7%) and good reproducibility with relative standard deviation (RSD) of $< 5.16\%$.

Keywords: biopolymers blended, incorporation of MWCNTs, NSAIDs, adsorption.

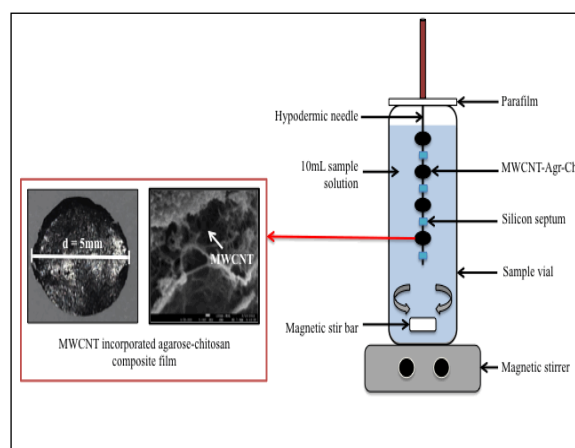


Figure 1: Schematic of -Agarose-chitosan-MWCNT and extraction of drugs form aqueous matrices.

References:

- Crini, G. (2005). Recent Developments in Polysaccharide-Based Materials Used as Adsorbents in Wastewater Treatment. *Prog. Polym. Sci.* 30, 38-70.
- Mustafa, A., Kusworo, T. D., Busairi, A., Ismail, A. F., and Budiyo. (2012). Increasing the Performance of PES-CNTs Mixed Matrix Membrane using Carbon Nanotubes Functionalization. *Int. J. Waste Resources* 2(1), 22-24.

Tailoring the Magnetization Distribution in Ferromagnetic Nanowires and Nanotubes for (Bio) Applications

K. Zuzek Rozman,^{1*} S. Trafela,¹ D. Pecko¹, M.S. Arshad¹, N. Kostevsek¹, S. Sturm¹, S. Kobe¹
¹Jozef Stefan Institute, Department for Nanostructured Materials, Jamova 39, Ljubljana, Slovenia

Abstract: Fe-Pd and Co-Pt nanowires (NW) and nanotubes (NT) with lengths of $\sim 2 \mu\text{m}$ were produced electrochemically in anodized alumina templates having pores diameter of 200 nm. Potential -1.1 V vs Ag/AgCl was used for $\text{Fe}_{50}\text{Pd}_{50}$ NWs and -2.1V, was used to produce $\text{Co}_{65}\text{Pt}_{35}$ NWs and $\text{Co}_{50}\text{Pt}_{50}$ NTs for which polycarbonate templates were used. Texturing of the hcp Co_3Pt phase in the [001] direction and of the fcc CoPt_3 phase in the [111] direction, perpendicular to the long axis of the Co-Pt nanowire axis was observed, that resulted in a very unique periodic magnetization distribution observed with magnetic force microscopy (MFM). The reason for that behavior was in the local magnetic moment deviating away from the nanowire's axis and modulating its orientation within the plane spanned by the nanowire's axis and the c-axis to lower the total energy. The large magnetocrystalline anisotropy HMA of the hcp phase will tend to align the magnetic moments in a plane perpendicular to the nanowire's axis, whereas the shape anisotropy tends to align them parallel to the nanowire's axis. As a result the local magnetic moment deviates from the nanowire's axis and modulates its orientation within the plane spanned by the nanowire's axis and the c-axis to lower the total energy (Figure 1). By using an adopted equation to calculate the period of the stripes or the domain width [1] for the nanowires we estimated a domain width of $W_{\text{cal}} \approx 250 \text{ nm}$ to minimize the total energy, which is in excellent agreement with the present observations. Finite-element calculations have also shown that the transverse magnetization configuration in such a type of domain pattern is the state with the lowest energy.

On the other hand the $\text{Fe}_{50}\text{Pd}_{50}$ NWs were found to possess fcc crystal structure with no preferred crystal orientation that caused the magnetization to be aligned with the long NWs axes as suggested by the shape anisotropy.

Additionally $\text{Co}_{50}\text{Pt}_{50}$ NTs were examined with using MFM, that revealed an even more specific magnetization distribution i.e. a single vortex-type of structure, exerting no stray fields, in the remnant state, despite their elongated shape, which would enable their usage in targeted drug delivery with high drug loads, as was shown for a model drug paracetamol. Examined NWs with parallel and perpendicular magnetization show huge potential to be used in biomed-

ical applications, as they can be easily aligned with the magnetic field to fit the electrodes, or can be used for selective magnetic separation. For that reason we have combined the FePd NWs with Au segments of different lengths, that were additionally functionalized with citric acid (proved by FTIR) to provide -COO- groups for further biological binding.

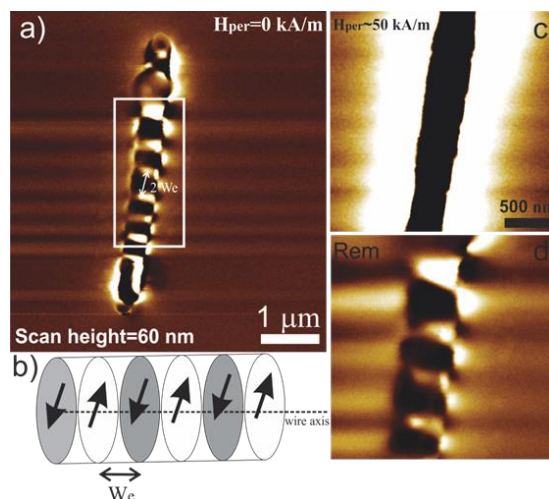


Figure 1: (a) The MFM image of an individual Co-Pt nanowire. (b) Schematic picture of possible magnetization modulation in the nanowire. (c) Saturation magnetization state of an individual Co-Pt nanowire at applied field of $H_{\text{per}} \approx 50 \text{ kA/m}$. (d) Remanent magnetization of an individual Co-Pt nanowire.

Keywords: ferromagnetic nanowires and nanotubes, electroplating, single domain, magnetization modulation, single-vortex, drug delivery

References:

- [1] Lebecki, K. M., Donahue, M. J., Comment on "Frustrated magnetization in Co nanowires: Competition between crystal anisotropy and demagnetization energy", (2010) Phys. Rev. B 82, 096401

Multimodal FePt/SiO₂/Au nanoparticles with a combined magneto-photothermal effect for nanomedical applications

Sašo Šturm,^{1*} Nina Kostevšek,¹ Kristina Žužek Rožman,¹ Spomenka Kobe¹

¹Department for nanostructured materials, Jožef Stefan Institute, Jamova 39, Ljubljana, 100 Slovenia

Abstract: Surgical incisions along with chemotherapy are the doctrine therapies for cancer therapy. Although effective in termination of cancer, these pose a variety of unwanted side effects due to the delocalized performance, raising the desire for less invasive treatments, to avoid damaging interventions to surrounding healthy tissue. Recently emerging treatment routes, referred as smart drug delivery system utilize targeted drug delivery and controlled drug release systems. Using such therapeutic routes, drug doses needed for therapy and toxicity to the surrounding healthy tissues are minimized. Research directions and implementation of targeted drug delivery and controlled release systems based on inorganic nanoparticles (NPs) incline towards utilization of magnetic particles for so-called hyperthermia actions. Drug carrying magnetic particles can be efficiently manipulated by an external magnetic field gradient. Depending on the therapeutic needs, such particles can either be moved through the body or concentrated in target areas. Noble-metal solid spherical NPs, in their turn, are good candidates for the photothermally induced drug release [1,2]. They exhibit enhanced scattering and absorption properties in the visible (VIS) wavelength regime due to the strong resonance upon excitation of free electrons at the particle surface known as the surface plasmon resonance. If such functionalized particle is excited by the same wavelength (using low-energy laser light) as its absorption peak it will dissipate heat leading to the photothermally induced treatment.

Designing a hybrid system, which will be simultaneously active in a magnetic and optical domain will have huge advantage in diagnostics, targeted delivery, drug release, treatment and extraction, which can be easily tailored to the specific needs. In view of this, developed the smart drug delivery systems, which is based on hybrid optically and magnetically active NPs.

In this study we focused on hybrid nanomaterials serving as tools for localized therapy by combining several physic-chemical phenomena in a single nanoparticle. This was realized by combining photothermal and magnetic entities in a FePt/SiO₂/Au hybrid nanoparticles. The magnetic cores of FePt exhibit the superparamagnetic properties, which facilitate guiding and retention of the nanoparticles at the infected site. On the other hand, photo-thermal

response is achieved by forming a thin layer of Au on the surface of the hybrid particles, which mediate strong plasmon induced surface heat flux upon absorption of the near NIR light. Combining both materials in a multifunctional FePt-Au core/shell structures represents a novel approach to combine and upgrade magnetic and optical properties of each single component and permit potential applications as optical agents and magnetic carriers for bio assay.

Keywords: hybrid nanoparticles, FePt, Au nanoshells, photothermal effect, magnetic manipulation

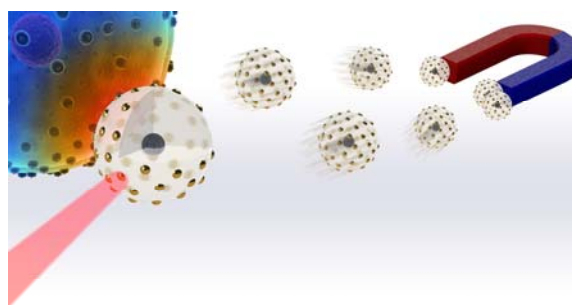


Figure 1: Schematic representation of multimodal hybrid NP functionalities with a combined magneto-photothermal effect for nanomedical applications

References:

- [1] X. Huang, P. K. J., I.H. El-Sayed, M.A. El-Sayed. Plasmonic photothermal therapy (PPTT) using gold nanoparticles. *Lasers Med Sci.* **2008**, 23, 217-228.
- [2] Bañobre-López, M.; Teijeiro, A.; Rivas, J. Magnetic nanoparticle-based hyperthermia for cancer treatment. *Reports of Practical Oncology & Radiotherapy* **2013**, 18, 397-400.

Synthesis and characterization of iron oxide nanoparticles for potential biomedical applications

Maïssa DARDOURI^a, Amel DAKHLAOUI OMRANI^{a,*}

a)Laboratory of Physical Chemistry of Mineral Materials and their Applications, National Center for Research in Material Sciences, CNRSM, Technologic Park of Borj Cedria B.P. 73, 8020 Soliman, Tunisia

*dakhlaoui_amel@yahoo.fr

Abstract: For the past three decades, iron oxide nanoparticles, especially magnetite Fe_3O_4 and maghemite $\gamma\text{Fe}_2\text{O}_3$ nanoparticles, have been established as a promising platform because of their numerous biomedical applications such as, targeted drug delivery, hyperthermia, magnetic scaffolds for bone defect repair, magnetic resonance imaging (MRI) contrast enhancement,...[1-3].

Till now several popular methods have been reported for the synthesis of magnetic iron oxide nanoparticles (MNPs), such as chemical precipitation, sol-gel processes, thermal decomposition, hydrothermal synthesis, emulsion/microemulsion methods, etc....

In the present communication, we focus on the synthesis of iron oxide NPs using the co-precipitation and the hydrothermal approaches. The effect of the alkaline ratio on the size and the morphology of the as-elaborated NPs will be detailed. The X-ray diffraction (XRD) revealed that all the powders correspond to pure magnetite (Fe_3O_4) nanoparticles. The Atomic Force Microscopy (AFM), the Scanning Electron Microscopy (SEM) and the Transmission Electron Microscopy (TEM) of these magnetic nanoparticles present a spherical morphology with a diameter size ranging from 10 to 50 nm depending on the alkaline ratio (Figure1).

Key Words: Magnetic Iron oxide, nanoparticles, magnetite, hydrothermal process, co-precipitation, biomedical application

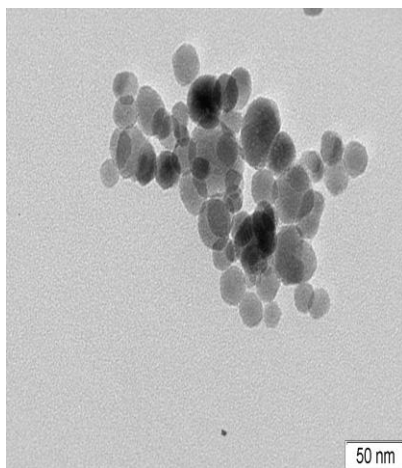


Figure 1: TEM micrographs of iron oxide nanoparticles obtained at an alkaline ratio of 2.75.

References:

- [1] Ch. Chen., X. Jiang., Y. V. Kaneti., A. Yu., *Powder Technology*, 236 (2013), pp. 157–163
- [2] M. Mahdavi., M. Bin Ahmad., M. J. Haron., F. Namvar., B. Nadi., M. Z. AbRahman., J. Amin, *Molecules*, 18 (2013), pp. 7533-7548
- [3] N. Bock., A. Riminucci., C. Dionigi., A. Russo., A. Tampieri., E. Landi., V.A. Goranov., M. Marcacci., V. Dediu., *Acta Biomaterialia* 6 (2010), pp.786–796.

Proteins as an alternative to synthetic surfactants for stabilizing nanoemulsions in the pharmaceutical field.

G. Mekhloufi^{1,2*}, A. Ali^{1,2}, E. Bouyer^{1,2}, M. Chéron³, F. Agnely^{1,2}

¹ Univ Paris-Sud, Faculté de Pharmacie, Châtenay-Malabry, France

² CNRS UMR 8612, Institut Galien Paris-Sud, Châtenay-Malabry, France

³ Pierre et Marie Curie University, Laboratoire Jean Perrin, Paris, France

Abstract: In the pharmaceutical field, emulsions are commonly used for the encapsulation, solubilisation, entrapment, and controlled delivery of active ingredients. Since emulsions are not thermodynamically stable and can phase separate, synthetic surfactants are added to allow the formation and the stabilization of dispersed droplets. However, these emulsifiers may raise toxicity and environment issues. In our group, we aimed to replace synthetic surfactants by “natural” emulsifiers, such as biopolymers, in order to answer the increasing demand of natural and biodegradable products (Bouyer et al., 2012). β -lactoglobulin (β -lg), a whey globular protein, was one of the selected biopolymers for our study to formulate oil-in-water emulsions for pharmaceutical use. We showed that β -lg enabled the formulation of emulsions at protein concentration as low as 0.5 (w/w)% (with a droplet mean diameter of 16 μ m they are macroscopically stable for 20 days). β -lg rapidly adsorbs at the oil–water interface and lowers significantly the interfacial tension. It forms interfacial elastic films that prevent droplet coalescence (Figure 1) (Bouyer et al., 2011). This primary study showed the interest of proteins for the formulation of new pharmaceutical emulsions without synthetic surfactant and thus more respectful towards sustainable development. Recently we aimed to formulate and stabilize oil-in-water nanoemulsions by β -lg. Nanoemulsions are emulsions with very small droplet size (\sim 200 nm). They raise a growing interest in the pharmaceutical field. Nanoemulsions present many advantages compared to conventional emulsions such as kinetic stability, high solubility and bioavailability of active ingredients, and improvement of transdermal drug permeability. Even if food grade nanoemulsions stabilized by proteins have been obtained very recently, to our knowledge, no pharmaceutical nanoemulsions stabilized by proteins are formulated. Indeed, small molecule surfactants are more effective at producing small droplets in nanoemulsions than proteins.

In the first step of the formulation and the stabilization of nanoemulsions by β -lg, the effects of different parameters (process and physicochemical) on the droplets size and the nanoemulsions stability were investigated to determine the optimized conditions for nanoemulsions formulation. The most stable nanoemulsions (over 30 days at least) were obtained

when the less viscous oil (5% oil volume fraction) was dispersed in 1(w/w)% β -Lg solution at a homogenization pressure of 100 MPa, applied for 4 cycles. The nanoemulsions droplet size was about 200 nm with a narrow size distribution. The next step will be to determine the effectiveness of this optimized formulation as a delivery system of a hydrophobic active pharmaceutical ingredient for topical application.

Keywords: Emulsions - Nanoemulsions - Stability - Protein - Interface - High-pressure homogenization

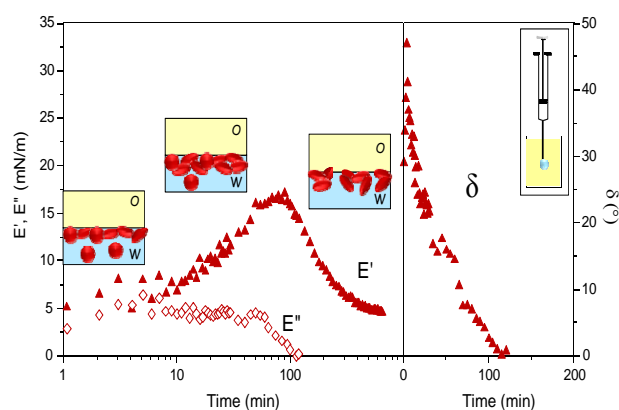


Figure 1: Time evolution of elastic (E') and viscous (E'') interfacial moduli, and phase angle (δ) for the interface sweet almond oil / β -lactoglobulin solution at 2.5 (w/w)% concentration. β -lactoglobulin organization over time at the oil-water interface is depicted.

References:

- Bouyer, E., Mekhloufi, G., Le Potier, I., du Fou de Kerdaniel, T., Grossiord, J.L., Rosilio, V., Agnely, F. (2011). Stabilization mechanism of oil-in-water emulsions by β -lactoglobulin and gum Arabic. *J. Colloid Interface Sci*, 354(2), 467-477
- Bouyer, E., Mekhloufi, G., Rosilio, V., Grossiord, J.L., Agnely, F. (2012). Proteins, polysaccharides, and their complexes used as stabilizers for emulsions: alternatives to synthetic surfactants in pharmaceutical field? *Int. J. Pharm*, 436 (1-2), 359-378.

Fabrication of Silver Nanoparticles using different Egyptian *Lactobacillus* sp. and their antibacterial and antifungal activities

¹Sawsan A. Abdellatif and ²El-Sayed Shabaan

¹Genetic Engineering and Biotechnology Research Institute, City of Scientific Research and Technology Applications, New Borg El-Arab City 21934, Alexandria, Egypt.

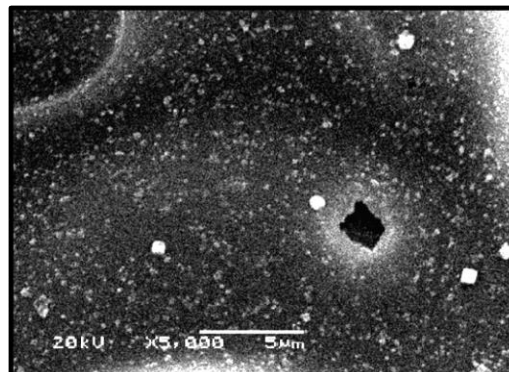
²Plant Protection and Biomolecular Diagnosis Department, Arid Lands Cultivation Research Institute, City of Scientific Research and Technology Applications, New Borg El-Arab City 21934, Alexandria, Egypt.

Abstract: In the present study, an eco-friendly process for the synthesis of nanomaterials using different *Lactobacillus* sp. Isolated from different sources. Supernatant of seed culture was used for the biosynthesis of silver nanoparticles. The aqueous silver ions were reduced to silver metal nanoparticles when treated with the bacterial supernatant. Addition of NaOH at a conc. Of 0.02 mM enhance the reduction vary greatly; silver nanoparticles obtained were in the range of 15–105 nm as obtained from SEM (Fig. 1). The nanoparticles were characterized by UV, FTIR, SEM and XRD. The use of supernatant of the seed media of the said *Lactobacillus* sp., opens up the exciting possibility of rational strategy of biosynthesis of nanomaterials.

Key words: silver Nanoparticles, FTIR, SEM and XRD, biocontrol, bacterial, fungal pathogens.

Silver nanoparticles are an effective antimicrobial agent against various pathogenic microorganisms, and various chemical and biochemical methods are being explored for its production (Naik *et al.*, 2002). Various microbes are known to reduce metal ions to metals (Chen *et al.*, 2003; Ahmad *et al.*, 2003; Sastry *et al.*, 2003). The reduction of silver ions by several *Fusarium oxysporum* strains has been attributed to a nitrate-dependent reductase and a shuttle quinone extracellular process (Duran *et al.*, 2005). Active metal transformation processes require viable microbes which enzymatically catalyze the alteration of the metal. The novelty of the work lies in the fact that we have used the biomass for production of an industrially useful metabolite, compactin. The same seed culture was utilized for Nanoparticles biosynthesis. This approach gave silver nanoparticles as a coproduct that is as useful as the metabolite for which the culture was utilized. It is industrially attractive, feasible and commercially possible.

Figure 1: Figure illustrating synthesis of silver Nanoparticles with different size



References:

- Naik RR, Stringer SJ, Agarwal G, Jones SE, (2002), Stone MO. Biomimetic synthesis and patterning of silver nanoparticles. *Nature Materials*,1, 169–72.
- Chen JC, Lin ZH, Ma XX.(2003), Evidence of the production of silver nanoparticles via pretreatment of *Phoma* sp. 3.2883 with silver nitrate. *Letters in Applied Microbiology*, 37(2),105–8.
- Ahmad A, Mukherjee P, Senapati S, Mandal (2003). Khan MI, Kumar R, et al. Extracellular biosynthesis of silver nanoparticles using the fungus *Fusarium oxysporum*. *Colloids and Surfaces B Biointerfaces*, 28, 313–8.
- Sastry M, Ahmad A, Islam Khan M, Kumar R. (2003). Biosynthesis of metal Nanoparticles using fungi and actinomycetes. *Current Science*. 85(2), 162–70.
- Duran N, Marcato PD, Alves OL, DeSouza GIH, (2005), Esposito E. Mechanistic aspects of biosynthesis of silver nanoparticles by several *Fusarium oxysporum* strains. *Journal of Nanobiotechnology*, 3:8.

CVD growth of single crystalline metal oxide nanomaterials and their application to gas sensing

S. Roso, F. E. Annanouch, E. Llobet

¹Minos-EMaS, Universitat Rovira i Virgili, Tarragona, Spain

Abstract: In the last few years, n-type metal oxide semiconductors (i.e., SnO₂, In₂O₃, ZnO or WO₃) with different morphologies such as nanoparticle films or one-dimensional nanostructures, have been intensively explored as potential building-blocks for gas sensors. The research on one-dimensional (1-D), single crystalline metal oxide nanostructures including nanowires, nanotubes, nanoneedles, nanorods and nanobelts, has been favored in the recent years, since their ultrahigh surface-to-volume ratio, low number of defects and good stability within a wide range of operating temperatures, make them an excellent building-block for micro/nanoscale gas sensors. Yet, the lack of selectivity together with humidity cross-sensitivity still remain the major drawbacks to be overcome. Many works have shown that by adding catalyst nanoparticles onto the metal oxide matrix (i.e., surface functionalization of the low-dimensional metal oxide), the selectivity toward a target gas can be significantly increased. Chemical vapor deposition is a flexible and scalable method for synthesizing nanostructured metal oxides with remarkable gas sensing properties. Here we will report on the use of standard chemical vapor deposition (vapor-liquid-solid growth at high temperatures) and aerosol assisted chemical vapor deposition (vapor-solid growth at moderate temperatures) for growing ZnO, WO₃ and In₂O₃ nanowires. Due to its simplicity, relatively low setup and running costs and its scalability, chemical vapor deposition is an industrially attractive technique. Because it is an atmospheric pressure process the rates of deposition that are typically orders of magnitude higher than those of low pressure processes, which allows for the direct and fast growth of nanomaterials onto a wide spectrum of substrates. The crystalline phase, chemical composition and morphology of the metal oxides grown will be reported based on XRD, XPS, TEM and SEM studies. Finally, the gas sensing properties to different gases such as H₂, NO₂, H₂S, C₆H₆ will be reported at different moisture levels and detection mechanisms will be discussed in detail. Figure 1 shows an example of tungsten oxide nanowires decorated with copper oxide nanoparticles synthesized via an aerosol-assisted CVD process. Figure 2 shows the response of a tungsten oxide nanowire sensor to hydrogen sulphide.

Keywords: vapor-liquid-solid, vapor-solid, metal oxide nanowire, metal and metal oxide nanoparticles, gas sensing

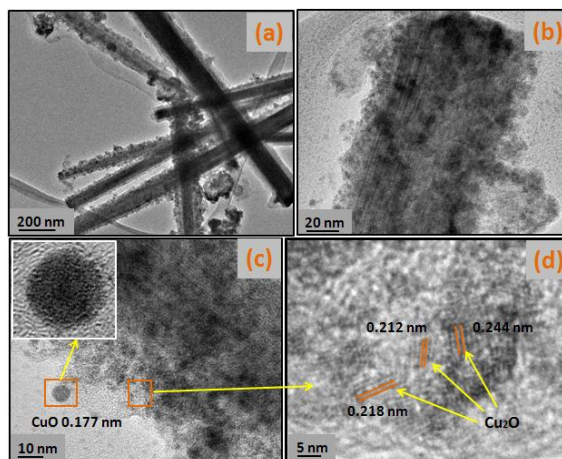


Figure 1: TEM (a & b) and HR-TEM (c & d) images of aerosol-assisted CVD grown copper oxide functionalized tungsten oxide nanowires.

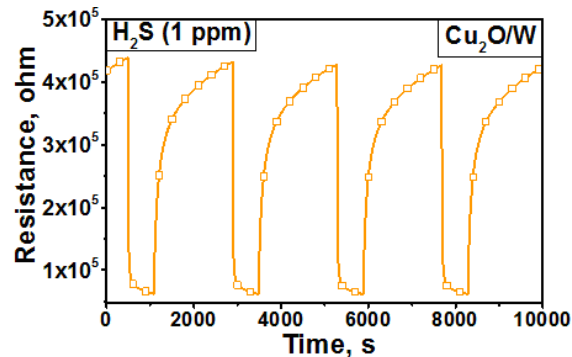


Figure 2: Several response-recovery cycles of a copper-oxide decorated tungsten oxide nanowire sensor to hydrogen sulphide at the operating temperature of 390°C.

References:

F. E. Annanouch, Z. Haddi, S. Vallejos, P. Umek, P. Guttman, C. Bittencourt, E. Llobet (2015), Aerosol assisted CVD grown WO₃ nanoneedles decorated with Cu₂O nanoparticles for the selective and humidity resilient detection of H₂S, Submitted.

The fabricated surface was able to detect betaine, an organic compound found in biological systems (Figure 3). It is worth mentioning that porous alumina substrates without the WO_3 layer do not produce desorption/ionization of analytes.

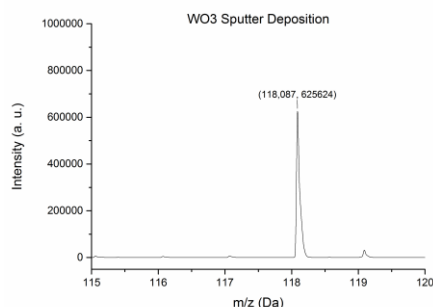


Figure 3: LDI peak spectra for betaine obtained using porous alumina covered by a WO_3 surface.

The desorption and ionization capability of the nanostructured WO_3 obtained has been compared with the standard NIMS substrate using different standard aqueous diluted organic molecules. Figure 4 shows the signal-to-noise ratio comparison where both surfaces are found to be complementary because some of the checked molecules were ionized just in only one of the surfaces.

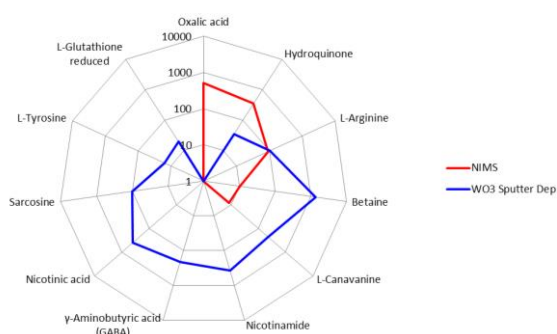


Figure 4: Signal-to-noise ratio comparison for 8 organic standard molecules between porous silicon NIMS (red) and nanostructured WO_3 (blue).

Figure 5 shows the LDI mass spectra obtained for urine analysis using porous silicon substrate (Figure 5 a) and porous alumina covered by WO_3 (Figure 5 b). To identify the molecules from the substrate, its mass spectra is shown in blue and the urine mass spectra in red. The surface spectra for porous silicon is clean from 200 Da onwards, so this surface is ideal for detecting molecules whose molecular weight exceeds this figure. The spectrum of a nanostructured WO_3 surface has an interesting range, from 100 Da to 200 Da, where it is clean. This allows to lower the detectable mass range, which is important because detecting low-mass organic molecules is essential in metabolic disease research. Therefore, WO_3 is a good candidate surface for detecting low mass range molecules in biological samples.

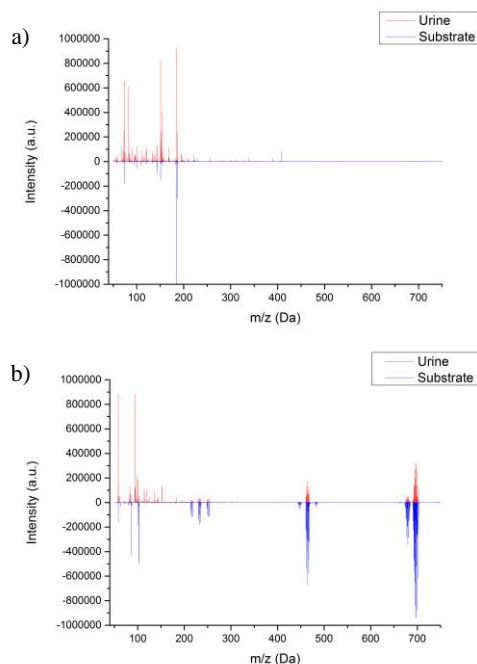


Figure 5: Urine LDI mass spectra obtained using porous silicon (a) and nanostructured WO_3 (b) as substrates. The substrate (blue) and urine spectra (red) have been compared.

Keywords: porous alumina, metabolomics, anodising, tungsten oxide, sputtering.

References:

- Northen T. R, Yanes O, Northen M. T, Marrinucci D, Uritboonthai W, Apon J, Golledge S. L, Anders Nordström A, Siuzdak G. Clathrate nanostructures for mass spectrometry. *Nature Letters* 2007;449:1033-6
- Okuno S, Arakawa R, Okamoto K, Matsui Y, Seki S, Kozawa T, et al. Requirements for laser-induced desorption/ionization on submicrometer structures. *Anal Chem* 2005;77:5364-9.
- Yang X, Hu XK, Loboda AV, Lipson RH. Microstructured tungsten oxide: a generic desorption/ionization substrate for mass spectrometry. *Adv Mater* 2010;22:4520-3.

A Disposable Electrochemical Sensor based on Protein G for High-Density Lipoprotein (HDL) Detection

H. Chammem^{1,2}, L. Mora^{3,4}, I. Hafaiedh^{1,2}, A. Garcia⁵, O. Meilhac⁶, A. Abdelghani^{1*}

¹Carthage University, National Institute of Applied Science and Technology, Centre Urbain Nord, Bp676, 1080 Charguia Cedex, Tunisia.

²Carthage University, Unité de Recherche de Synthèse et Structure de Nanomatériaux (UR11ES30), Faculté des Sciences de Bizerte, Jarzouna, 7021, Tunisia.

³INSERM U1148, LVTS, Institut Galilée, Université Paris 13, Sorbonne Paris Cité, Villetaneuse, France

⁴Université Paris 13, Sorbonne Paris Cité, Laboratoire des Sciences des Procédés et des Matériaux, CNRS (UPR 3407), F-93430 Villetaneuse, France.

⁵Inserm U1188 Diabète athérombose Thérapies Réunion Océan Indien (DÉTROU), Université de La Réunion, CHU –CIC de La Réunion, Saint-Denis, France

*Corresponding author: hanen-chammem@hotmail.fr, Tel: +216 53661068

Abstract: Nowadays, a considerable progress has been achieved in the development of biomarker detection techniques of cardiovascular disease (CVD) which is the leading cause of death due to heart disease and stroke. Indeed, the biosensor technologies is a powerful alternative to conventional techniques, harnessing the specificity and sensitivity of biological systems in small, low cost devices with fast measurements, allowing the health monitoring and are expected to enable proactive personal health management and better treatment of various medical conditions.

In this context, the biosensor system has been applied to the detection of High-density lipoprotein (HDL) and reconstituted HDL (CSL111), which are attractive agents for treating dyslipidemia and atherosclerosis. The main role of these proteins is to increase HDL levels and enhance therapeutic activities associated with HDL, including reverse cholesterol transport (RCT). In this work, we study the electrochemical properties of protein layer grafted on interdigitated electrode for HDL and CSL111 protein detection. We used a method based on oriented antibody Anti-ApoA1 with protein G onto the gold surface [1]. Two immunosensors were developed. The first was tested against HDL antigen and the second against CSL111 antigen in phosphate buffer saline solution.

The molecular structure of two biosensors was characterized by Atomic Force Microscopy (AFM), cyclic voltammetry and impedance spectroscopy. And the detection was controlled by surface Plasmon resonance (SPR) and impedance spectroscopy. The two developed biosensors able to detect the HDL and CSL111 respectively with the

detection limit of 50 ng/mL and 1 ng/mL (Figure 1).

Keywords:

Protein G ,HDL, CSL111, AFM, SPR, , impedance spectroscopy.

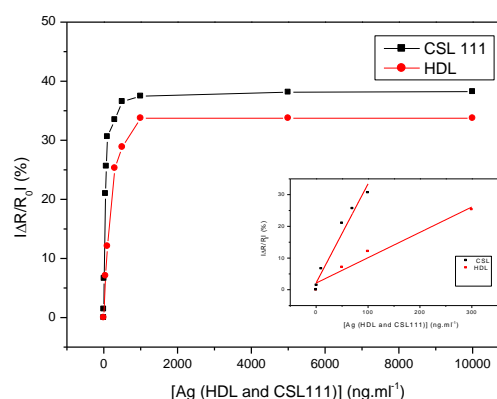


Figure 1: response sensor for HDL and CSL 111 detection.

References:

[1] I. Hafaiedh, H.Chammem, A.Abdelghani, E.Ait, L.Feldman, O.Meilhac, L.Mora, (2013), Supported protein G on gold electrode: Characterization and immunosensor application, Talanta, 116, 84–90.

Development of an impedimetric immunosensor for human serum albumin detection

N.Bohli^{1,2}, H.Chammam^{1,2}, L.Morra³, Olivier Meilhac^{4,5}, A.Abdelghani¹

¹ Carthage university, National Institute of Applied Science and Technology, Centre Urbain Nord, Bp676, 1080 Chargaia Cedex, Tunisia.

² Carthage university, Unité de recherche de Synthèse et Structure de Nanomatériaux UR11ES30, Faculté des Sciences de Bizerte, 7021 Jarzouna, Tunisia.

³Inserm U698, Bio-ingénierie Cardiovasculaire, Institut Galilée, Université Paris13, Sorbonne Paris Cité, F-93430 Villetaneuse, France.

⁴ INSERM UMR 698, F-75018 Paris, France.

⁵AP-HP, Bichat Stroke Center, F-75018 Paris, France.

Abstract: Human serum albumin is the most abundant protein in human blood plasma (Peters, 1995). For type two diabetics, this protein can be altered and advanced glycation end-products may be formed leading to numerous health complications such as vascular system alteration (Kajiyama, 2002). In this work, we report the fabrication and characterization of an impedimetric immunosensor based on a protein layer grafted on interdigitated gold microelectrode for Human Serum Albumin (HSA) detection.

The HSA-antibody immobilization method is based on oriented HSA-antibody with protein G intermediate layer. This method was used rather than the physisorption technique as it leads to improved immunosensor properties (Hafaiedh et al., 2013).

Preliminary experiments were performed in order to optimize the HSA-antibody concentration. The optimal HSA-antibody concentration for the developed immunosensor was determined to be $60 \mu\text{g}\cdot\text{mL}^{-1}$ (Figure 1).

The electrochemical characterization of each immobilized layer was achieved by cyclic voltammetry and electrochemical impedance spectroscopy.

The developed immunosensor was tested against HSA antigen in phosphate buffer saline solution with redox couple. Protein concentrations within the linear range of $100 \text{ ng}\cdot\text{mL}^{-1}$ to $250 \text{ ng}\cdot\text{mL}^{-1}$ were detected (Figure 2).

A detection limit of $100 \text{ ng}\cdot\text{mL}^{-1}$ antigen was observed.

Keywords: Human Serum Albumin, Electrochemical Impedance Spectroscopy (EIS), protein G, impedimetric immunosensor.

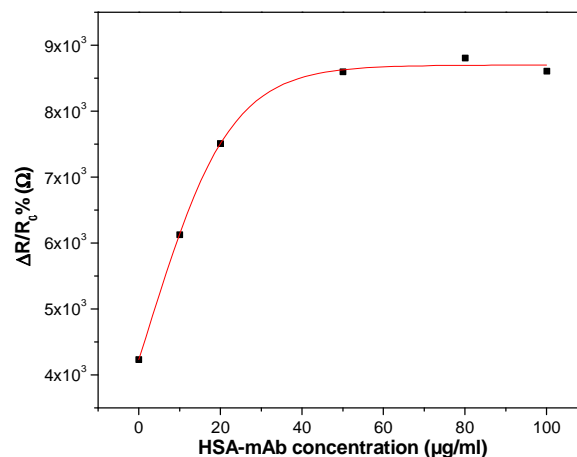


Figure 1: Optimization of the HSA Antibody concentration.

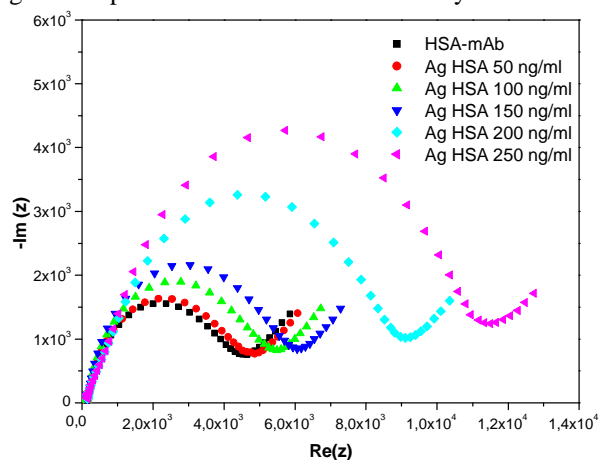


Figure 2: Nyquist impedance plots of modified gold electrode with PG and with HAS-mAb under various concentrations of HSA-antigen.

References:

- Peters, J.T. (1995), All About Albumin: *Biochemistry, Genetics, and Medical Applications*, Academic Press, San Diego, p. 1.
- Kajiyama, Y. (2002), Human albumin and AFP detection by ELISA in cultured cells Hu7 cells grown in 5% FCS. *Mol Cell Biol*, 2, 6122-30.
- Hafaiedh, I. Chammem, H. Abdelghani, A. Ait, E. Feldman, L. Meilhac, O. Mora, L. (2013), Supported protein G on gold electrode: Characterization and immunosensor application, *Talanta*, 116, 84–90.

Gas sensors based on WO₃ nanoneedles decorated with Pt and Au nanoparticles

A. Thamri¹, H. Baccar^{1,*}, E. Llobet², A. Abdelghani¹

¹Carthage University, Nanotechnology Laboratory, INSAT, Tunis, Tunisia

²MINOS-EMaS, Universitat Rovira i Virgili, Avda. Països Catalans, 26, 43007 Tarragona, Spain

Corresponding authors: hamdibaccar@yahoo.fr

Abstract: Scientific research is looking forward new materials that exhibit excellent performances together with high selectivity, rapidity and stability. Several techniques were used to improve the performances of tungsten oxide nanostructure [1]. Among these techniques, there is the technical of Aerosol Assisted by CVD (AACVD). This method is flexible, low cost and high performance for growing both polycrystalline or monocrystalline metal oxides and have a good properties for gas and vapors detection [2].

In this approach, we developed two sensors based on tungsten oxide (WO₃) nanoneedles decorated with Pt and Au nanoparticles deposited by aerosol assisted chemical vapor method for gases and vapors detection. The two decorated metal nanoparticles (Pt/WO₃ and Au/WO₃) film behave as n-type semiconductors. Various gases (NO₂ and H₂S) and vapors (ethanol, methanol, acetone, toluene and benzene) were used for detection. The morphology of the nanostructures was investigated by Scanning Electron Microscopy (SEM) and by Transmission Electron Microscopy (TEM). Impedance spectroscopy was used for vapors and gases sensors calibration.

The results shows that both sensors present a good sensitivity for gases. The sensor modified with Au/WO₃ present a better response for NO₂ than the sensors with Pt/WO₃. For vapors detection, the two sensors show better sensitivity to organic vapors than to the aromatic vapors. All detection were carried at moderate operating temperatures 250°C and 300°C respectively for Au/WO₃ and Pt/WO₃ [3].

Keywords: Nanoneedles, Aerosol Assisted Chemical Vapor Deposition (AACVD), Au decorated WO₃, Pt decorated WO₃, Gas detection, Vapor detection.

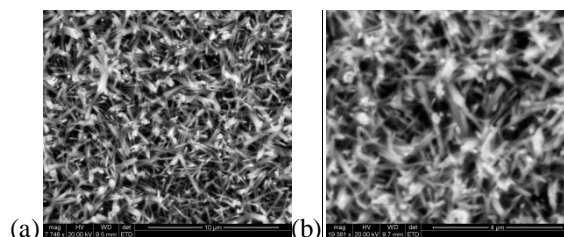


Figure 1: SEM image of WO₃ nanoneedles decorated with metal nanoparticles (a) Pt/WO₃, (b) Au/WO₃.

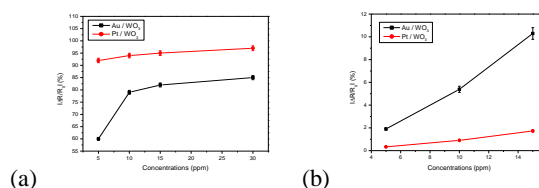


Figure 2: Calibration curves of sensors Au/WO₃ and Pt/WO₃ (a) for H₂S detection, (b) for NO₂ detection.

References:

- [1] Meng, D., Shaalan, N.M., Yamazaki, T. and Kikuta, T., *Sens. Actuator B-Chem.* 2012, 169, 113-117.
- [2] F.E. Annanouch, S. Vallejos, T. Stoycheva, C. Blackman, E. Llobet, (2013), Aerosol assisted chemical vapour deposition of gas-sensitive nanomaterials *Thin Solid Films*, pp. 703–70.
- [3] S. Vallejos, P. Umek, T. Stoycheva, F. Annanouch, E. Llobet, X. Correig, P. De Marco, C. Bittencourt, C. Blackman, (2013), Single-Step Deposition of Au- and Pt-Nanoparticle- Functionalized Tungsten Oxide Nanoneedles Synthesized Via Aerosol-Assisted CVD, and Used for Fabrication of Selective Gas Microsensor Arrays, *Funct. Mater.* 23 (2013), pp. 1313–1322.

Ecotoxic evaluation of cobalt and titanium silicon oxide nanomaterials in terrestrial ecosystem

^{1,2,*}S.Bouguerra, ^{2,3}A.Gavina, ¹M. Ksibi, ⁴M.G. Rasteiro, ⁵T. Rocha-Santos, ^{2,3}R. Pereira.

¹Laboratory of Water, Energy and Environment (3E), Engineering School of Sfax, University of Sfax, B.p.w.3038, Sfax-Tunisia;

²Department of Biology, Faculty of Sciences of the University of Porto, Rua do Campo Alegre, s/n, 4169-007, Porto, Portugal;

³CIIMAR - Interdisciplinary Centre of Marine and Environmental Research, Rua dos Bragas, n.289, 4050-123, Porto, Portugal;

⁴Department of Chemical Engineering & CIEPQPF & University of Coimbra, 3030-290 Coimbra, Portugal;

⁵ISEIT/Viseu, Instituto Piaget, Estrada do Alto do Gaio, Galifonge, 3515-776 Lordosa, Viseu, Portugal.

*E-mail contact:sirine.bouguerra@yahoo.fr

Abstract : In the last decade, metallic nanomaterials (NMs) display outstanding properties in different fields like chemistry, optics, magnetism, electricity which in turn have produced current exploitation and applications in catalysis, electronics, coatings and biomedical. For example, magnetic NMs like cobalt have shown big interest and important roles in the areas of medicine, biotechnology, drug delivery, cancer treatment and medical imaging. Nano Cobalt oxide (nano-Co₃O₄) are also attracting enormous interest owing to their unique size-and shape-dependent properties and potential applications in, for example, pigments, catalysis, sensors, electrochemistry, magnetism, energy storage, etc. While titanium silicon oxide (nano-TiSiO₄), are widely used in the ceramic, cosmetics, pharmaceutical, and paint industries as a coloring material because of its high stability, anticorrosion and photocatalytic properties. Considering the increased production and applications of inorganic NMs, assessing their safety has become a worldwide issue. Nevertheless, there is a few data and experience on environmental hazard evaluation of nano-Co₃O₄ and nano-TiSiO₄. Further, the hazard assessment for the soil ecosystem stills lacking. For this purpose, a battery of sub-lethal ecotoxicological tests was performed to assess the influence of both NMs on soil avoidance and reproduction of invertebrates *Eisenia andrei* and *Folsomia candida*, using the standard artificial soil OECD (5% of organic matter), spiked with aqueous suspensions of both NMs. Soil enzymes activity, potential nitrification, N-mineralization and basal respiration were also evaluated. For this purpose replicates composed by a natural soil spiked with a range of concentrations of aqueous suspensions of NMs (87.8 – 1000 mg kg⁻¹soil_{dw} by a factor of 1.5), were incubated for 30 days. The aqueous suspensions of NMs were characterized by Dynamic Light Scattering (DLS). The results showed significant avoidance ($p \leq 0.05$) of *Eisenia andrei* earthworms at concentration up to

1000 mg kg⁻¹ soil_{dw} of nano-Co₃O₄ and nano-TiSiO₄, while a significant ecotoxicological effects on springtails *Folsomia candida* ($F = 8.043$, $d.f_1 = 20$, $d.f_2 = 26$, $p = 0$) reproduction were recorded for all tested concentration (figure 1). In opposition no effects on invertebrates occurred within the range of concentrations of 100 – 1000 mg nano-TiSiO₄ Kg⁻¹soil_{dw} for long term exposures. In terms of soil microbial activity a significant inhibitory effect was recorded only for N-mineralization at the lowest concentration of nano-TiSiO₄. In opposition, high concentrations of these NMs stimulated the activity of some soil enzymes. In general, soil basal respiration was significantly stimulated at highest concentration of nano-Co₃O₄.

Keywords: *Eisenia andrei*, *Folsomia candida*, soil enzymes activity, potential nitrification, N-mineralization, soil basal respiration.

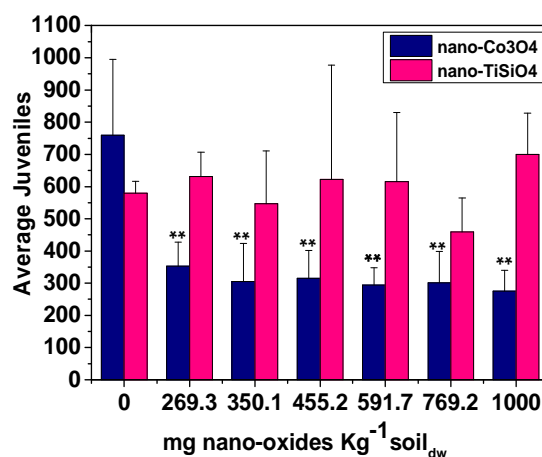


Figure 1: Reproductive output of *Folsomia candida* exposed to the OECD soil spiked with different concentrations of mg nano-Co₃O₄ Kg⁻¹soil_{dw} and mg nano-TiSiO₄ Kg⁻¹soil_{dw}; (** $p \leq 0.01$).

Analytical Efficient Model of the Tunneling Current in Ambipolar Schottky Barrier Carbon nanotube Field Effect Transistor

W. Ben Ayed¹, M. Najari^{1,2}, , H. Samet¹

¹ University of Sfax, Laboratory of Electronics and Information Technology LETI, Sfax, Tunisia

² University of Gabes, Faculty of Sciences of Gabes, Department of Physics, Gabes, Tunisia

Abstract: Carbon nanotubes are becoming more and more popular thanks to their mechanical and electrical properties. Recently, the conventional carbon nanotube transistor (C- CNTFETs) modeling is widely studied. However, the literature describing the model of Schottky barrier carbon nanotube transistor (SB-CNTFET) is limited. Since no analytical solution is carried out for the tunneling current in SB-CNTFET with ambipolar character, a new approach is proposed to find an analytical approximation of the tunneling current. The ambipolar behavior is treated. The proposed compact analytical model for SB-CNTFET can be implemented with a hardware description language (HDL). The simulation results, obtained using this model, are in close agreement with numerical calculation results.

Keywords: SB-CNTFET, ambipolar behavior, compact model

1. INTRODUCTION

Thanks to their excellent electrical, optical and mechanical properties, a lot of research studies have focused on the carbon nanotubes (CNTs) as candidates to overcome the present challenges related to the physical technology limits of silicon MOSFET (Appenzeller *et al.*, 2002).

Semiconducting carbon nanotube can be used as the channel in Carbon Nanotube Field Effect Transistor (CNTFET). The Schottky barrier source and drain contact between metal and CNT are always present in the fabricated devices, the tunneling current is the dominant mechanism across the contacts. If we neglect the SB effect, this overestimates the drain current. Moreover, the ambipolar behavior of Schottky barrier CNTFETs limits the performance of these devices in both 'On' and 'Off' regimes (Pourfath *et al.*, 2004) and consequently the ION/IOFF ratio is limited.

These limitations result from the decrease of the On current caused by barrier height between metal and CNT. However, the increase of the off current is due to the ambipolar characteristics resulting from the parasitic hole current injection at the drain contact through the valence band for n-type devices, or, from the parasitic electron current at the drain contact through the conduction band for p-type devices.

Two types of current tunneling or thermionic current can be present in SB-CNTFET. Carriers with energies above the Schottky barrier height reach the channel by thermionic emission. On the contrary, carriers with energies below the Schottky barrier height reach the channel by tunneling emission featuring a transmission function

Some research works have been carried out to obtain a numerical (Jiménez *et al.*, 2007) (Guo *et al.*, 2004), and analytical model in order to calculate the tunneling current in SB-CNTFET (Najari *et al.*, 2009 2010).

The main issue of this paper is to provide an accurate analytical model for the tunneling current of the n- type SB-CNTFET with ambipolar characteristics. The proposed model will be compared with numerical simulation results. A close agreement is obtained.

This paper is organized as follows: Section 2 describes the physical equations of the tunneling current through the Schottky barrier CNTFET and poses the mathematical problems. Section 3 gives an analytical solution for the tunneling electron current in SB-CNTFET. The obtained solution is validated by a comparison with numerical calculation. Section 4 presents an analytical model for the tunneling holes current in SB-CNTFET. This model is also validated by a comparison with numerical results. Section 5 presents the total tunneling current in SB-CNTFET; the agreement between the numerical calculation and the proposed model is satisfactory.

2. TUNNELING CURRENT IN THE SB-CNTFET

Assuming the ballistic transport, the ambipolar tunneling drain current is given by Landauer-Büttiker formula. It is composed of both carriers' electrons and holes, the electrons are transported from source to drain contact through conduction band. Whereas, the holes are transported from drain to source contact through the valence band as shown in figure 1.

$$I_{DS} = \frac{2e}{h} M \int_0^{\infty} [f_S(E) - (1 - f_D(E))] T_T(E) dE \quad (1)$$

Where f_S, f_D are Fermi Dirac distributions at the source and drain contacts respectively, and T_T is the total transmission function.

$$f_S = \frac{1}{1 + \exp\left(\frac{E - qV_{CNT}}{k_B T}\right)} \quad (2)$$

$$f_D = \frac{1}{1 + \exp\left(\frac{E - q(V_{CNT} + V_{DS})}{k_B T}\right)} \quad (3)$$

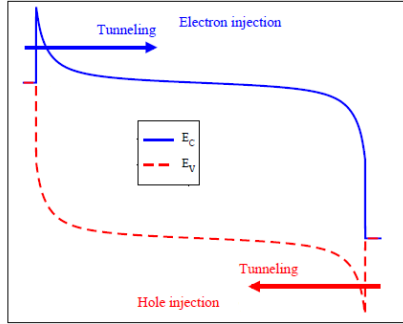


Figure.1 Band energy profile for ambipolar SB-CNTFET

There are two interfaces Schottky barrier contacts source/CNT interface and CNT /drain interface. The total transmission function $T_T(E)$ is expressed using the transmission function of source $T_S(E)$ and drain $T_D(E)$. By using the Wentzel- Kramers- Brillouin (WKB) approximation (Messiah, 1991) and assuming a triangular potential profile: $T_S(E)$ and $T_D(E)$ can be depicted as follows:

$$T_S(E) = \exp(-A(\Phi_{SB} - E - qV_S)^{3/2}) \quad (4)$$

$$T_D(E) = \exp(-A(\Phi_{SB} - E - qV_{DS})^3) \quad (5)$$

Where

$$A = 4 \frac{\sqrt{2m^*}}{3\hbar q E_{elec}} \quad (6)$$

m^* is the carrier effective mass, Φ_{SB} is the SB height, E_{elec} is the electrical field $E_{elec} = \frac{V_{cnt}}{\lambda}$, λ is the screening length, $\lambda = 3\text{nm}$ and \hbar is the Planck constant. Like in Fabry-Perot cavity, the total transmission function $T_T(E)$ over the whole structure is predicted to be (Datta, 1997):

$$T_T = \frac{T_S(E).T_D(E)}{T_S(E)+T_D(E)-T_S(E).T_D(E)} \quad (7)$$

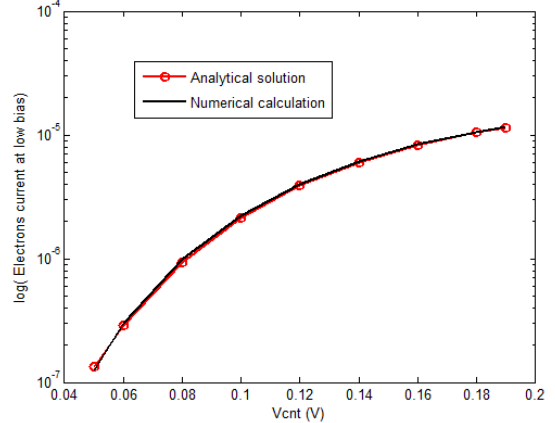
The total tunneling current given in equation (8) cannot be directly calculated since it has no analytical solution. So, it cannot be implemented in compact model.

3. ANALYTICAL SOLUTION OF ELECTRONS CONTRIBUTION

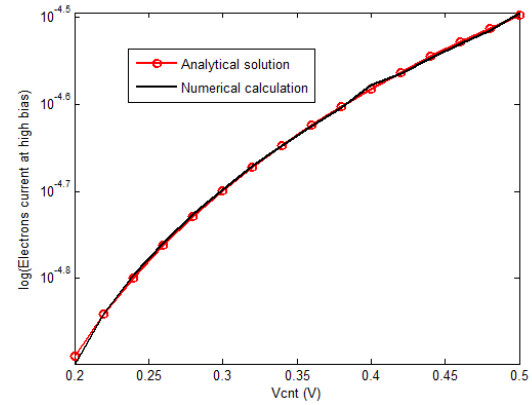
To overcome the complexity of implementing the tunneling current in equation (8) in compact model, an approximation method has to be used to extract an analytical solution.

Partial solutions have to be considered depending on the relative variation of the Fermi-Dirac distribution and the total transmission function.

Hence, the electrons and holes contribution are calculated by means of partial solutions over a large variation of the gate potential and for low, middle and high carrier energies. Figure 2 and figure 3 shows a comparison between these analytical solutions and the numerical calculation for the electrons current and the holes current respectively. A very good agreement is shown in both cases. The mean absolute percentage (MAP) error is equal to 0.05% and 3.46% for the electrons current and the holes current respectively.

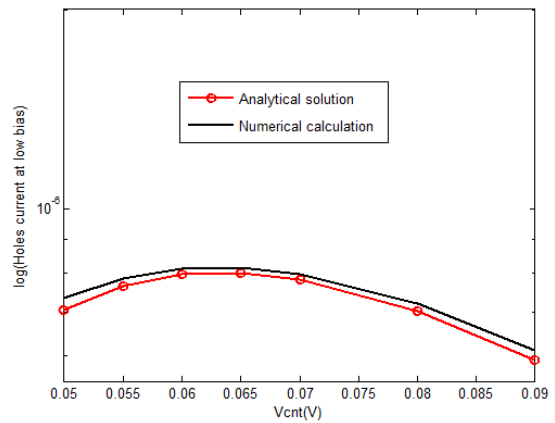


(a)



(b)

Figure 2. Comparison between numerical (solid line with circle) and analytical solutions (solid black line) for electrons contribution at low (a) and high (b) gate biases.



(a)

$$I_{DS} = \frac{4e}{h} \sum_{p=1}^{nb} \left[\int_{\Phi_{SB-V_{cnt-sbbd}}^{\Phi_{SB-qV_D}}} T_T(E) \cdot f_S(E) dE - \int_{\Phi_{SB-V_{cnt-sbbd}}^{\Phi_{SB-qV_D}}} T_T(E) \cdot (1 - f_D(E)) dE \right] \quad (8)$$

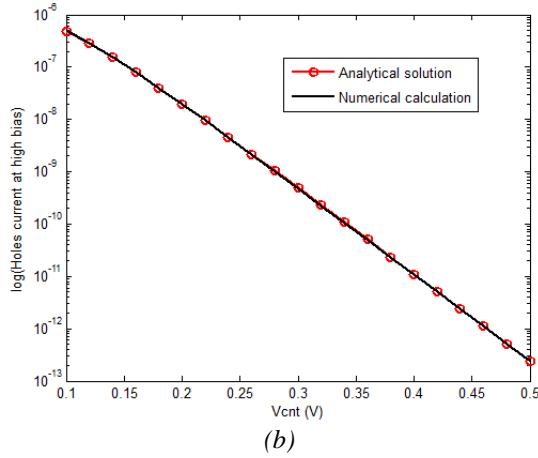


Figure 2. Comparison between numerical (solid line with circle) and analytical solutions (solid black line) for holes contribution at low (a) and high (b) gate biases.

4. TOTAL ANALYTICAL SOLUTION

Two smoothing functions F_{SMO_e} and F_{SMO_h} are used to obtain a complete analytical solution. These functions are introduced here to ensure both the accuracy and the numerical convergence of the model, which is a very common technique in compact modeling.

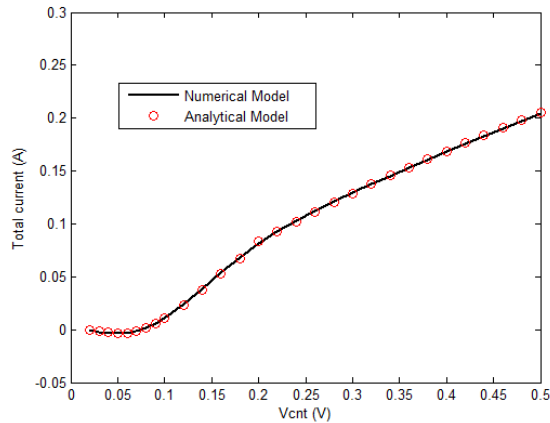


Figure 3. Comparison of numerical and analytical solutions for the total tunneling current in linear scale. The analytical solution (solid line with circle) agrees with the numerically calculated total tunneling current (solid line).

$$I_e = I_{L_e} * f_{SMO_e} + I_{H_e} (1 - f_{SMO_e}) \quad (9)$$

$$I_h = I_{L_h} * f_{SMO_h} + I_{H_h} (1 - f_{SMO_h}) \quad (10)$$

$$I_{analytical} = I_e - I_h \quad (11)$$

5. CONCLUSION

In this paper, an analytical model of tunneling current for ambipolar Schottky barrier CNTFET has been developed based on the approximation of the transmission function and the Fermi Dirac distribution of the electrons and holes in different gate bias.

To ensure the proposed analytical model accuracy, a comparison with the numerical calculation has been performed. A close agreement is obtained. Our proposed model presents the error in the total tunneling current less than 0.25%.

REFERENCES

- J.Appenzeller and al. "Carbon Nanotube Electronics" *IEEE Transaction On Nanotechnology*, Vol. 1, No. 4, December 2002
- M. Pourfath, E. Ungersboeck, A. Gehring, B.H. Cheongy, W. Park, H. Kosina, and S. Selberherr "Improving the Ambipolar Behavior of Schottky Barrier Carbon Nanotube Field Effect Transistors." *Solid-State Device Research conference*, 2004.
- D. Jiménez, X. Cartoixà, E. Miranda, J. Suñé, F. A. Chaves and S. Roche "A simple drain current model for Schottky-barrier carbon nanotube field effect transistors" *IOP science Nanotechnology*, Issue. 41, 2007
- J. Guo, S. Datta and M. Lundstrom "A numerical study of scaling issues for Schottky-barrier carbon nanotube transistors" *Electron Devices, IEEE Transactions on* Vol. 51, Issue. 2, 2004
- M. Najari, S. Frégonèse, C. Maneux, H. Mnif, T. Zimmer and N. Masmoudi "Efficient physics-based compact model for the Schottky barrier carbon nanotube FET" *solid state physics*, Vol.7, Issue. 11–12, 2010
- M. Najari, S. Frégonèse, C. Maneux, T. Zimmer, H. Mnif, and N. Masmoudi "Analytical modeling of the tunneling current in Schottky barrier carbon nanotube field effect transistor using the Verilog-A language" *Systems, Signals and Devices*, 2009.
- A. Messiah, *Quantenmechanik 1* DeGruyter 1991
- S. Datta "Electronic Transport in Mesoscopic systems" Cambridge University Press-1997

Flame retardant nanocomposite materials utilizing intumescent system and nano clay

J.-W. Park¹, H. Kim¹, J.-H. Lee¹, H.-J. Kim^{1†}, M.-J. Kwon² and J.-Y. Choi²

¹ Seoul National University, Laboratory of Adhesion & Bio-Composites, Program in Environmental Materials Science, Seoul, Republic of Korea

²Korea Environment Merchandise Testing Institute, Republic of Korea

Abstract: Fire is not only casualties but a social problem that to pay the enormous social cost. These fire problems are magnified larger by the combustion of the polymeric material, in order to solve these problems, various forms of flame retardent system have been proposed. In general, the most efficient flame retardant materials is halogen-based material, its use is limited by toxic substances occurs after combustion. Intumescent systems is a manufacturing technology of a composite material utilizing carbide and foaming system as a basic mechanism. By utilizing these intumescent system, when producing the flame-retardant material, it is possible to expect the higher flame retardant effect. However, the case of a simple intumescent system, some problems occurred such as durability because it will be form structure as open-cell. To overcome these drawbacks, it is to configure a hybrid composite material that utilizing the nano filler. By applying the clay that has excellent aspectratio among different nanofillers, induce carbonized layer formationed at surface, which was to produce high performance flame-retardant layer. In particular, formation of carbide layer that is formed by application of the clay are analyzed.

Keywords: flame retardant, composites, intumescent system, nano clay.

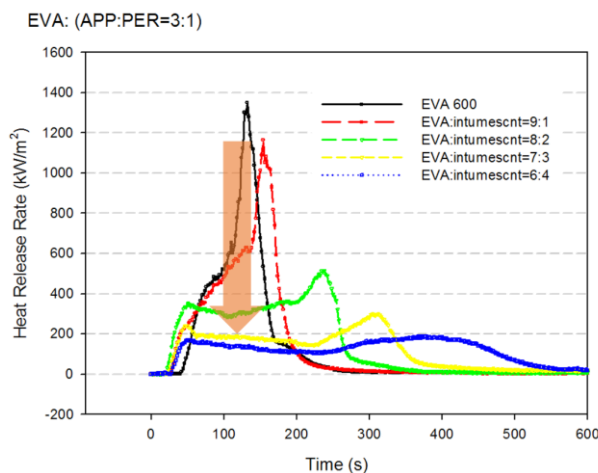


Figure 1: Effect of intumescent system on composites. When increased intumescent agent, maximum heat release rate is dramatically decreased. Reduce ratio is almost 80%, that is significantly result of flame retardant system.

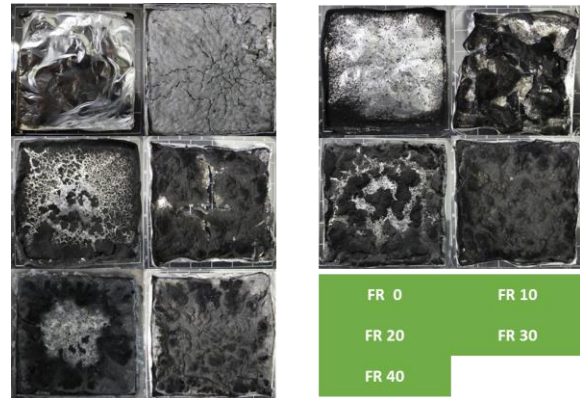


Figure 2: Comparison of clay effect on combustion ash. Left: non clay, Right : clay 5phr. Clay that dispersed composites can be form carbide layer on surface. Role of the layer is high efficiency heat insulator.

References:

- Beyer G. (2002) Nanocomposites: a new class of flame retardants for polymers. *Plast Addit Compd*
- Landrock AH. (1983) Handbook of plastics flammability and combustion toxicology. Park Ridge, NJ: Noyes Publications
- Lu SY, (2002) Hamerton I. Recent developments in the chemistry of halogen-free flame retardant polymers. *Prog Polym Sci*
- Irvine DJ, McCluskey JA, (2000) Robinson IM. Fire hazards and some common polymers. *Polym Degrad Stabil 2*
- Lomakin SM, Haslam E. (1999) Ecological aspects of polymer flame retardancy (new concepts in polymer science). Leiden, The Netherlands: Brill Academic Publishers

Magnetically Responsive Biological Waste Materials for Environmental Technology

I. Safarik,^{1,2,*} E. Baldikova,¹ Z. Maderova,¹ K. Pospiskova,² M. Safarikova,¹

¹Institute of Nanobiology and Structural Biology, Department of Nanobiotechnology, Ceske Budejovice, Czech Republic

²Palacky University, Regional Centre of Advanced Technologies and Materials, Olomouc, Czech Republic

Abstract: Food, agriculture and wood industries are responsible for the production of huge amounts of biological waste materials. In many cases, these materials can be used as efficient biosorbents for the removal of various organic and inorganic xenobiotics and radionuclides or as low-cost carriers for the immobilization of various biologically active compounds or affinity ligands. In order to improve manipulation with such non-magnetic materials, conversion into their magnetic derivatives can be very useful.

There are several possibilities for magnetic modification of non-magnetic materials. In most cases the magnetization procedure is based on the incorporation of magnetic iron oxide nano- or microparticles into the structure or on the surface of modified materials. Typical magnetization procedures (microwave-assisted procedures, mechanochemistry, application of water-based magnetic fluids etc.) will be presented during the talk, together with typical examples of successful applications of magnetically modified biological wastes in environmental technology (e.g., removal of dyes, heavy metal ions, and radionuclides) (Safarik et al., 2011).

Keywords: magnetic modification, magnetic adsorbents, xenobiotics removal

References:

Safarik, I., Horska, K., Safarikova, M. (2011), Magnetically responsive biocomposites for inorganic and organic xenobiotics removal. In: *Microbial Biosorption of Metals* (Kotrba, P., Mackova, M., Macek, T., Editors), Springer, pp. 301-320.

Safarik, I., Pospiskova, K., Horska, K., Safarikova, M. (2012), Potential of magnetically responsive (nano)biocomposites, *Soft Matter*, 8, 5407-5413.

Safarik, I., Horska, K., Pospiskova, K., Maderova, Z., Safarikova, M. (2013), Microwave assisted synthesis of magnetically responsive composite materials, *IEEE Trans. Magn.*, 49, 213-218.



Figure 1: Appearance of original sawdust suspension (left), suspension of sawdust after magnetic modification (middle) and demonstration of magnetic separation of magnetically modified sawdust (right) (Safarik et al., 2013).

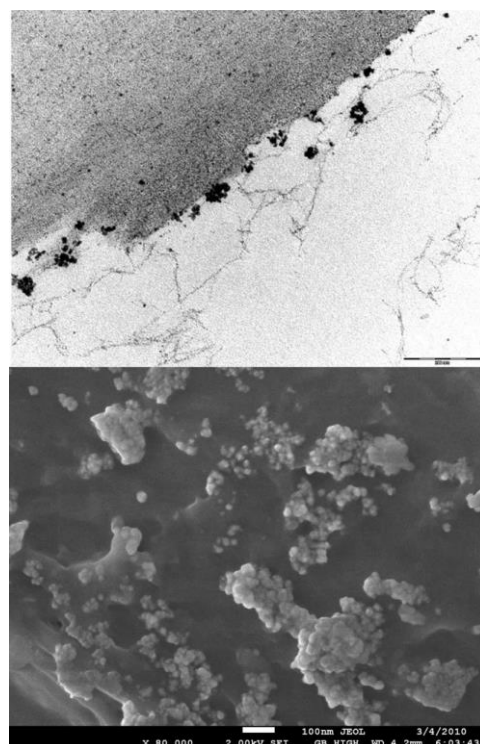


Figure 2: Top - Ultrathin section of magnetic sawdust particle observed in TEM (bar = 200 nm). Bottom - SEM image of ferrofluid modified peanut husk particle (bar = 100 nm) (Safarik et al., 2012).

Increment of Solar Cell Efficiency by Selected Anti-Reflection Coating

Khalid Omar^{1*}, Khalidun A. Salaman², Z. Hassan³

¹National Chair of Material Science and Metallurgy, University of Nizwa, 616 Nizwa, Oman

²Al-Nahrin Nanorenewable Energy Research Center, Solar Cell Research Department, Al-Nahrin University, Baghdad, Iraq

³School of Physics, University of Science Malaysia, 11800 Penang, Malaysia

*Corresponding author email: khalidomar@unizwa.edu.om

Increasing the conversion efficiency of the solar cell device with low cost, the formation and characterization of the porous silicon layers on n-type Si with (100) orientation was using simple photoelectrochemical etching technique. The fabrication of the PS layers was carried out at the etching time of 20 min and by fixing the concentration of the electrolyte solution of HF/ethanol at a ratio of 1:4 by volume and current density of 60 mA/cm². The n-PS (100) sample with the optimal etching time at 20 min was selected to be used as an anti-reflection coating layer on solar cell device. It was used with the ZnO film deposited by radio frequency (RF) sputtering system. The surface morphology was characterized using scanning electron microscopy (SEM), and the findings revealed that nanopores with average pore diameter of 5.73 nm were produced on the n-PS (100) layer (Figure 1).

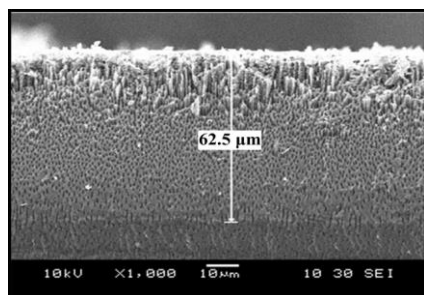


Figure 1: SEM cross-section of the n-PS (100) layer at 20 min etching time.

The ZnO/n-PS (100) layers were characterized using SEM, which revealed that the ZnO film deposited along the walls partially covered the tiny pores of the n-PS (100) layer during the RF sputtering process. The PL emission peaks indicated the nanocrystalline characteristic of the n-PS (100) layer and the ZnO film. Raman measurements of the ZnO/n-PS (100) layers are excellent ARC that exhibit exceptional light trapping at wavelengths ranging from 400 to 1000 nm, leading to the production of a solar cell device with high efficiency of 18.15 %. The efficiency of a solar cell device compared with other energy conversion devices. The efficiency of the solar cell device refers to the fraction of the incident light energy converted to electrical energy.

ZnO has a wide direct energy band gap (3.37 eV), a high exciton binding energy (60 meV) at room temperature, and a hexagonal crystal structure. ZnO thin film as a front contact or solar cells has been fabricated in commercial products. More recently, ZnO has become one of the preferred materials for use as ARC for solar cells because it has good transparency and appropriate refractive index.

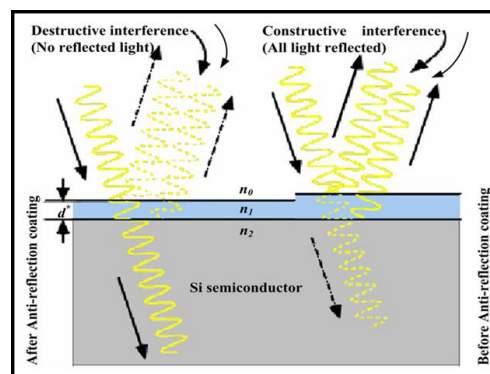


Figure 2: Reflection and transmission of light for the Si solar cell.

The photovoltaic (PV) effect indicates the generation of a potential difference at the junction of two different semiconductor materials in response to visible radiation and other types of radiation (Figure 2).

The conversion efficiency (η) of the solar cell is the ratio of the maximum power P_m to the incident solar power P_{in}

$$\eta = \frac{I_{sc} V_{oc} FF}{P_{in}}$$

Keywords: solar cell, anti-reflection coating, SEM, AFM, efficiency.

References:

- Kasap, S.O. Capper, P. (2006) Springer handbook of electronic and photonic materials, Springer.
- Yen, T. (2010) Zinc oxide thin film deposition, characterization, and its applications, Ph.D thesis in, State University of New York at Buffalo, New York.
- Ye, Z.Z. Lu, J.G. Zhang, Y.Z. Zeng, Y.J. Chen, L.L. Zhuge, F. Yuan, G.D. He, H.P. Zhu, L.P. Huang, J.Y. Zhao, B.H. (2007) ZnO light-emitting diodes fabricated on Si substrates with homobuffer layers, Applied Physics Letters, 91, 113503-113505.

Photoelectrochemical Water Splitting on Tungsten Oxide Nanorod Arrays *via* Anodizing Al/W Metal Layers

M. Bendova,^{1,2,*} A. W. Hassel,² A. Mozalev³

¹Centre of Sensor, Information and Communication Systems, Faculty of Electrical Engineering and Communication, Brno University of Technology, Brno, Czech Republic

²Christian Doppler Laboratory for Combinatorial Oxide Chemistry at the Institute for Chemical Technology of Inorganic Materials, Johannes Kepler University Linz, Linz, Austria

³Central European Institute of Technology (CEITEC), Brno University of Technology, Brno, Czech Republic

Abstract: Hydrogen can be used as a non-toxic energy storage and transport medium. Hydrogen that is made from water by electrolysis using solar energy is a sustainable and renewable home energy supply. In this work, we have synthesized a novel type of nanostructured metal-oxide semiconductor photoanode *via* electrochemically anodizing Al/W metal layers sputter-deposited onto a Si wafer and assessed its applicability for water oxidation reactions in acidic aqueous conditions.

The initial samples were Al-on-W metal layers sputtered by dc magnetron method onto an oxide-coated n-type Si wafer. Anodizing was done in an organic acid aqueous solution at potentials ranging from 150 to 450 V, so that a layer of nanoporous anodic alumina was first formed and then used as a mask for anodizing the underlying tungsten (Mozalev *et al.*; 2008). The films derived from the anodized Al/W bilayers after selective alumina dissolution were composed of arrays of well-defined, size-tailored, long-aspect-ratio rod-like metal-oxide protrusions, about 130 nm in diameter and up to 1 μm long (Mozalev *et al.*; 2014). The as-prepared (amorphous) and annealed (crystalline) arrays of WO_3 nanorods vertically aligned on the substrate were tested by photoelectrochemical scanning droplet cell microscopy (PE-SDCM), which is an extremely versatile tool for the screening of water splitting photoelectrodes, allowing for multiple most important photoelectrochemical experiments on the same sample within a diameter of 100 μm (Kollender *et al.*; 2013). The electrolyte used in this study (0.1M Na_2SO_4 , pH5.0) enabled selective water oxidation on the surface of tungsten oxide nanorods instead of undesired anion oxidation and produced no destructive effect on the anode material.

The present findings revealed that the photoactivity of the tungsten-oxide semiconductor electrode prepared here was three times higher than that of a planar WO_3 anodic film used as reference and was further enhanced due to annealing the samples in a vac-

uum atmosphere and especially in air at 500°C. Thus, the WO_3 nanorod array derived from so-called porous-alumina-assisted anodizing of tungsten layers appeared to be capable of effectively performing solar-driven water splitting.

The technology is advantageous in that it provides a simple, cost effective and environmentally friendly way for fabricating materials for solar hydrogen production by electrolysis.

Research leading to these results was supported in part by GAČR grant no. 14-29531S and by project CZ.1.07/2.3.00/30.0005 of Brno University of Technology.

Keywords: renewable hydrogen production, tungsten oxide nanostructures, photoelectrochemical water splitting, porous-alumina-assisted anodizing.

References:

Mozalev, A., Khatko, V., Bittencourt, C., Hassel, A. W., Gorokh, G., Llobet, E., Correig, X. (2008), Nanostructured Columnlike Tungsten Oxide Film by Anodizing Al/W/Ti Layers on Si, *Chem. Mater.*, 20, 6482–6493.

Mozalev, A. et al. (2014), Smart Anodizing of Tungsten through the Alumina Nanopores: from Nanocolumns to Nanocapsules and Nanotubes. 65th Annual Meeting of the International Society of Electrochemistry, Ubiquitous Electrochemistry, 460.

Kollender, J. P., Mardare, A. I., Hassel, A. W. (2013), Photoelectrochemical Scanning Droplet Cell Microscopy (PE-SDCM), *Chem. Phys. Chem.*, 14, 560–567.

Magnetic Nano-Structured Coatings for Corrosion Resistance

Taleb H. Ibrahim* and Khalil M. Abed
American University of Sharjah
Department of Chemical Engineering
P.O. Box 26666, Sharjah, UAE

Abstract:

Carbon steel is the most widely used metal in the oil and gas industry due to its abundance and low cost. However, it is susceptible to corrosion. Protecting carbon steel structures against uniform corrosion in wet environments has always been a major interest to scientists and engineers. The use of coatings and paints is a primary method in corrosion control of carbon steel in the industry. Inorganic coatings have proved potency in corrosion control over organic ones; however, they have always been associated with negative impact on the environment. Therefore, scientists and engineers are working in the direction of improving the corrosion resistance of more environmentally friendly organic coatings by different methods. This work is an attempt to enhance the corrosion resistance performance of an organic coating by incorporating Fe_3O_4 magnetic nanoparticles and Fig leaves extract as green inhibitor. This process is believed to improve the adhesion of the coating to the metal surface as the magnetic nanoparticles will work as shear connectors or nano nails and will help pin the coating to the carbon steel surface. On the other hand, the natural inhibitor will get adsorbed on the metal surface and both, the nanoparticles and the green extract are believed to increase the Time To Failure (TTF) of the coating. Electrochemical Impedance Spectroscopy technique was used to determine the coat performance using a

three electrode cell and collected over a period of twenty one days. The EIS measurements indicated an improvement on the corrosion protection properties of reinforced Fe_3O_4 -Fig Extract-alkyd based coating.

Keywords: Alkyd coating coatings, green inhibitor, waterborne coatings, Nano- Fe_3O_4 , Magnetic Nanoparticles, Corrosion resistance, EIS

*corresponding Author: italeb@aus.edu

Thermodynamic modeling and design of a solar lithium bromide-water absorption chiller

CH. Hamdi¹, A Farhat²

¹National Engineering School of Tunis, Tunisia,

²The Energy Technologies Research center of Borj Cedria, B.P. 95, 2050. Hammam-lif, borj cedria, Tunis. Tunisia

Abstract: The solar lithium bromide-water, absorption chillers have been the subject of intensive research in the past few years, due to a number of attractive properties, such as the energy Economy, environmental protection and low-cost [1-4].

This paper presents the modeling and design of the solar lithium bromide-water, absorption chillers of 8 to 20 Kw. The solar lithium bromide-water absorption chiller shown in figure1 is mainly composed of two systems: the solar system which is composed of collector and tank and the absorption refrigeration system which is essentially composed of heat exchangers that all have the same principles such as: condenser, evaporator, absorber, solution heat exchanger and generator. Each system has its own loop and characteristics. The parameters of each component are calculated by using the basic concepts of thermodynamic principles, mass and energy balance and the correlations provided in the literature for evaporation, condensation and liquid to liquid heat transfer[5-8].

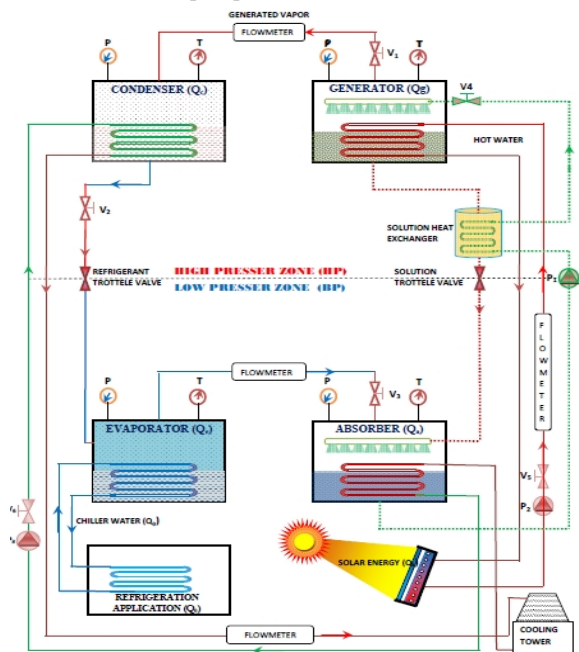


Figure1: Schematic diagram of a solar lithium bromide water absorption chiller.

The algorithm displayed in Figure 2 describes the steps of design solar lithium bromide-water, absorption chillers. Enthalpies, temperatures, mass flow rate and the heat exchangers area in each compo-

nent, were calculated, the numerical results are tabulated and discussed.

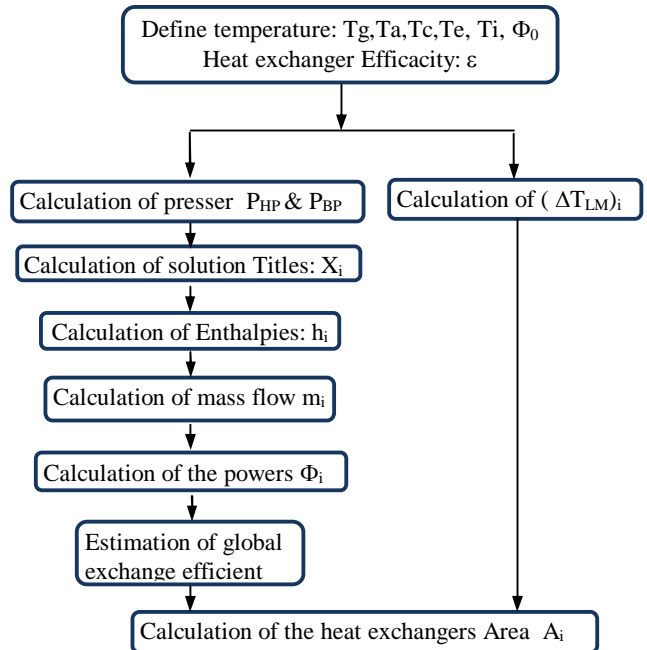


Figure2: the steps of design solar lithium bromide-water, absorption chillers

Keywords: Absorption chiller, Lithium bromide-water, Thermodynamic modeling, design, Heat Exchangers...

References:

Tawatchai Jaruwongwittaya, Guangming Chen “A review: Renewable energy with absorption chillers in Thailand”

Arun Bangotra, Anshul Mahajan “Design Analysis Of 3 TR Aqua Ammonia vapour Absorption Refrigeration System” Mechanical Engineering Department, Government Polytechnic College, Jammu, J&K, India, 180004

Horuz, T.M.S Callander, “Experimental investigation of a vapour absorption refrigeration system” Department of Mechanical Engineering, University of Uludag, Bursa, Turkey.

Bakhtiari, B., Fradette, L., Legros, R., Paris, J., 2011. « A model for analysis and design of H₂OeLiBr absorption heat pumps” Energy Convers. Manage. 52, 1439e1448.

DRINKING WATER MICROPOLLUTANTS EVALUATION IN TUNISIA, CASE OF: Pb, Hg, Cd, F

W. Guissouma, J. Tarhouni,

¹ National School of Agronomy, Department of Rural Engineering, Tunis, Tunisia

Abstract: This study aims to quantify the burden of Pb, Cd, Hg and F of water distributed by the Tunisian National Water Distribution Utility (SONEDE). A sampling campaign was conducted on 100 points of water consumption throughout the Tunisian territory. The results revealed that there are no significant cases of exceeding quality standards for Cadmium and Mercury in public distribution networks. However the fluoride analyzes reveal concentrations ranging from 0 to 2.4 mg/L. Some levels do not meet the national standards and the World Health Organisation (WHO) guidelines on water quality limits for human consumption. As WHO mentioned, the presence of fluoride in the drinking water is a real health problem for regions whose fluoride content exceeds 2 mg/L. The overtake cases are located primarily in southern Tunisia (Medenine Gabes, Gafsa and Tataouine). However, some other regions, are fed by water very poor in fluoride (<0.1 mg / L). A fluorides risk characterization step was performed to identify the most sensitive population and subsequently the health effect (tooth decay, dental fluorosis and skeletal fluorosis).

Keywords: Drinking water, Assessment risk, fluoride, sensitive population.

1- INTRODUCTION

In recent years, an important effort has been made to the mastery of the bacteriological quality of drinking water that has been translated to a decrease in diarrheal diseases. However, previous studies have not supported all chemical hazards for the evaluation of such risks. Only few studies have been conducted to evaluate consumer exposure to some micropollutants; i.e. fluoride and heavy metals.

The aims of this study are to:

- Help disseminate knowledge about the levels of some micropollutant in drinking water;
- Assess compliance ranging compared to national and international standards.
- Contribute to assess of risk exposure through drinking water (distributed by SONEDU).
- Contribute to the awareness of the Tunisian drinking water quality problems and mainly in specific regions.

2- METHODS

A sampling plan was developed to define the number and sampling points. A levy of 100 samples of drinking water distributed on the 24 governorates of Tunisia was made following a probing of second degree with reasoned choice involving the importance of networks according to the mass of population served by SONEDU water.

2.1. Conformity assessment of the quality of drinking water in Tunisia

After laboratory analysis of water samples, the conformity assessment of the quality of drinking water was conducted. It is based on a comparative analysis between the laboratory analysis results and the standards of water portability for selected parameters (lead, mercury, cadmium and fluorine). The conformity assessment we allowed locate areas of exceeding quality limits of drinking water on the Tunisian territory.

2.2. Risk assessment of fluoride content in drinking water

As mentioned in [1], the risk assessment process is conventionally structured in four basic steps :

- Hazard identification,
- Selection of toxicological reference values (TRV),
- The exposure assessment,
- Risk characterization.

2.2.1. The exposure assessment

The exposure assessment was determined according to international recommendations of WHO [2]; by compiling data usage (in water) and concentrations obtained through laboratory analyzes (concentrations of fluoride element contained in the drinking water).

The consumption habits of drinking water considered in this evaluation are those observed for high consumers express (L/d), the choice of high values of water consumption is justified by:

- The approach of the study is intended protective
- The geographic area affected by high levels of fluoride are located in southern Tunisia, arid and temperatures sometimes exceed 40 ° C, under the hot breath and dry Sirocco, so

an important need of water for allowing the regulation of body temperature.

The estimate of daily consumer exposure through drinking water (E_w) expressed in (mg/kg/day) is formulated as follows:

$$E_w = C \times C_i / B_w$$

With:

- C_i : Concentration of fluoride in drinking water
- C : the daily consumption of drinking water (L / d): The reference values used by WHO are: 2 liters per adult, 1 liter for a child, 0.75 liter for infants.
- B_w : is the average body weight: The reference values used by WHO [3] are: 60 kg for adults, 10 kg for a child, 5 kg for an infant,

2.2.2. The risk characterization

The risk characterization combines the information of daily exposure in water and the adverse effects observed at higher exposures VTR toxicological reference values [4]. The most population exposed at risk is defined by comparing daily exposure levels to fluoride in water depending on the age. The comparative approach of the level of the daily exposure with the referential toxicological values, allows us to estimate some risk indicators illuminating the health dimension of the situation investigated, such as the hazard quotient (QD). This is the ratio between the level of exposure and the toxicological reference value. Adverse effects may occur when the r exceeds the value of 1 [5]. So, the calculation of this ratio is a tool for identifying risk areas.

3- RESULTS

3.1. Descriptive analysis of results

The levels of fluoride in drinking water in Tunisia changing from north to south (figure1), they are less than 0.1 mg / L in Jendouba and Beja and exceed 2 mg / L in several southern regions, particularly in the region of gabes, Gafsa, Medenine and Tataouine where fluoride levels reach 2.4 mg / L. These signify an important interregional variability in levels of fluoride in the drinking water in Tunisia associated with the intense intra-regional variability in the region of Gabes, marked by significant fluctuation of levels of fluoride in drinking water (levels between 0.29 mg/L and 1.94 mg/L in El Hamma and Mareth).

3.2. The conformity assessment results

The results of the conformity assessment drink water compared to national standards [4] and international shows that:

- For fluoride, 7% of samples are classified non-compliant; These cases are located primarily in southern Tunisia (Medenine, Gabes, Gafsa and Tataouine).

- For mercury 2% of samples are classified non-compliant: These cases exceeded indicate accidental contamination of drinking water which could be the subject of an investigation by regulators and water dispenser (SONEDE) in to define the origin or source of spill responsible for this non-compliance.

- No case of non-compliance is detected for Cd and Pb.

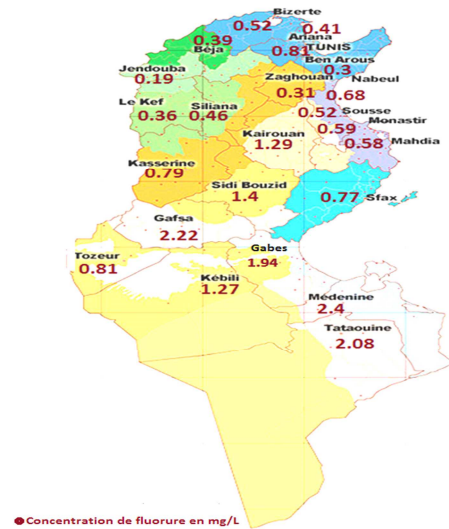


Figure 1: Representative map of the concentration of fluoride in drinking water

Only the fluoride element was quantified while for the other 3 elements are insufficient data to estimate the exposure of consumers to the health risk associated with Pb, Hg, Cd in drinking water (98% of values are below the limits of quantification).

3.3. The risk characterization

3.3.1. The most population exposed at risk of fluoride through drinking water

Infants and children have higher exposure of fluoride than adults. Hence infants and young children are the age groups most exposed to risk of fluoride; they are regarded such as the population particularly sensitive at overruns even low levels. The explanation for this sensitivity can be reflected in the fact that for these age groups the growth skeletal rate is high and the mineralization of tooth buds of permanent teeth is triggered during this period.

3.3.2. Risk areas in Tunisia

The Tunisian consumer is protected from acute toxicity to fluoride through drinking water.

3.3.2.1 Risk areas of tooth decay

75% of the regions in Tunisia (18 governorates out of 24), have lower than recommended nutrient value

by WHO for prevention of tooth decay (figure2). These regions are located mainly in the north of Tunisia, this deficiency of fluoride in drinking water is more pronounced in the north west (Beja and Jendouba) where levels of fluoride are below the limit of quantification in these regions, the supplementation in children is required, it can be done on the one hand, by the kitchen salt fluorinated whose real contributions are not known and secondly, in the form of fluorinated drugs [6].

3.3.2.2. Risk areas of dental fluorosis

We find that 25% of the regions in Tunisia (6 regions out of 24) have exposure levels exceeding the referential dose of dental fluorosis, this exposure is exclusively coming from drinking water (100% of the referential dose coming from water). It should be noted that the excess can appear in another region if we associate to water exposure, the food exposure and that provided by the drink (tea) and toothpastes. Children's exposure in the region of Medenine is greater by a factor of 2 compared with the toxicological reference value to effects associated with dental fluorosis.

3.3.2.3. Risk areas of skeletal fluorosis

The value of the fluoride exposure by water exceeds the reference value of occurrence of skeletal fluorosis in localized regions in Medenine, Gabes, Gafsa, Tataouine and Zidi Bouzid: where a QD > 1 in 20% of regions of Tunisia (figure3).

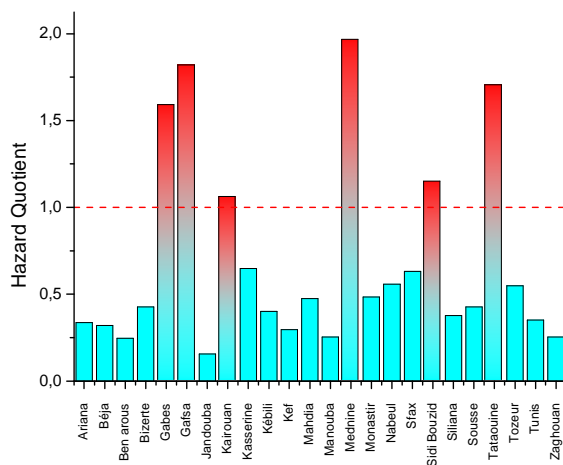


Figure 2: Presentation of the hazard quotient in different regions

4- CONCLUSION

The physical and chemical nature of the water in Tunisia does not present the problem related to the presence of mercury, cadmium and lead except in accidental cases, while the real problem related to drinking water in Tunisia is fluoride that is present naturally in waters in south of Tunisia. Fluoride is an ambivalent element, provided with beneficial effects and harm effects to human health [7]. Intakes levels

produce opposite effects of fluoride are not very far from each other, so that an estimation of the optimal level of fluoride seems essential.

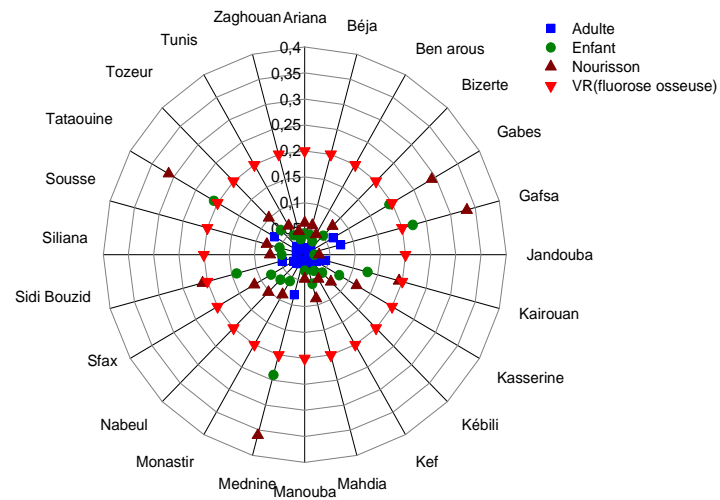


Figure 3: Definition of regions at risk to producing skeletal fluorosis

REFERENCES

- 1- InVS/Afsset. Estimation de l'impact sanitaire d'une pollution environnementale et évaluation quantitative des risques sanitaires. Ed. InVS/Afsset 2007 ; 162p.
- 2- WHO ; 2011 : Guidelines for drinking-water quality, fourth edition World Health Organization 2011
- 3- OMS : 2003 : Rapport sur la santé dans le monde – façonner l'avenir, n.d.
- 4- Parent-Massin, D. : Évaluation des risques toxicologiques et nutritionnels liés à l'utilisation des additifs et auxiliaires de fabrication. In : Additifs et auxiliaires de fabrication dans les industries agroalimentaires, Paris : Tec&Doc 2002, 746 p.
- 5- Afssa ; Evaluation des risques sanitaires liés aux situations de dépassement des limites et références de qualité des eaux destinées à la consommation humaine 2005 ; 96 p.
- 6- NT09.14 : Norme Tunisienne relative à la qualité des eaux destinées à la consommation humaine ; 2013, 14 p.
- 7- Viswanathan G., Jaswanth A, Gopalakrishnan S, Siva Ilango S, Aditya G.; 2009: Determining the optimal fluoride concentration in drinking water for fluoride endemic regions in South India. Department of Pharmaceutical Chemistry, Manonmaniam Sundaranar University, Abishekapatti, Tirunelveli - 627012, Tamil Nadu, India.

Poster Presentations

Structural, microstructural and thermal stability of FeSiB nanopowders alloys prepared by mechanical alloying

M. Ibrir,^{1,*} S. Alleg,² S.LAKEL,³ Saadi BERRI,¹ N.E. Fenineche,⁴ J.J. Suñol⁵

¹Laboratoire de Physique des Matériaux et ses Applications, Département de physique, Université de M'sila B.P. 166 Route de Ichbilia, M'sila 28000, Algérie.

²Laboratoire de Magnétisme et Spectroscopie des Solides, Département de Physique, Université de Annaba B.P. 12, Annaba 23000, Algérie

³Laboratory of Metallic and Semiconducting Materials, University of Biskra, B.P. 145 RP 07000 Biskra, Algérie

⁴LERMPS, Université de Technologie de Belfort-Montbéliard (UTBM), 90010 Belfort, Cedex France

⁵Dep. de Física, Universitat de Girona, Campus Montilivi, Girona 17071, Spain

*E-mail: ibirmiloud@yahoo.fr

Abstract: Fe–Si alloys are of significant commercial and academic interests due to the large diversity of their physical properties. Fe–Si alloys can be used as starting materials for many multicomponent technical alloys. The addition of B to the Fe–Si alloys hinders coarsening of the bcc grains, increases the possibility of forming an amorphous phase and, thereby, provides good magnetic properties, and gives a better thermal stability of the residual amorphous phase (Ono et al., 1999). Therefore, Fe–Si–B amorphous alloys have been widely used as magnetic core materials (Swartz et al., 1981). Some efforts were made to synthesize Fe–B–Si alloys from elemental powders using MA (Pekala et al., 2001). It has been reported that ball milling produced NC solid solution (Shultz et al., 1988) or only partial transformation to the amorphous state. Consequently, determination of the extent to which B and Si are incorporated in the Fe crystallites during ball milling is of great interest. It has been observed that the steady state concentration of B and Si in solution during the milling process of the Fe–13B–7Si (at.%) powder mixture, in a spex mill, required 128 h. In the ball-milled Fe78Si9B13 powders, the dissolution of B and Si in the Fe lattice occurred simultaneously with crystallite size reduction.

In this work, the structural, microstructural and thermal stability of FeSiB nanopowders alloys prepared by mechanical alloying from elemental powder mixture Fe75Si15B10 were studied as function of milling times. X-ray diffraction results show the formation of Fe₂B after 5 h of milling, and Silicon diffraction peaks disappeared after 50 h of milling. Rietveld refinement of XRD patterns reveals the presence of 74 % Fe(Si, B) solid solution and 26 % Fe₂B boride with crystallite size about 13 nm and 6 nm, respectively. Differential scanning calorimetry (DSC) measurements on FeSiB alloy present an exothermic peak at 580 °C, which is associated with the crystallization of the α -Fe(Si, B) and Fe₂B phases.

Keywords: Nanomaterials; Mechanical alloying; nanopowder; DSC; X-ray diffraction.

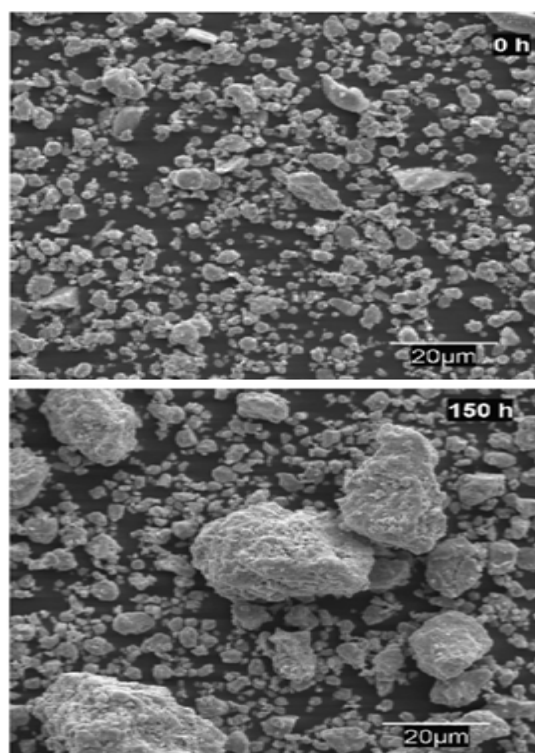


Fig. 1. SEM micrographs of the as-received (0 h) and Fe75Si15B10 powders milled for 150 h.

References:

- Ono, Y., Ichirku, T., Ohnaka, I., Yamauchi, I. (1999) Spinning phenomena, structure and magnetic properties of Fe–6.5 mass% Si alloy fiber produced by the in-rotating-liquid-spinning process, *J. Alloys Compd.* 289, 220–227.
- Swartz, J.C., Kossowsky, R., Hahgh, J.J., Krause, R.F. (1981) *J. Appl. Phys.* 52, 3324–3330.
- Pekala, M., Jachimowicz, M., Fadeeva, V.I., Matyja, H., Grabias, A. (2001), *J. Non-Cryst. Solids*, 287, 380–384.
- Shultz, L., Hellstern, E., Zorn, G. (1988) *J. Phys. Chem.* 157, 203–208.

Cupric oxide nanomaterials: Hydrothermal synthesis and electrochemical properties

F. Janene ^{a*}, H. Dhaouadi ^a and F. Touati ^b

^a Useful Materials Laboratory. National Institute of Research and Physicochemical Analysis (INRAP), Sidi Thabet technopole, 2020-Ariana, Tunisia.

^b Methods and Analysis Techniques Laboratory. National Institute of Research and Physicochemical Analysis (INRAP), Sidi Thabet technopole, 2020-Ariana, Tunisia.

Abstract: Nanomaterials have attracted much attention in recent years because of their outstanding properties and potential applications. As the size of the particles reduces into nanoscale, materials exhibit novel properties that cannot be explored by their bulk counterpart and they are considered to be very fruitful for new scientific and technological developments. Among the various types of nanomaterials, semiconductor metal oxide nanoparticles are a special class of advanced materials which have been used to fabricate different types of technological devices [1]. Among them, copper oxide is inexpensive and non toxic with a narrow band gap of 1.2 eV at room temperature. Owing to its unique physicochemical properties, the material has a wide range of applications in, for example, solar energy conversion[2] and lithium batteries [3]. In addition it can also be used to prepare a variety of organic-inorganic nanostructures composites with high thermal and electrical conductivity, high mechanical strength, and high temperature durability. In this paper we described a simple one step hydrothermal route for the synthesis of CuO nanoplatelets from copper nitrate trihydrate as a copper source and 1,3-diaminopropane which, acts as a reducing and structure-directing agent. The impact of the reaction time on the particles size, morphologies and the crystalline phases was investigated. The electrochemical properties of the CuO nanoplatelets films deposited on indium-tin-oxide (ITO) coated glass has been investigated using cyclic voltammetry (CV) in the presence of Li^+ in propylene carbonate electrolytic solution. Although many methods have been developed to elaborate nanostructured copper, to the best of our knowledge, it is the first report of CuO nanoplatelets synthesis using $Cu(NO_3)_2 \cdot 3H_2O$ as starting inorganic precursor and 1,3-diaminopropane which, acts as a reducing and structure-directing agent.

Keywords: Hydrothermal synthesis, CuO nanostructures, Electrochemical properties, Optical properties.

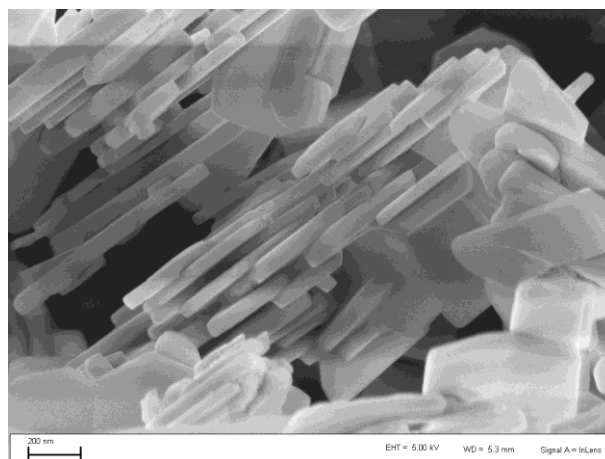


Figure 1: Figure illustrating the SEM micrographs of the samples synthesized at 180°C for 2 hours.

References:

- Rai, A., K., Anh, L., T., Park, C., J., Kim, J. (2013), Electrochemical study of NiO nanoparticles electrode for application in rechargeable lithium-ion batteries, *Ceram. Inter.*, 39,6611-6618.
- Anandan, S., Wen, X., Yang, S. (2005), Room temperature growth of CuO nanorod arrays on copper and their application as a cathode in dye-sensitized solar cells, *Mater. Chem. Phys.*, 93,35-40.
- Zhang, W., Wang, H., Zhang, Y., Yang, Z., Wang, Q., Xia, J., Yang, X. (2013), Facile microemulsion synthesis of porous CuO nanosphere film and its application in lithium ion batteries, *Electrochim. Acta*, 113,63-68.

Nucleic Acid Induced Assembly of Gold Nanoparticles

Ramla Gary^{1,*}, Giovanni Carbone¹, Gia Petriashvili^{1,2}, Riccardo Barberi¹

¹Physic Department and IPCF-CNR Cosenza, University of Calabria, 87036 Cosenza, Italy

²Institute of Cybernetics of Georgian Technical University, 0175 Tbilisi, Georgia

*gary-ramla@hotmail.com

Abstract:

The understanding of the physical nature of the fundamental interactions between nucleic acid (DNA) and gold nanoparticles (AuNPs) has primary importance due to its significance in biomedical applications, particularly in therapeutics and diagnostics [1,2].

In this work, a combination of laser confocal microscope (LSCM) and scanning electron microscope techniques (SEM) show an AuNPs assembly when the DNA was added to the solution. This aggregation is due to electrostatic and hydrophobic interactions between positive charged CTAB capped AuNPs and negative charged DNA phosphate backbone.

Our studies would help in the use of DNA molecules as templates to realize linear nanoparticle assemblies since that the ordered arrangement of nanoparticles in two- and three-dimensional structures is an important research problem of practical goal (Figure)[3,4].

Keywords:

DNA-gold nanoparticles, Gold nanoparticles assembly, electrostatic/hydrophobic interactions.

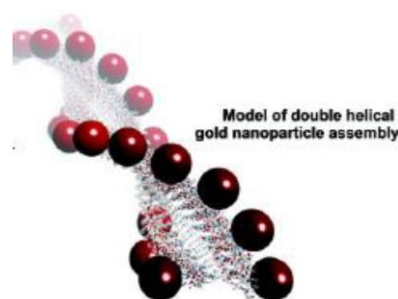


Figure 1: AuNPs assembly in 3-D structure following the twisted peptides morphology[4]

References:

- [1] Liping Sun, Zhaowu Zhang, Shuang Wang, Jianfeng Zhang, Hui Li, Lei Ren, Jian Wen, Qiqing Zhang, Effect of PH on the interaction of Gold nanoparticles with DNA and Application in the Detection of Human p53 Gene Mutation, *Nanoscale Res Lett* (2009) 4:216-220.
- [2] Ziyang Zhang, Yongjian Liu, Chad Jarreau, Michael J. Welch, and John-Stephen A. Taylor, Nucleic Acid-directed Self-assembly of Multifunctional Gold Nanoparticle Imaging Agents, *The Royal Society of Chemistry* 2013.
- [3] KRISHNA N. GANESH AND MURALI SASTRY., DNA-amine interactions: From monolayers to nanoparticles., *J. Indian Inst.Sci.*, Mar.-Apr., 2002, 82, 105-112.
- [4] Chun-Long Chen, Peijun Zhang, and Nathaniel L. Rosi., A New Peptide-Based Method for Design and Synthesis of Nanoparticles Superstructures: Construction of Highly Ordered Gold Nanoparticles Double Helices., *J. Am. Chem. Soc.*, 2008, 130(41)

Formation of nanocrystalline B2-structured (Fe,Ni)Al in mechanically alloyed Fe₅₀Al₃₀Ni₂₀ (%.wt) powder

C. Nakib^{1,*}, A. Otmani¹, A.Djekoun², J.M. Grenèche³

¹Laboratoire de Recherche sur la Physico-Chimie des Surfaces et Interfaces, LRPCSI, Université 20 Août 1955, BP 26, Route d'El-Hadaïek, Skikda 21000, Algeria

²Laboratoire de Magnétisme et Spectroscopie des solides, LM2S, Université Badji Mokhtar, BP 12, Annaba 23000, Algeria

³LUNAM, Université du Maine, Institut des Molécules et Matériaux du Mans, UMR CNRS 2, France

Abstract: The results of the ball milling process are various. So we can obtain the formation of amorphous phases by milling pure elements [1-3] or by milling elemental metal ribbons [4,5] and the formation of intermetallics for pure elements [6,7]. Also, mechanical alloying (MA) is a process used for producing powders at nanometer scale [8].

B2-structured (Fe,Ni)Al was synthesized by an abrupt reaction during mechanical alloying (MA) of the elemental powders of Fe, Al and Ni. The structural, microstructural and morphological changes occurring in the studied material during MA were investigated by X-ray diffraction (XRD) and scanning electron microscopy (SEM). Two crystalline phases were found, a majority one corresponding to FeAl bcc phase with a crystallite size less than 10 nm (figure.2), a lattice strain up to 1.6% and a dislocation density of about $2.3 \cdot 10^{16} \text{m}^{-2}$. The other phase in low proportion corresponding to Fe (Al,Ni) solid solution. SEM images (figure.1) showed an irregular morphology of powder particles.

Keywords: Mechanical alloying, ternary composition, dislocation density, structural properties.

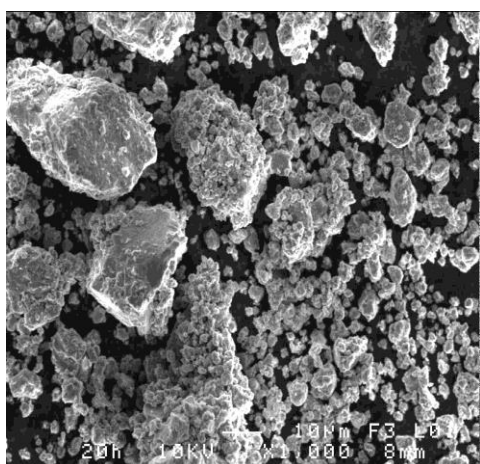


Figure 1: SEM images of the powder mixture of Fe, Al and Ni milled for 20 h.

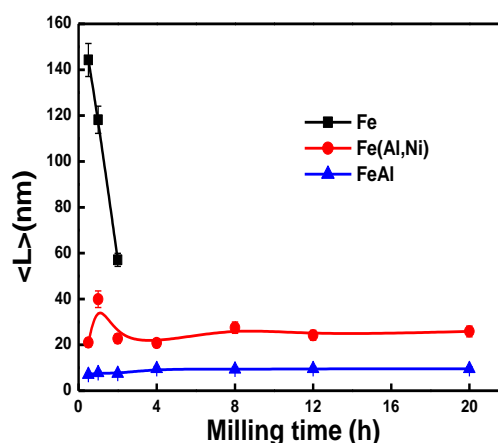


Figure 2: Evolution of the estimated crystallite size of Fe₅₀Al₃₀Ni₂₀ powder as a function of milling time.

References:

- [1] E.Gaffet, Mater.Sci.Engng. A 136, (1991) 161.
- [2] E.Gaffet and M. Harmelin, J. less-common Metals.157, (1990) 201.
- [3] M. Sherif El-Eskandany, Kyoshi Aoki, Haruko Itoh and Kenji Suzuki, J.less common Metals.169, (1991) 235.
- [4] F. Bordeaux and A.R.Yavarr, J.Appl.Phys.67, (1990) 2385.
- [5] A. Calka, A.P. Pogany, R.A. Shanks, H. Engelman, Mater. Sci. Engng A128, (1990) 107.
- [6] T.J. Tianen, R.B.Schwarz, J.less-common metals. 140, (1998) 99.
- [7] M.S. Kim, C.C. Koch, J. Appl. Phys. 62, (1987) 3450.
- [8] C. Suryanarayana, F.H. Froes, Nanostruct. Mater. 1, (1992) 191.

Vanadium oxide nanorods: Hydrothermal synthesis

F. Ferhati^{1-2,3}, A.Simo¹⁻², M.S. Belkaid³, M. Maaza¹⁻²

1-LATAGE Laboratory of Advanced Technologies of Genie Electrics, Faculty of Electrical and Computer Engineering, Mouloud Mammeri University BP17.RP 15000, Tizi-Ouzou, Algeria.

1-UNESCO-UNISA Africa Chair in Nanosciences/Nanotechnology, College of Graduate Studies, University of South Africa, Muckleneuk ridge, POBox 392, Pretoria-South Africa.

2-Nanosciences African Network (NANOAFNET), iThemba LABS-National Research Foundation, 1 Old Faure Road, Somerset West 7129, POBox 722, Somerset West, Western Cape Province, South Africa.

Abstract: Nanomaterials, which are often superior to their corresponding bulk materials, have attracted much attention due to their crucial roles in future technological applications. It is well known that the properties of materials such physical, optical and electronic ones are greatly dependent on their shapes when their sizes were reduced to micrometer or nanometer scale. So, many efforts have been devoted to synthesis of materials with different shapes and sizes.

Vanadium oxides are typical polyfunctional materials and have attracted strong interest over the past years for their electrical, optical, electrochemical properties: metal-to-insulator transitions, electrical switching of V_2O_5 , high ion interaction capacity, high sensitivity of active elements for gas sensors, etc... (A.Dhayal Raj et al. *Current Applied physics* 10, 531-537, Nirton CS Vieira et al. *Nanoscale Research Letters* 7:310).

Vanadium pentoxide in different forms has been intensively studied (Jacques Livage *Appl.phys.Lett.* 94, 103107). Vanadium oxide nanoparticles like-rods were synthesized by hydrothermal process treating $V_2O_5 \cdot 1,6H_2O$ precipitate derived from aqueous solution of V_2O_5 powder and H_2O_2 . The morphology and structure of products were investigated by means of scanning electron microscopy (SEM), transmission electron microscope (TEM), X-ray diffraction (XRD) and energy-dispersive X-ray spectroscopy (EDS) revealed that the composition of nanorods contain only V and O elements and it can be indexed as the orthorhombic V_2O_5 (space group Pmmn, $a=11.516 \text{ \AA}$, $b=3.566 \text{ \AA}$, $c=4.373 \text{ \AA}$, JCPDS card n°. 41-1426) and a preferential growth for (110) plan. The as-prepared products are composed of a large quantity of one-dimensional V_2O_5 nanorods with the widths about 50nm and the lengths of 128-416nm. The influences of synthetic parameters, such as reaction time and reaction temperature of the precursor, on the crystal structures and morphologies of the resulting products have been investigated. Time-dependent experiments show that $V_2O_5 \cdot 1,6H_2O$ are dehydrated gradually and converted into orthorhombic V_2O_5 single-crystalline nanorods. High reaction temperature of prepartion of the precursor also favors the formation of orthorhombic nanorods.

Keywords: Vanadium oxide, Nanostructure, Nanorods, V_2O_5 , Hydrothermal synthesis, gas sensing

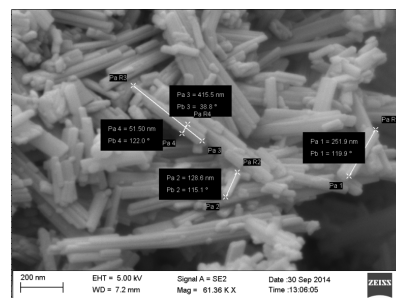


Figure1: SEM image of V_2O_5 nanorods synthesized by hydrothermal method

References:

- Jinxing Wang*, Weijie Yu, Shun Xu, Songyan Dai, Jiadong Wang, Chenxi Wang, Wen Zeng, Peishan Cao (2014) A Study on the precursor of vanadium pentoxide by the hydrothermal method, *Ceramics International* 40, 317-321.
- A.Dhayal Raj^{a,b}, T. Pazhanivel^b, P.Suresh Kumar^b, D.Mangalaraj^{a,c,*}, D.Nataraj^{a,b}, N.Ponpandian^{a,c} (2010) Self assembled V_2O_5 nanorods for gas sensors, *Current Applied physics* 10, 531-537.
- Yin Hu, Zhengcao Li, Zhongjun Zhang, and Daqiao Meng (2009) Effect of magnetic field on the visible light emission of V_2O_5 nanorods, *Appl.phys.Lett.* 94, 103107.
- Jacques Livage (2010) Hydrothermal Synthesis of Nanostructured vanadium oxides, *Materials* 3, 4175-4195.
- Nirton CS Vieira^{1,*}, Waldir Avansi², Alessandra Figueiredo¹, Caue Ribeiro³, Valmor R Mastelaro¹ and Francisco EG Guimaraes¹ (2012) Ion-sensing properties of 1D vanadium pentoxide nanostructures, *Nanoscale Research Letters* 7:310.
- Weijie Yu, Jinxing Wang*, Zhongping Gou, Wen Zeng, Weiwei Guo, Liyang Lin (2013) Hydrothermal synthesis of vanadium pentoxide nanostructures and their morphology control, *Ceramics International* 39, 2639-2643.
- Jie Ding, Hongrui Peng, Guicun Li*, Kezheng Chen* (2010) Conversion of $V_2O_5 \cdot xH_2O$ into orthorhombic V_2O_5 single-crystalline nanobelts, *Materials Letters* 64, 1562-1565.

Theoretical prediction of the optical properties of $Zn_{1-x}Be_xO$ Alloys based optoelectronic devices

Said LAKEL^{1,2}, Fatima Elhamra², M. Ibrir, K. Almi², F. Okbi²

¹ Laboratoire de physique des Matériaux - Université de LAGHOUAT – BP 37G, Laghouat, Algeria

² Laboratoire de Matériaux Semi Conducteurs et Métalliques, Université de Biskra, Algeria

Abstract: There is a growing interest in $Zn_{1-x}Be_xO$ (ZBO)/ZnO hetero structures and quantum wells since the band gap energy of ZBO solid solutions can be turned over a very large range (3.37–10.6 eV) as a function of the Be composition. ZBO/ZnO has been utilized in ultraviolet light emission diodes and lasers, and may find applications as active elements of various other electronic and optoelectronic devices. Band gap engineering by Be substitution enables the facile preparation of barrier layers and quantum wells in device structures. The optical properties of $Zn_{1-x}Be_xO$ were studied by first principle using the density functional theory. The dielectric functions and optical constants are calculated using PP-PW method with the generalized gradient approximation (GGA). The theoretical calculated optical properties yield a static dielectric constants for $Zn_{1-x}Be_xO$ are 4.08, 3.86, 3.60, 3.12 and 2.85 along polarization direction (001). It indicates that the static dielectric constants reduce with increasing Be concentration. However a static refractive indices for $Zn_{1-x}Be_xO$ are found to be 2.05, 1.98, 1.88, 1.77 and 1.70 with the increasing x , respectively. The obtained results agree well with the available theoretical and experimental values.

Keywords: First principle calculations, Optical Properties, optical constants, DFT.

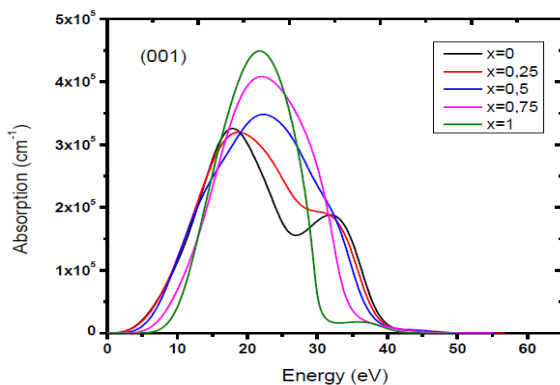


Figure 1: Varieties of absorption of $Zn_{1-x}Be_xO$ alloys along (001) direction.

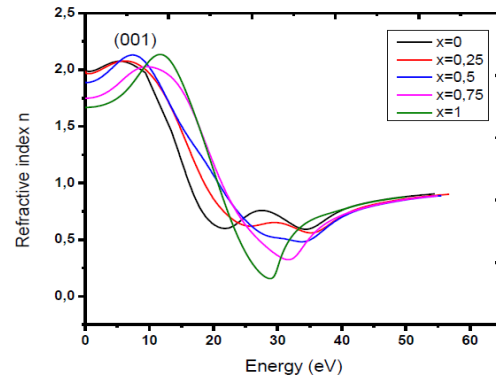


Figure 2: Varieties of refractive index of $Zn_{1-x}Be_xO$ alloys along (001) direction.

Acute hepatotoxicity of zinc oxide nanoparticles in Wistar rats

H.Ben Miled¹, Z.Ben Barka¹, Y.Baratli¹, M. Tlili¹, H.Abdelmelek¹, M. Sakly¹, K. Ben Rhouma¹, Olfa Tebourbi¹

⁽¹⁾Laboratory of Integrated Physiology, Science Faculty of Bizerte, 7021 Jarzouna, Carthage University, Tunisia.

Abstract: Various engineered nanomaterials have already been introduced into a number of industrial processes and innovative products. However their potential hazards on mammalian and humans remain largely unknown (Aschberger et al., 2011). As a result of their unique physicochemical properties, nanoparticles are becoming present in sunscreens, toothpastes, sanitary ware coatings and even food products. Currently, researchers are focusing on many areas such as applied physics and chemistry, mechanical and electrical engineering, nanotoxicology, nanobiology and nanomedicine, industrial applications and environmental investigations (Ferreira et al., 2013).

Zinc oxide nanoparticles (ZnO NPs) are used in a wide range of products including cosmetics, food packaging, imaging, etc. The present study was conducted on Wistar male rats and aimed to investigate the acute oral toxicity of ZnO NPs (0.5 and 1g/kg of body weight). The rats were sacrificed after 24h, 48h, 7, 15 and 30 days of ZnO NPs administration and blood samples were collected for assaying serum biochemical parameters. Liver histopathological examination was also performed.

Our results showed a significant accumulation of nanoparticles in the liver leading to cellular

injury shortly after ZnO NPs treatment. The liver of treated animals showed many pathological lesions in the liver morphology, including steatosis, inflammation, hepatocyte ballooning and later necrosis. Such damage was confirmed by the increase of serum activities of alanine aminotransferase (ALT) and aspartate aminotransferase (AST), creatinine, uric acid and total proteins.

These findings showed that acute oral exposure to 15 nm- sized ZnO NPs in Wistar rat leads to an accumulation of nanoparticles in the liver and blood vessel alteration which may contribute to liver dysfunction. These results also suggest the need for a complete risk assessment of any new engineered nanoparticle before its arrival into the consumer market.

Key words: ZnO nanoparticles, rats, liver, toxicity

References:

Aschberger ,K., Micheletti,C., Sokull-Klüttgen,B., Frans M. Christensen,F.M. (2011) Analysis of currently available data for characterising the risk of engineered nanomaterials to the environment and human health — Lessons learned from four case studies, *Environ. Int.*, 37, 1143–1156.

Ferreira, A.J., Celyn-Jones, J., Robalo-Cordeiro, C. (2013) Nanoparticles, nanotechnology and pulmonary nanotoxicology . *Rev. Port. Pneumol*, 19, 27-38.

Synthesis, characterization and optical properties of ZnO nanostructures via solvo-hydrothermal process

A. Moulahi,^{1*} F. Sediri^{1,2}

¹Laboratory of Condensed Matter Chemistry, IPEIT, University of Tunis,
2, Jawaher Lel Nehru 1008, B.P. 229 Montfleury,(Tunisia).

²Chemistry Department, Sciences Faculty of Tunis, Tunis El Manar University,
2092 El Manar, Tunisia.

Abstract: In recent years, controlling the morphology and size of inorganic materials has attracted intensive attention due to the fact they play very important roles in determining optical, electrical, and other physicochemical properties on the porous glass surface that we have enlightened with potential optical applications. Efforts have been devoted to controllable synthesis of inorganic materials with various morphologies for exploring its potential applications in various fields. Among the wide variety of nanoparticles in materials science, the semiconductor ZnO has caught special attention of researchers by their enhanced optical and electrical properties (Pudukudy et al., 2014, Moulahi et al., 2014). In this study we reported the synthesis, characterisation and optical properties of ZnO nanostructures prepared via the hydro-solvothermal reaction of zinc acetate $Zn(CH_3COO)_2 \cdot 2H_2O$, THF, H_2O and sodium decyl sulfate (DSS) as structure-directing templates. The structure, the crystallinity, the morphology and the composition of the materials were investigated by scanning electron microscopy (SEM), X-ray diffraction (XRD), Raman spectroscopy and Fourier transform infrared spectroscopy (FTIR). The optical properties of the as-synthesized ZnO were investigated by UV-visible absorption and room temperature photoluminescence (RTPL). The influence of the solvents and surfactant on the morphology of ZnO samples are discussed. The photoluminescence spectra have identified several kinds of defects in as-synthesized ZnO materials, such as oxygen vacancy (V_o), zinc vacancy (V_{Zn}) and interstitial zinc (Zn_i).

Keywords: ZnO nanostructures, hydro-solvothermal process, Semiconductors, Surfactants, Optical properties, Polarity, DSS.



Figure 1: Figure illustrating the SEM micrographs of the samples synthesized with H_2O

References:

- M. Pudukudy, Z. Yaakob, 30 (2014), Simple chemical synthesis of novel ZnO nanostructures: Role of counter ions, *Solid state sci.*, 30, 78-88.
- A. Moulahi, F.Sediri, 40 (2014), ZnO nanoswords and nanopills: Hydrothermal synthesis, characterization and optical properties, *Ceram. Int.*, 40, 943-950.

Correlation between structural and optical properties of SiO₂/(Ni:TiO₂) Bragg reflectors processed by dip-coating sol-gel method: The effect of annealing duration and Ni content

H. Sedrati^{1,2} and R. Bensaha¹

¹Laboratoire de Céramique, Département de Physique, Université Constantine 1, Route de Aïn El-Bey, Constantine 25000, Algérie

²Département des Sciences de la Matière, Faculté des Sciences, Université 20 Août 1955, BP 26 El-Hadaïk, Skikda 21000, Algérie

Abstract: The main objective of this paper is the study of the correlation between structural and optical properties of SiO₂/(Ni:TiO₂) Bragg reflectors, under the effect of annealing duration and Ni content, obtained by the dip-coating sol-gel process. The obtained samples have been analyzed with several investigation methods: X-ray diffraction (XRD), Raman spectroscopy, UV-VIS-IR and Photoluminescence spectroscopy. XRD diagrams show that our films crystallize in anatase phase only, whatever are the annealing duration and the Ni content. Moreover, the grain size raises from 11.76 to 14.45 nm with the increase of annealing duration from 10 to 20 minutes while it decreases from 14.45 to 13.96 nm when Ni content increases from 2 at. % to 5 at. %. These results have been confirmed by Raman spectroscopy. However, the recorded Raman spectra show symmetric vibration modes (A_{1g}+2B_{1g}+3E_g) of anatase phase identified at 144.9 cm⁻¹ (E_g), 198.1 cm⁻¹ (E_g), 396.6 cm⁻¹ (B_{1g}), 515.9 cm⁻¹ (A_{1g} + B_{1g}) and 637.3 cm⁻¹ (E_g) (Ohsaka, 1980). Spectra obtained by UV-Vis-IR analysis (Figure 1) show that increasing the annealing duration from 10 to 20 minutes diminishes the transmission coefficient (T%) from 2.24 to 1.46, broadens the stop band width from 172.01 to 185.30 nm and shifts the transmission curves towards the higher wavelengths. Inversely, raising Ni content from 2 to 5 at. % increases the transmission coefficient (T%) from 1.46 to 3.39, narrows the stop band width from 172.01 to 185.30 nm and shifts the transmission curves towards the lower wavelengths. Furthermore, the photoluminescence intensity increases when the annealing duration increases from 10 to 20 minutes, which may be probably due to the increase of the recombination rate of electrons-hole and to the growth of the grain size (Sedrati *et al.*, 2014). In return, The PL intensity decreases with the raise of the Ni content. This decrease may be attributed to the introduction of new defect sites that can act as trapping level in the band-tail states (Umebayashi *et al.*, 2002).

keywords: Bragg reflectors, Nickel doped TiO₂, Photoluminescence, Raman spectroscopy, recombination rate, band-tail state.

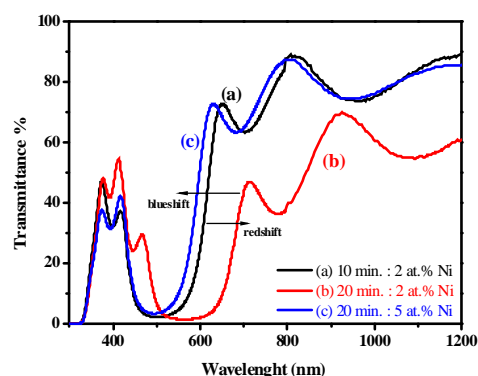


Figure 1: Figure illustrating UV-vis-IR spectra of (5/5) SiO₂/(Ni:TiO₂) Bragg reflectors annealed at 550°C : (a) during 10 min. and doped with 2 at. % Ni, (b) during 20 min. and doped with 2 at. % Ni and (c) during 20 min. and doped with 5 at. % Ni

References:

- Ohsaka, T. (1980) Temperature Dependence of the Raman Spectrum in Anatase TiO₂, *Journal of Physical Society of Japan*, 48, 1661-1968.
- Sedrati, H., Bensaha, R., Bensouyad, H., Miska, P. and Robert, S. (2014), Structural, optical and waveguiding properties of SiO₂/TiO₂ Bragg reflectors processed by the sol-gel method under the effect of Ni-doped TiO₂ and annealing duration, *Materials Research Bulletin*, 57, 287-292.
- Umebayashi, T., Yamaki, T., Itoh, H., Asai, K. (2002), Analysis of electronic structures of 3d transition metal-doped TiO₂ based on band calculations, *Journal of Physics and Chemistry of Solids*, 63(10), 1909-1920.

Age Modulates Fe₃O₄ Nanoparticles Liver Toxicity

Y. Baratli,^{1,2,*} M. Tlili,¹ H. Ben Miled,¹ Z. Ben Barka,¹ L. Ben Taher,³ H. Abdelmelek,¹ O. Tebourbi,¹ B. Geny²

¹ Université de Carthage, Laboratoire de physiologie intégrée, Faculté des Sciences de Bizerte, Tunisie

² Université de Strasbourg, Laboratoire Mitochondries, Stress Oxydant et Protection Musculaire, Strasbourg, France

³ Université de Carthage, Laboratoire de Synthèse et Structures de Nanomatériaux, Faculté des Sciences de Bizerte, Tunisie

Abstract: Owing to their ultra-fine sizes, iron oxide nanoparticles (ION) can elicit a spectrum of tissue responses including cell activation, generation of reactive oxygen species (ROS), and cell death (Zhu et al., 2011). Particularly, reports indicated that the liver is a key organ largely involved in body iron detoxification. Also mitochondrial dysfunctions appear as early signs of cells damage in several experimental settings (Charles et al., 2011) but mitochondrial implication in ION toxicity remains poorly known and controversial. Furthermore, age might modify the susceptibility of mitochondria to ION.

The ION was mixed with a solution of NaCl 9%. The mixture was then stirred vigorously and sonicated for 60 min to break up aggregates. Isolated liver mitochondria were extracted using differential centrifugations and were incubated with different concentrations of Fe₃O₄ (0, 250, 300 and 350 µg/mL) during 30 min. To discriminate if the results obtained might be due to the size or to a general response pattern in front of iron oxide exposure, we submitted middle-aged liver mitochondria to a Fe³⁺ solution with concentration of 350 µg/mL Fe₃O₄. To obtain free Fe³⁺ ions a precise mass of Fe₃O₄ nanoparticles was dissolved in a small volume of concentrated HCl under gentle heating (Cornell and Schwertmann, 1996).

We examined the effects of ION on mitochondrial respiratory chain complexes activities and mitochondrial coupling in young (3 months) and middle-aged (18 months) rat liver.

Maximal oxidative capacities V_{max} , V_{succ} and V_{tmpd} together with mitochondrial coupling were determined in controls conditions and after exposure to 250, 300, and 350 µg/ml Fe₃O₄ in young and middle-aged rats.

Keywords: Nanoparticles, Iron oxide, Coupling, Mitochondria, Mitochondrial respiratory chain, Middle-aged liver, Young liver.

In young liver mitochondria, exposure to ION did not alter mitochondrial function. In contrast, ION dose-dependently impaired all complexes of the mitochondrial respiratory chain in middle-aged rat liver using Fe₃O₄ (350 µg/ml). Mitochondrial coupling also decreased. Interestingly, 350 µg/ml Fe₃O₄ in the form of Fe³⁺ solution did not impair liver mitochondrial function in middle-aged rats. In summary, we demonstrate for the first time that old rats are more susceptible to ION exposure in terms of liver mitochondrial respiration and coupling. These age-related changes in liver mitochondrial respiratory chain activity should perhaps be taken into consideration in preclinical and clinical studies of particulate contrast agents.

References:

Zhu, M.T., Wang, B., Wang, Y., Yuan, L., Wang, H.J., Wang, M., Ouyang, H., Chai, Z.F., Feng, W.Y., Zhao, Y.L. (2011), Endothelial dysfunction and inflammation induced by iron oxide nanoparticle exposure: risk factors for early atherosclerosis, *Toxicol. Lett.*, 203, 162–171.

Charles, A.L., Guilbert, A.S., Bouitbir, J., Goette-Di Marco, P., Enache, I., Zoll, J., Piquard, F., Geny, B. (2011), Effect of postconditioning on mitochondrial dysfunction in experimental aortic cross-clamping, *Br. J. Surg.*, 98, 511–516.

R. M. Cornell and U. Schwertmann, *The Iron Oxides Structure, Properties, Reactions, Occurrence and Uses*, Wiley-VCH, Weinheim, Germany, 1996.

The application of electrochemical impedance spectroscopy to study of enzyme kinetics

Z. Fohlerová,^{1*} M. Jílek,¹ M. Pospíšilová,¹ J. Hubálek¹

¹ CEITEC BUT, Brno University of Technology, Technická 10, Czech Republic

Abstract: The application of electrochemical impedance spectroscopy (EIS) in theory and experiment for investigation of redox enzyme kinetics has been already described. The impedance studies are quite sensitive to the changes at the interface caused by adsorption of charged species and therefore can be used to study the kinetics of adsorption of macromolecules and also enables us to study enzyme kinetics since the action of the enzymes on their substrates involved modification and generation of charged species. In this work, we would explore the potential of electrochemical impedance technique to follow the kinetics of glucose oxidase–substrate reaction on the electrode surface. The enzyme is allowed to interact with different concentrations of its substrate and the resulting reaction is recorded in real time. Change in the imaginary component of the impedance at various substrate concentrations will be expected to follow Michaelis–Menten kinetics. Subsequently, when the suitable frequency from the spectrum is selected, the substrate conversion will be recorded online at the fix frequency. This method is expected to be simple and sensitive enough to study redox systems such as model of glucose oxidase and should be partially eliminate interferences commonly interfering during amperometric detection.

Keywords: biosensors, impedimetric biosensor, enzymes, kinetics of enzyme reaction, glucose oxidase

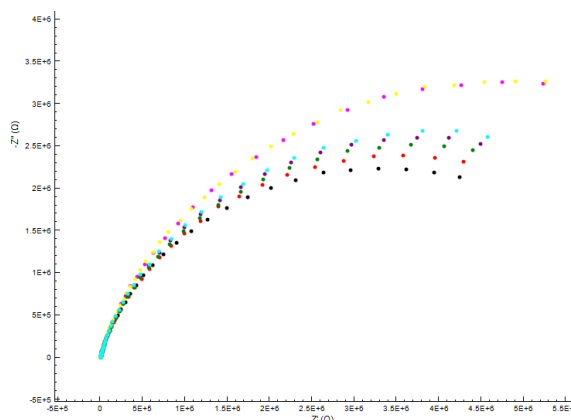


Figure 1: The plot illustrating the time-dependent increase of impedance parameters during enzymatic conversion of glucose.

References:

- Shervedani, R.K., Mehrjardi, A.H. (2006), Electrochemical characterization of directly immobilized glucose oxidase on gold mercaptosuccinic anhydride self-assembled monolayer, *Bioelectrochemistry*, 69, 201–208
- Kohma T., Hasegawa H., Oyamatsu D., Kuwabata S. (2007), Utilization of AC Impedance Measurements for Electrochemical Glucose Sensing Using Glucose Oxidase to Improve Detection Selectivity, *Bull. Chem. Soc. Jpn.*, 80, 158–165
- Shrikrishnan, S., Sankaran, K., Lakshminarayanan, V. (2012), Electrochemical Impedance Analysis of Adsorption and Enzyme Kinetics of Calf Intestine Alkaline Phosphatase on SAM-Modified Gold Electrode, *J. Phys. Chem. C*, 116, 16030–16037

optimization of the electromagnetic wave propagation in a tri-layer electrode ZnO/Ag/ZnO for solar cells application

¹D. Htem, ¹MS. Belkaid¹, M. Mesrouk

¹Laboratory of Advanced Technologies of Electrical Engineering (LATAGE), Faculty of Electrical and Computer Engineering, Mouloud Mammeri University (UMMTO), BP 17 RP, 15000, Tizi-Ouzou, Algeria

Abstract: In this paper we have simulated using COMSOL 4.3, a tri-layer electrode TCO/Metal/TCO with silver (Ag) as a metallic layer. The silver layer is used to reduce the sheet resistance of the transparent electrode. We have optimized the electromagnetic wave propagation for different combination of thickness at the wave length of 500 nm for ZnO/ Ag /ZnO electrode. The optimal thickness of different layers are respectively 42 nm / 2nm / 51 nm. ZnO/ Ag /ZnO presents a high transmittance up to 95%. The obtained results shows that this structure is the most appropriate in terms of using as a transparent electrode in solar cells application

Keywords: Electromagnetic wave propagation , tri-layer, solar cells application.

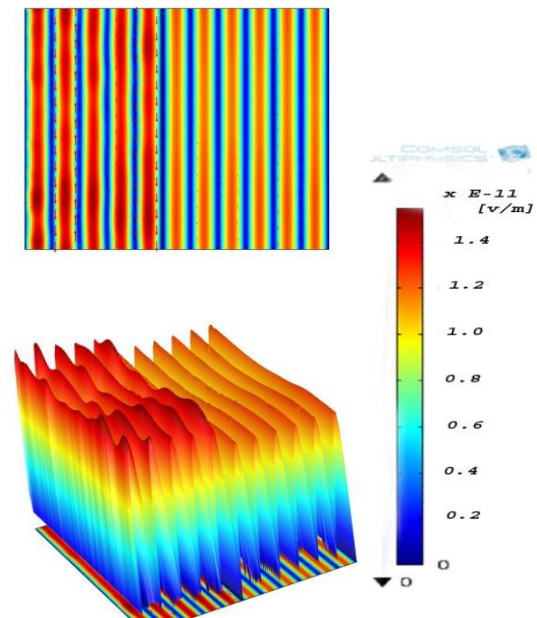


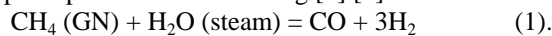
Figure 1. Electromagnetic wave propagation in ZnO/Ag/ZnO electrode

Use Hydrogen in The Steel IndustryT

M. Kahalerras, M. T. Abedghars,

Welding and NDT Research center (CSC) / Unit for Applied Steel and Metals. URASM /CSC-Annaba, BP 196 Annaba

Abstract: The use of hydrogen as a clean and storable energy is involved in the substitution of coking coal from natural gas for the reduction of iron oxides by the process of direct reduction [1]. The resulting product called "pre reduces or synthetic scrap" is the biggest load of arc furnaces in steel production. To meet the needs and steel products to prevent the importation of coal as expensive and polluting matter, we focused our studies and research work to the enhancement of our natural resources including the use of Gara iron ore Djebilet and Algerian natural gas. The main objective of this work is to produce a rich reducing gas hydrogen from natural gas at a lower cost by the principle of steam reforming [4] [5].



The producing a reducing gas [2] consists primarily of hydrogen (H_2) and carbon monoxide (CO), from natural gas and water vapor in a re-driver is used as a reducing agent for iron ore (pellets or calibrated) in a direct reduction pilot module [3] with a capacity of one ton.



Keywords: Energy and applications; Energy conversion, Hydrogen, gas reducing, sponge iron., steel, pollution.

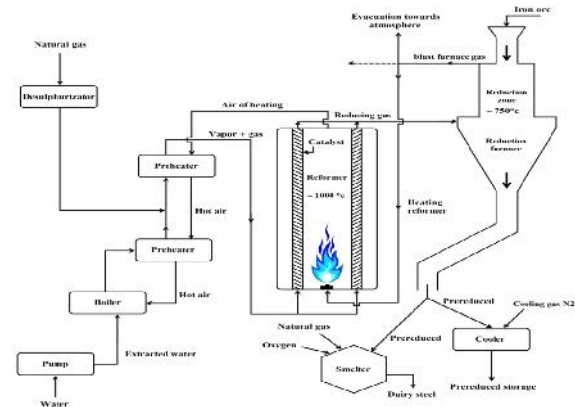


Figure 1: General view of the installation of hydrogen production, sponge iron and steel.

References:

- [1] ASTIER (J.). – Réduction directe. [M 7 580]. Traité Matériaux métalliques.
- [2] ASTIER (J.). – Usines sidérurgiques fondées sur la réduction directe. [M 7 110]. Traité Matériaux métalliques.
- [3] JENKINS (J.H.) and STEPHENS (T.W.). – Kinetics of catalytic reforming. Hydrocarbon Processing (USA) Nov. 1980
- [4] JONCHERE (J.P.) et BAUDOIN (C.). – Production d'hydrogène à Grande échelle à partir des hydrocarbures. L'actualité Chimique, 20-25 déc. 2001.
- [5] RAGUIN (J.). – Protection de l'environnement: Stratégie. M 7 150, M 7 151, traité Matériaux métalliques volume ME1

Single and binary adsorption system of lead and zinc ions from aqueous solution, by use of ammonium activated clays: kinetics and thermodynamics study.

A. Gharsalli, ^{1,*}, M. Bagane, ¹, S. Ammar ²

¹National Engineering School of Gabes, Department of Chemical Engineering and Processes, Gabes, Tunisia.

²University of Gabes, Faculty of science, Department of Chemistry, Tunisia.

Abstract: The sorption of two divalent metal ions -zinc and lead- from aqueous solution onto the ammonium activated clay in single and binary component systems has been studied. The effects of initial pH, contact time, adsorbent dose and initial metal concentration on the adsorption process have been investigated. The experimental data were analyzed using Langmuir and Freundlich adsorption models. The maximum percent removal 99% for Pb(II) and 66% for Zn(II) of the metal ions has been reached at the optimum adsorbent dosage 4g/l.

At the optimum pH of 5 and in the single adsorption system, the maximum adsorption capacities of the ammonium activated clay for Pb(II) and Zn(II) were found to be 25 and 16.95 mg g⁻¹, respectively. However, in the binary adsorption system, the maximum adsorption capacities were 17.24 mg/g for Pb(II) and 9.35 mg/g for Zn(II). Indeed, The ammonium activated clay has showed the high selectivity and interference resistance from coexisting ions for the adsorption of Pb(II). The experimental data obtained for both metals has been well-described by the Langmuir model while the kinetic studies have showed the adsorption process following the pseudo second-order rate model.

Keywords: ammonium activated clay, Heavy metals, lead (II), zinc (II), Adsorption, Kinetics, Thermodynamic

3-D Design, Electro-Thermal Simulations of Metal Oxide Gas Sensor Based on a High Temperature and Low Power Consumption Micro- Heater Structure and Geometrical Optimization of Spiral Platinum Micro-heaters using COMSOL

Aimer Amer Abdeslam,¹ Dr. Fouad Kerrou,¹ Pr. Khalifa Aguir²

¹ Lab. of MODERNa. of Constantine, Univ. of Constantine 1, Constantine, Algeria

² Aix Marseille University, CNRS, IM2NP UMR 7334, Av. E.N. Neimen 13397 Marseille, France

Abstract: Metal oxide gas sensors have many qualities that make this kind of sensor one of the most studied in laboratories and used in companies: it is low cost and very sensitive and fast responses to gases. To have these two last characteristics, the sensor must desorb easily the gases molecules in interaction with the sensible layer, what is the role of the micro-heater. The higher the temperature is, the easier the desorption is. To make an embeddable sensor the power consumption must be as low as possible.

A compromise should be found between these two parameters. That's why a metal oxide gas sensor, based on a micro-heater structure on a membrane able to work until 600 °C (with a power consumption equal to 60 mW at this temperature), has been developed. The technological process is the following: the bi-layer SiO₂/SiN_x membrane is grown on a silicon substrate; the heater and sensible electrodes metalization in platinum are deposited by evaporation; a SiO₂ passivation layer is grown; the contact open is realized by a wet etching; the membrane is released by a dry etching; the sensitive layer is deposited by inkjet. The electro-thermal simulation of this structure with COMSOL 4.3 has been realized. For this purpose, the Joule Heating physics interface has been used and a stationary study has been executed in order to: check the temperature distribution on the surface (Figure 1). Three different patterns of micro-heaters which are spiral, meander and ring are simulated, it was found that the spiral shape is the most suitable, in temperature uniformity and power consumption (Figure 2). The spiral form was used after introducing the SnO₂ tin oxide as a sensitive layer, and the tungsten oxide WO₃ thereafter and results are compared (Figure 3), and observe the influence of a sensitive layer with different thickness on the maximum temperature for different power consumptions (Figure 4). Our low power and high temperature structure has been successfully modeled. In addition, it has been observed that the temperature uniformity is suitable for our application. These results are promising and

the model developed will be helpful for the next step in which we will optimize our sensor.

Keywords MEMS, Gas Sensor, Micro-hotplates, COMSOL.

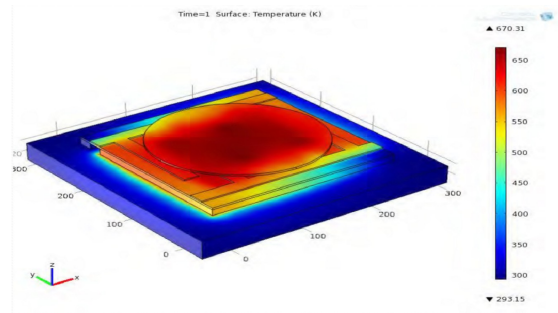


Figure 1: 3D temperature distribution in the micro-hotplate for heater voltage = 2 V.

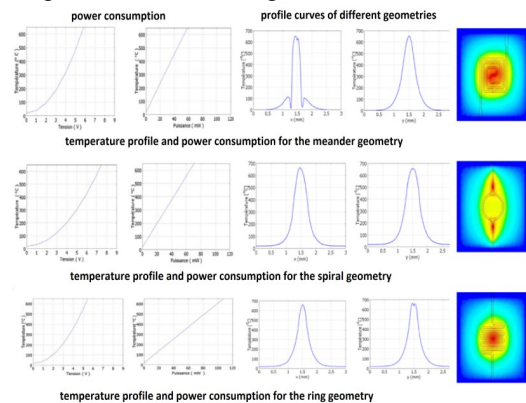


Figure 2: Temperature versus power consumption at the surface of the passivation layer with COMSOL: comparison between three geometries .

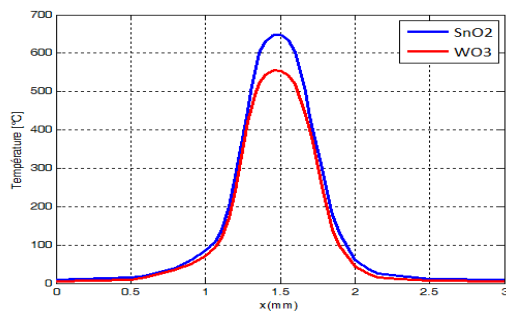


Figure 3: comparing the thermal profile of SnO₂ and WO₃.

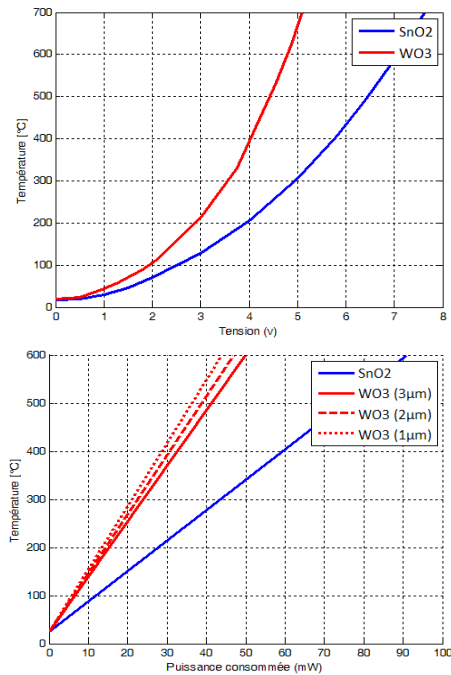


Figure 4: voltage and power consumption in function of the temperature.

References:

1. J. Courbat & al., Drop-coated metal-oxide gas sensor on polyimide foil with reduced power consumption for wireless applications, *Sensors and Actuators B*, 161, 862– 868 (2012).
2. Monika, Dr. Arti Arora, Design and Simulation of MEMS based Microhotplate as Gas Sensor, (*IJARCET*) Volume 2 Issue 8, August (2013).
3. F. Biró, C. Dücső, Optimisation of Low Dissipation Micro-hotplates – Thermo-mechanical Design and Characterisation, *IEEE, Thermic*, September Berlin, Germany, (2013).
4. N. Dufour, K.Aguir, P. Menini Increasing the Sensitivity and Selectivity of Metal Oxide Gas Sensors by Controlling the Sensitive Layer Polarization, *IEEE*, Toulouse, (2013).

Effect of cavity length of quantum well laser

K. Aouni,^{1,2,*} F. Kerrou

¹University of Constantine, Laboratory of Devices Modeling in Renewable Energy and Nanometric, Constantine, Algeria

²University of Constantine, Laboratory of Devices Modeling in Renewable Energy and Nanometric, Constantine, Algeria

Abstract:

Quantum well laser (QWL) is such semiconductor laser is one of the most important light sources fibre optical and integrated optical systems (A.Yariv.1997). Since the invention of semiconductor lasers people have strived to describe them mathematically (Hammadou.A. 2011), yet only in recent years did the fully microscopic calculation of the optical properties of semiconductor heterostructures become possible and was shown to give very good agreement with experimental gain data.

Quantum well lasers have drawn considerable attention because of their low threshold current high, internal efficiency, and fast dynamics, as compared with those of conventional semiconductor lasers.

In this research the dynamic effects of (QWL) GaAs/AlGaAs characteristics in the mid-infrared range of $\lambda \cong 9 \mu m$ is investigated by solving the numerical equations.

One of advantages of semiconductor injection quantum well lasers is their potentially high power conversion efficiency. In this paper the dynamic effects of quantum well laser is investigated by solving the numerical equations. Developing of the rate equation model for a coupled electromagnetic and electronic system can obtain some important structural parameters (Vahed S. 2013)

Calculating of the photons density and the carriers density and the output power are the objectives of the presented study. The effects of cavity length are taken into account (Figure 1). It has been found that the output power becomes more important at lower length cavity.

Keywords: Quantum well laser, rate equation, output power, length cavity.

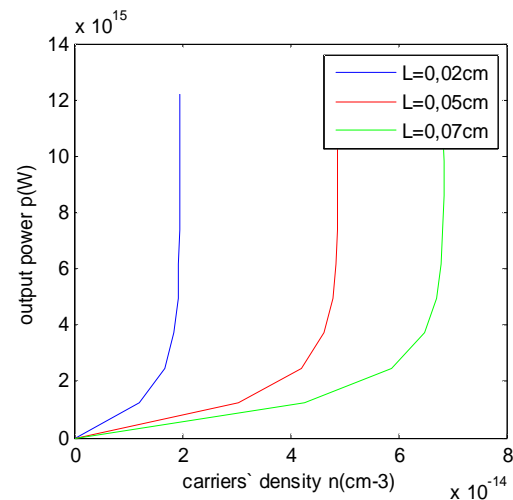


Figure 1: Show the output power versus the carriers density for third cavity length $L=0,02\text{cm}$, $L=0,05\text{cm}$, $L=0,07\text{cm}$. We observe that the output power increases rapidly with the carriers density and decreased of the cavity length leads to the increase of the output power.

References:

Vahed S. (2013), Dynamic analysis of Ga As based Quantum cascade laser, INT J Appl ELECTR PHYS and ROBOT.vol.1, n0.2. Pp.10-12.

Hammadou.A. (2011), Optical external efficiency calculation formid -in Quantum cascade laser, optica applicata . vol.XLI.N0.3.

A.Yariv. (1997), Optical electronics in modern Communication, Oxford,U.K: Oxford Univ. Press, 1997

White organic light-emitting diode using Rubrene

A.Sidi said,^{1*} M.Belkaid,¹ R. Antony,² and S.Oussalah,³ D.Hatem¹

¹ University of Mouloud MAMMERRI, Laboratory of Advanced Technology of Electrical of Engineering
Tizi-Ouzou, Algeria

² University of Limoges, Laboratory of X-LIM-CNRS, Limoges, France

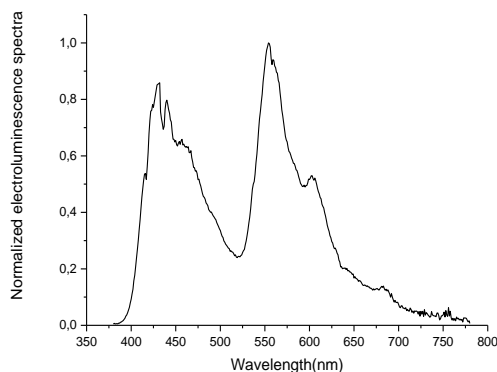
³ Center for Development of Advanced Technologies, Microelectronics and Nanotechnology Division,
Algiers, Algeria.

Abstract: White organic light-emitting diode (OLED) has been fabricated using an ultrathin yellow-emitting layer of 5,6,11,12-tetraphenylanthracene (rubrene) inserted at two sides of interface between two N,N' -bis-(1-naphthyl)-N,N'-biphenyl-1,1'-biphenyl-4,4'-diamine (NPB) layers as a hole transporting and blue emissive layer, respectively (Huang *et al.*, 2008). The configuration of the device is ITO/(NPB) (45 nm)/rubrene (0.3nm)/NPB (29 nm)/(BCP) (31 nm)/Al (90 nm).

The results showed that a maximum luminance of the device reached to as high as 30 cd/m² at 17 V. The peaks of electroluminescent (EL) spectra locate at 430 and 560 nm corresponding to the Commissions Internationale De l'Eclairage (CIE) coordinates of (0.312, 0.320), which is independent of bias voltage (Yu et al 2008).

Keywords: Organic light-emitting diode, rubrene, emissive layer, electrical properties, luminance, EL, PL, efficiency.

Figure 1: Figure illustrating the electroluminescence spectra of device.



References:

Huang, H. H., Chu, S. Y., Kao, P. C., Chen, Y. C. (2008), High efficiency white organic light emitting diodes using Rubrene doped N, N' -bis-(1-naphthyl)-N,N' -diphenyl-1,1' -biphenyl-4,4' -diamine as an emitting layer, *Thin Solid Films* 516, 5669–5672.

Yu L, Li, J., Tang, X., Wang, T., Li, W., Jiang, Y, (2008), Efficient bright white organic light-emitting diode based on non-doped ultrathin 5,6,11,12-tetraphenylanthracene layer, *Journal of Luminescence*, 128, 1783–1786.

Laser-assisted photocatalysed degradation of pollutants using semi-conductors in electronic contact with gold nanoparticles

Z. Chehadi ^{1,2*}, J. Toufaily ², J-S. Girardon ³, M. Capron ³, F. Dumeignil ³, T. Hamieh ², R. Bachelot ¹, S. Jradi ¹.

¹ Laboratoire de Nanotechnologie et d'Instrumentation Optique, Institut Charles Delaunay, STMR-UMR 6281 CNRS, Université de Technologie de Troyes, 12 rue Marie Curie - CS 42060, 10004 Troyes Cedex - France.

² Laboratory of Materials, Catalysis, Environment and Analytical Methods, Faculty of Sciences I, Doctorate School of Science and Technology, Lebanese University, Beirut, Lebanon.

³ Université Lille Nord de France, F-59000, Lille, France; CNRS UMR8181, Unité de Catalyse et Chimie du Solide, UCCS, F-59655 Villeneuve d'Ascq, France.

Abstract: Metal oxide semiconductors hold great promise for applications in energy conversion and storage, environmental remediation optoelectronics, and other areas. However, critical factors such as the high rate of charge-carrier recombinations and limited light absorption have restricted more practical and viable applications (Saji et al, 2013). Plasmonic nanostructures of noble metals have been attracting significant attention for their ability to interact with light from visible to near IR range through the creation of resonant surface plasmon (Stewart et al, 2008). Plasmonic nanostructures of noble metals in combination with semiconductors offer a promising future for the next generation of energy needs (Figure 1).

Various methods have been described for the synthesis of TiO₂ and metal nanoparticles hybrid. In this study, GNPs were fabricated in a thin film of nanocrystalline TiO₂ by sol-gel spin coating method. The thickness can be adjusted by repeating the cycle from adding the Titanium alkoxide precursor on the substrate after calcination at 450°C. The morphology of the nanocomposite and the phases of the films were determined by SEM and Raman. The interaction with noble metal and semiconductor nanostructures under visible light is investigated. Particularly, we study the photocatalytic degradation of Methylene Blue (BM) and Bisphenol A (BPA) under visible light using Au-TiO₂ and Au-ZnO as photocatalysts. Green laser emitting at 532 nm was used to excite the resonance band of the GNPs. The influence of various parameters such as irradiation time, laser power, and catalyst type and amount has been studied.

the role of plasmonic noble metals in enhancing the photocatalytic activity.

Keywords: noble metal nanoparticles, semi-conducteur, visible light, photocatalyst, green laser.

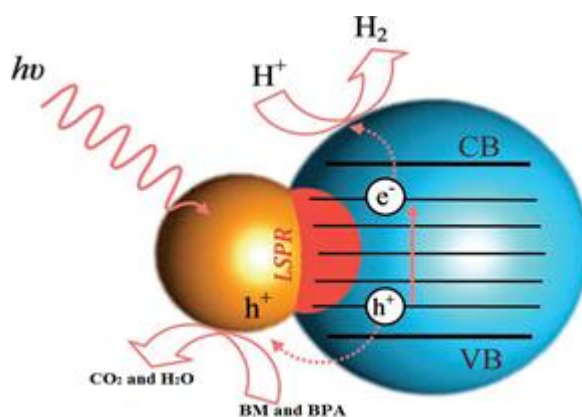


Figure 1: Figure illustrating the proposed photocatalytic process for efficient photodegradation of pollutant using Au-TiO₂ nanostructures, based on excitation of the LSPR under visible light irradiation.

References:

Saji Thomas Kochuveedu, Yoon Hee Jang and Dong Ha Kim (2013) A Study for the interaction of light with noble metal-oxide semiconductor nanostructures for various photophysical applications, RSC publishing, Chem soc Rev.

Stewart M.E., Anderton C.R., Thompson L.B., Maria J, Gray S.K, Rogers J.A and Nuzzo R.G (2008) Nanostructured plasmonic sensors, Chem. Rev, 108, 494.

Surface Potential Decay and Potential Return of Corona Charged Biomedical Polymer: Simulation and Experimental

N. Hitoum¹, S. Sahli¹, Z. Ziari¹, A. Bellel²

¹University of Constantine, Microsystems and Instrumentation Laboratory (LMI), Constantine, Algeria

²University of Constantine, Laboratory of Electronic Material Study for Medical applications, Constantine, Algeria

Abstract: Surface potential measurements have been implemented for many years for analyzing charging/polarization phenomena in dielectrics (polymers) (A. Dolatabadi; 2003). In this work, we have measured the surface potential of a medical polymers charged with corona discharge for different initial voltages. A numerical model, previously developed to reproduce the space charge behavior in polymeric materials, has been then used to simulate the behavior of the surface potential in this biomedical polymer after its charging by a negative corona discharge. The model is one-dimensional, and considers only electrons. It features electron transport using a constant effective mobility, trapping and detrapping in a single deep trapping level and extraction of charge at the ground electrode. Electrons from the discharge are considered as being deposited in the first micrometers inside the polymer. Charges move under the field that they induce in the polymer. The simulated results concern the potential decay and the potential return in the polymer as a function of time. Simulation results show a 'normal' dependence of the potential decay with the different parameters of the model. The results of the decay and the return potential surface obtained through our simulation model are similar to those found experimentally by generating electrostatic charges due to the application of corona discharge on the surface of the dielectric material. Our model is one-dimensional, according to the thickness of the dielectric one, and described the transport of charge in a material after a corona discharge. The trapping, the detrapping and the recombination are taken into account. The charge (electrons and holes) can be mobile or trapped. Like agreed, a mobile electron in the band of conduction (hole in the valence band) has a constant effective mobility, lower than the mobility of band, and which takes account of the trapping and detrapping charge in not very deep traps (G. Chen; 2010). There exists only one level of major trapping for the electrons and the holes, with a maximum density of traps for each type of charge. These trapped loads can be detrapped thanks to a thermo active mechanism. Lastly, the recombination is taken into account for each type of charge, mobile or is trapped.

Keywords: Surface potential, Potential decay, Return potential, Charge injection, Medical polymers.

The figure 1 presented the variation of experimental surface potential decay out on a film of polyforme and surface potential decay obtained thanks to our model according to time.

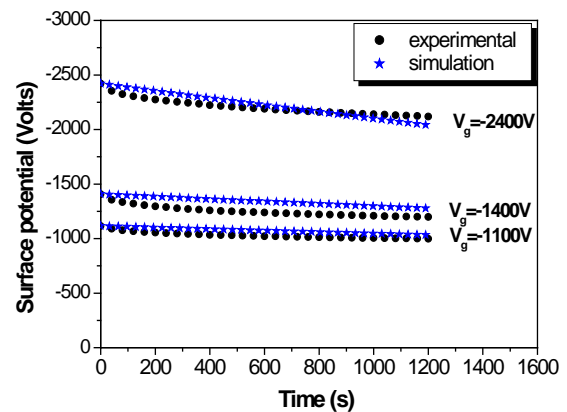


Figure 1: Comparison between experimental surface potential decay curves and calculated for various initial potential.

The figure 2 presented the spatial distribution of the electrostatic charges simulated by COMSOL on Polyforme.

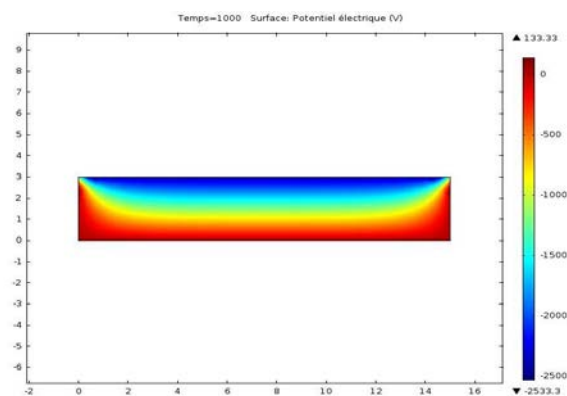


Figure 2: The spatial distribution of the electrostatic charges simulated by COMSOL on Polyforme.

The return of potential consists in neutralizing the charge previously deposited by corona discharge, practically by rubbing the surface of the sample with a piece of cotton soaked with alcohol (J. Kindersberger; 2008). The surface potential is thus tempora-

rily cancelled, and one follows then the variation of the surface potential after neutralization. Generally, this neutralization is made a few seconds at a few minutes after the stop of the discharge. The figure 3 presented the variation of experimental surface potential return out on a film of polyforme and return obtained thanks to our model according to time.

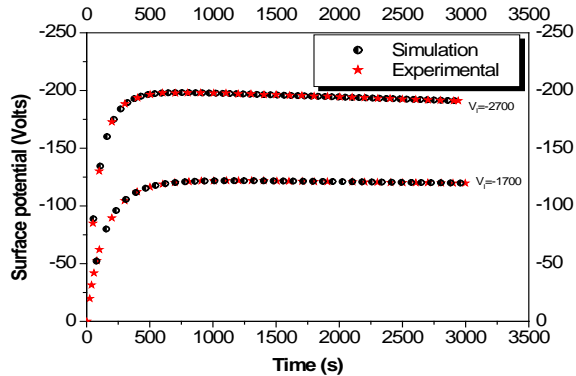


Figure 3: Comparison between experimental surface potential return and calculated for various initial potential.

The study of surface potential on corona charged polyforme films 3 mm thick has revealed that the initial decay rate and the injection coefficient increase with increasing charging level. Model of the potential decay has been constructed via a system of partial differential equations for the space and time dependencies of the field across the sample and the transport parameters contained in this model has been determined by fitting procedure. The model, accounting for the above times, yields a good agreement even for higher charge levels, and this confirms the influence of these times on decay. For weak times of potential return, the model shows a reaugmentation of the surface potential, of the same sign than the initial potential. The maximum value of potential return strongly depends on the density of charge present in the dielectric one but especially of its position (maximum impact when the load penetrated with moist of the sample).

References:

A. Dolatabadi, J. Mosatghimi, V. Pershin (2003) A New Design for Coating Thin Film Alumina on Stainless Steel for Biomedical Applications, *IEEE*, 0-7695-1947-4/03.

G. Chen. (2010), A new model for surface potential decay of corona-charged polymers, *J. Phys. D: Appl. Phys.* 43 (2010) 055405 (7pp)

J. Kindersberger, C. Lederle. (2008), Surface Charge Decay on Insulators in Air and Sulfurhexafluorid – Part I: Simulation, *IEEE Transactions on Dielectrics and Electrical Insulation* Vol.15, No. 4; August 2008.

The 3rd International Nanotech Conference & Exhibition

Nanotech Tunisia 2015



April 22 - 24, 2015 | El Mouradi Hotel, Yasmine Hammamet, Tunisia

www.setcor.org

www.setcor.org